UNIVERSITY OF OKLAHOMA

GRADUATE COLLEGE

INVESTIGATION OF FLEXURAL BEHAVIOR OF REINFORCED CONCRETE WITH 3D PRINTED GLASS FIBER REINFORCED POLYMER

A THESIS

SUBMITTED TO THE GRADUATE FACULTY

in partial fulfillment of the requirements for the

Degree of

MASTER OF SCIENCE

By

ABDIRAHMAN AHMED HAIBE
Norman, Oklahoma
2022

INVESTIGATION OF FLEXURAL BEHAVIOR OF REINFORCED CONCRETE WITH 3D PRINTED GLASS FIBER REINFORCED POLYMER

A THESIS APPROVED FOR THE
SCHOOL OF CIVIL ENGINEERING AND ENVIRONMENTAL SCIENCE

BY THE COMMITTEE CONSISTING OF

Dr. Shreya Vemuganti, Chair

Dr. Royce Floyd

Dr. Jeffery Volz

DEDICATION

I would like to dedicate this thesis my cousin, Safiya Mohamoud who is fighting the good fight against cancer. My parents, Fadumo Osman and Ahmed Haibe, and my advisor Dr. Shreya Vemuganti for her endless support to help me succeed.

ACKNOWLEDGEMENTS

I want to thank my advisor, Dr. Shreya Vemuganti, for her guidance, help, support, and motivation throughout this journey. This work could not be completed without her guidance and advice, and I am honored to work under her supervision. Also, I would like to thank my committee members, Dr. Jeffery Volz and Dr. Royce Floyd for their support and guidance.

I would like to thank Mr. John Bullock for his assistance in conducting experiments throughout the program. I would like to thank my research team, Alexandra Liever, Ali Akbarpour, and Stephanie Castillo for their help and assisting for casting and experimental testing.

Lastly, I want to acknowledge and thank, Matthew Reed, Stephen Roswurm, Jake Choate, Jackson Milner, Omar Yadak, and Jacob Starks for assisting and training me. Also, I want to thank my family and friends from home for their unlimited support and motivation.

DEFINITIONS

Terms	Definitions
FRP	Fiber Reinforced Polymer
GFRP	Glass Fiber Reinforced Polymer
VAHT	Vacuum Assisted-Hand-Layup Technique
PolC	Polymer Concrete
PCC	Portland Cement Concrete
MMA	Methyl Methacrylate

Abstract

More than 40 years of Fiber Reinforced Polymers in Civil Engineering has shown the widespread use and advantages of these unique composites. FRP composites are high strength, lightweight, corrosion resistant materials that are known for their long-term durability and performance in infrastructure applications. FRP composites are available in the form of sheets, rods, grids and winding strands that are used for a wide range of civil engineering applications. In the last decade, 3D printing technology for manufacturing FRP composites for construction applications has gained increased attention. With 3D printing technology, FRP composites can be printed with radical shapes and properties resulting in varied mechanical performances. Precise angles, optimized designs and radical shapes are also some of the several advantages that 3D printed FRP composites can offer. With increasing demand for 3D printed composites and with interest in using these composites for construction applications, it is very important to understand the behavior of these composites in concrete when used as reinforcement. Concrete - FRP bond behavior plays a significant role in controlling debonding failures in FRP-strengthened flexural elements ultimately contributing to their structural performance. In addition, compared to conventional Portland cement-based concrete, polymers in concrete can have a much different behavior due to better engagement with increased bond strength with the constituents. Polymers have known to have higher bond strength with other materials compared to cement due to lack of saturation in the latter. Therefore, the behavior of FRP, especially 3D printed FRP may be different in these different concretes. This work investigates the flexural behavior, failure modes and ductility of conventional FRP composites, conventionally manufactured and 3D printed, used as a reinforcement in concrete. Two types of concrete are investigated for understanding the flexural response of FRP composites. A Methyl Methacrylate based polymer concrete and Portland cement-based concrete

reinforced with Glass FRP reinforcement. The results of this work show that both conventional and 3D printed FRP composites used as reinforcements in Portland cement concrete and Polymer concrete improve the moment capacity and flexural capacity of the beams. However, on average, 3D printed GFRP in Polymer concrete has improved flexural response than the 3D printed GFRP in Portland cement concrete. Microscopic analysis was conducted to observe damage in all the beams subjected to flexural testing. These investigations indicated that polymer concrete shows better engagement with the reinforcement.

The outcomes of this work show that 3D printed FRP composites are suitable for use in construction applications. Further understanding of the behaviors of 3D printed FRP composites in concrete lead a way to advanced concrete based reinforced composites that can be 3D printed in radical shapes and designed for tailored mechanical properties and performance for construction applications.

Table of Contents

List of Figures

List of Tables

Chapter 1: Introduction

1.1 Background

Fiber-reinforced polymers (FRP) were introduced in the aerospace industry in the middle of the 20th century due to their high strength, corrosion resistance, durability, and lightweight (Gunaslan, Karasin, and Öncü 2014; Sonnenschein, Gajdosova, and Holly 2016). The construction industry has adopted FRP for these advantages over the years. The interest in using FRP composite in new construction like concrete structures and rehabilitating older structures increased in the last few decades.

3D printing technology is taking engineering to new heights. The current manual fabricated reinforcements can be 3D printed with more precision as shown in Figure 1 (a). Radial shapes and optimized designs can constructed using concrete 3D printer. Combining these two novel methods, simultaneously 3D printed the concrete and reinforcement, is currently being investigated.

(a) (b)

Figure 1: (a) 3D printing reinforcement (Del Giudice and Vassiliou 2020) and (b) 3D printing concrete (Wu, Memari, and Duarte 2022)

3D printed FRP is an emerging material with lower production cost, that can produce complex shapes and designs, which have the conventional FRP benefits (Pervaiz et al. 2021). The

technology is utilized in various industries, and 3D printed FRP can be used as reinforcement for concrete. Currently, 3D printed FRP composites are not used in the construction industry due to limited information on the behavior of 3D printed FRP. Therefore, this thesis investigates the flexural response of concrete reinforced with 3D printed GFRP.

1.2 Scope of Research

This study will focus on understanding the flexural behavior of reinforced concrete with 3D printed glass fiber reinforced polymers, (GFRP). The scope of this investigation includes using Vacuum Assisted Hand layup Technique (VAHT) to fabricate glass fiber reinforced polymer composites at unidirectional (0°) layup and 3D printing techniques to fabricate 3D printed unidirectional (0°) layup and debonded 3D printed pseudo-ductile FRP designs (multidirectional 3D printed GFRP for construction). Two types of concrete are studied in this research including Portland cement concrete (PCC) and Polymer concrete (PolC).

1.3 Hypotheses

The following hypotheses can be made based on existing knowledge.

i. Conventional and 3D printed GFRP may have better engagement in polymer-based concretes compared to cementitious concretes due the polymer-polymer high bond strength.
ii. Polymer concrete may have higher flexural strength than Portland cement concrete with 3D printed GFRP compared to conventional GFRP.
iii. 3D printed multidirectional GFRP will preserve its pseudo ductile behavior in flexural response due to the different orientations with appropriate load transfer
iv. The VAHT unidirectional GFRP will have higher fiber volume fraction and overall stiffness than 3D printed unidirectional GFRP.

v. 3D printed unidirectional GFRP, and multidirectional 3D printed GFRP for construction can be used in concrete as a reinforcement.

1.4 Objectives

The primary aim of this study is to understand the flexural behavior of 3D printed GFRP when used as a reinforcement in concrete. The following are proposed:

i. Determine flexural response of PCC reinforced with VAHT unidirectional GFRP, 3D printed unidirectional GFRP, and multidirectional 3D printed GFRP for construction.

ii. Determine flexural response of PolC reinforced with VAHT unidirectional GFRP, 3D printed unidirectional GFRP, and multidirectional 3D printed GFRP for construction.

iii. Provide a comprehensive comparison between the flexural behavior of the concretes with different reinforcements.

1.5 Thesis Outline

- **Chapter 1** : Discusses background information on FRP and describes the progress that has been made in past several decades. The research scope, hypotheses, and objectives are discussed as well.
- **Chapter 2**: Covers the literature review on FRP composite manufacturing, benefits and drawbacks, applications in the construction industry, and the future of the material.
- **Chapter 3**: Provides comprehensive explanation of the methodology and the materials needed to conduct this study successfully.
- **Chapter 4**: Presents the results of the different test methods, volume fiber fraction, tensile, compression, modulus of rupture, and flexural.
- **Chapter 5**: Compares and discusses the results of presented in chapter 4.
- **Chapter 6**: Presents the conclusion, recommendations, and future work.

Chapter 2: Literature Review

2.1 Fiber Reinforced Polymer Composites

Fiber reinforced polymers are a composite material made of two major components, high strength fibers and homogenous epoxy which holds the fibers together (Gowayed 2013). The primary function of fibers in the composite is taking the load while providing stability, stiffness and strength (Sonnenschein, Gajdosova, and Holly 2016) and the polymer matrix holds the fibers in place, prevents damages from the environmental changes and protects the fibers during manufacture (Sonnenschein, Gajdosova, and Holly 2016). An example of the composite is shown in Figure 1 illustrating the functionality of both the fiber and the matrix.

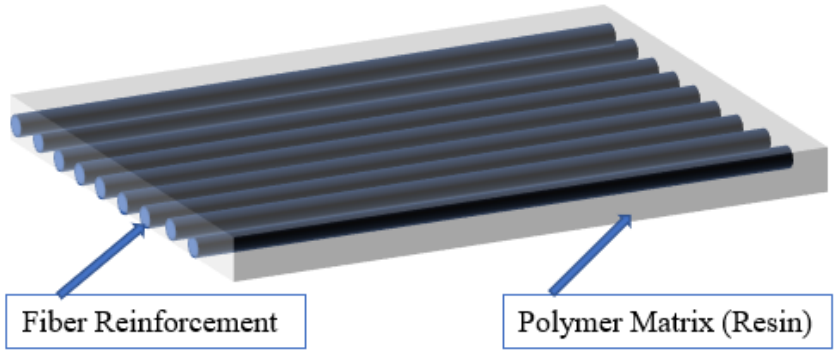

Figure 2: Schematic representation of typical unidirectional fiber reinforced polymer composite

FRP was first discovered in the early 20th century by Leo Hendrik Baekeland; however, it was not utilized for commercial reasons until 1930s (Bai 2013). The aircraft industry was facing production problems because every design change required new molds. The primary material was metals and molding metals was a time consuming and costly process (Bai 2013). Furthermore, plastic molds did not have the desired strength to withstand the loads which led to the idea of adding reinforcing

glass fiber to the plastic to increase its strength. (Bai 2013). A list of advantages and disadvantages of FRP are provided in Table 1.

Table 1: Advantages and disadvantages of fiber reinforced polymers (Gunaslan, Karasin, and Öncü 2014)

Advantages	**Disadvantages**
• High strength to weight ratio • High stiffness to weight ratio • Corrosion resistance • Long term durability • High workability • Low transport cost due to lightweight • Easy formability • High fatigue and impact strength • Low heat conductivity • Electrical insulation and conductivity	• High initial cost • Brittle failure at high strength • Poor shear strength • Anisotropic (complex failures)

Composites with fibers arranged in a parallel fashion to the loading direction give their maximum performance and therefore, provide the highest strength and stiffness. The arrangement of a weave or mat demonstrates limited strength but in more directions. For applications with low structural demand, fibers chopped to short lengths are randomly distributed in the matrix for strength enhancements. The fiber type is essential to obtain an FRP composite with the necessary stiffness and strength. There are several different types of fibers used for FRP like Aramid, Basalt, Carbon, Kevlar, and Glass.

A comparison of properties of different fiber types of FRP with steel is shown in Table 2.

Table 2: Comparison of properties of different fiber types with steel (Goh, Yap et al. 2018)

Materials	**Tensile Strength (MPa)**	**Modulus of Elasticity (GPa)**
GFRP	1050	55
AFRP	1400	76
CFRP	1500	180
Steel	400-1000	200

Even though Aramid fiber reinforced polymers (AFRP), Carbon fiber reinforced polymers (CFRP), and Glass fiber reinforced polymers (GFRP) are the main types used in the civil engineering industry, (Gunaslan, Karasin, and Öncü 2014), GFRP is by far the most predominant type due to its low cost yet comparable strength to carbon (Sonnenschein, Gajdosova, and Holly 2016). Glass fibers are produced by melting silica and other raw materials at a very high temperature, 1500 to 1700 C. The molten glass is extruded through "a heated platinum spinneret containing very small holes" (Gowayed 2013). Then the fibers are treated with a coupling agent which improves the adhesion of the fiber to the matrix material in the composite (Gowayed 2013). FRP are available in the form of sheets, rods, grids and winding strands that are used for a wide range of civil engineering applications. The tensile strength of FRP is superior to steel, however, they have a linear elastic behavior to failure. The high strength and stiffness composites lack ductility which leads to failure before yielding as shown in Figure 2. This inadequate ductility does not satisfy the requirements for civil infrastructure applications. Even in automobile, recreational and aerospace applications, where components are subjected to impact or dynamic loading, progressive, gradual, and controlled failure mechanisms are desirable for energy dissipation. Therefore, the brittle behavior of FRP and lack of ductility causes a major drawback of FRP composites which limits their wide scale use in the construction industry.

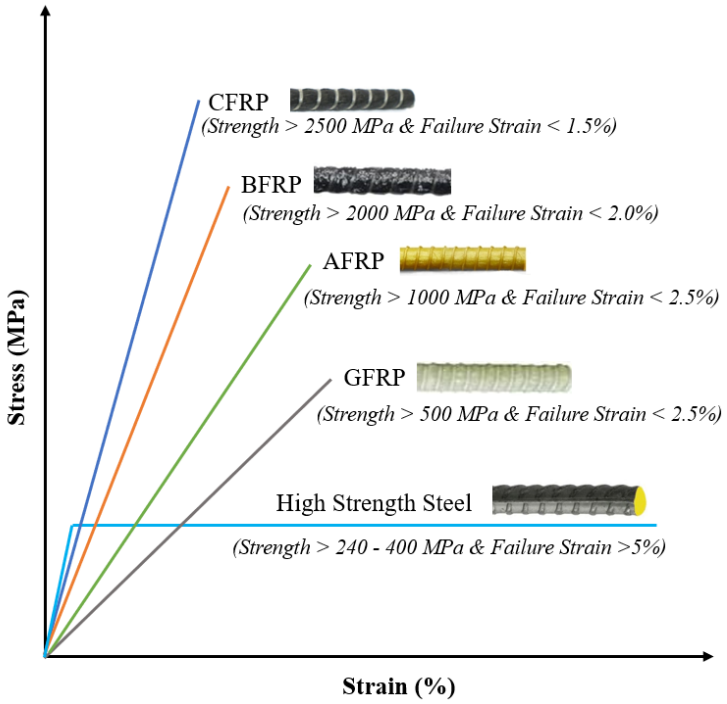

Figure 3: Response of different types of FRP in comparison to steel

2.2 Conventional FRP Composites

Conventional FRP composites have limited fiber orientation due to their manufacturing processes. The most common FRP composites are rebars as concrete reinforcement; tendons for prestressed concrete; and stay-in-place formworks for concrete members (Bank 2006). All these forms of FRP composites are used in the civil engineering industry of different scales.

(a) FRP Rebar (b) FRP Stay-in-Place (c) FRP Prestress Tendons

Figure 4: Prefabricated common FRP composites used in construction

(Courtesy of Google Images)

There are numerous FRP composite manufacturing methods FRP used in construction are mainly manufactured using lay-up or pultrusion methods. The manual hand lay-up can be open molding, spray up, or vacuum assisted hand lay-up technique. The advantages of this technique are simple manufacturing process, low cost, and no special training required (El-Hajjar, Tan, and Pillai 2013; Krishna and Kumar 2016).

In the late 1980s, hand-layup FRP composites became popular in Japan for retrofitting concrete structures. Tow sheets, a unidirectional carbon fiber sheet, were mainly developed and commercialized (Bank 2006). The United States adopted the usage of FRP composite, following Japan, for rehabilitating deteriorating structures (Bank 2006; Sonnenschein, Gajdosova, and Holly 2016). A schematic drawing of the hand-layup used for FRP wraps and sheets is show in Figure 4.

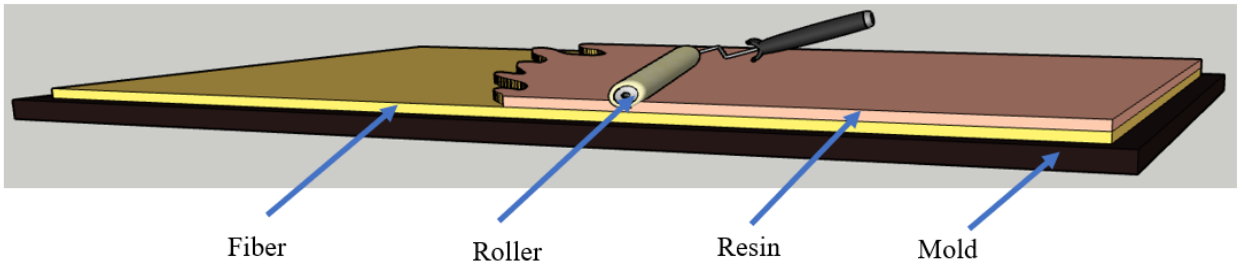

Figure 5: Schematic of manual hand lay-up technique

The prefabricated FRP composites in Figure 3 (a) ; rebars, stay in place formworks, and tendons; are produced using the pultrusion process. In pultrusion process, different continuous fiber reinforcements are mechanically guided into a resin saturation unit, surfacing veil, and then drawn into heating chamber to cure, (Figure 5)(El-Hajjar, Tan, and Pillai 2013).

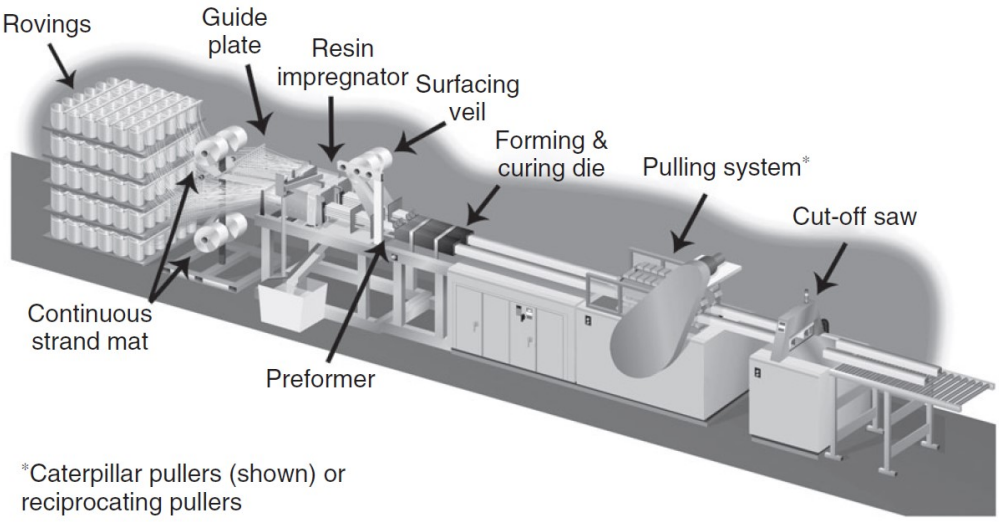

Figure 6: FRP pultrusion process (El-Hajjar, Tan, and Pillai 2013)

The mechanical properties of three different types of FRP bars, Glass/Vinyl ester (G/V), Basalt/Vinyl ester (B/V), and Basalt/Epoxy (B/E) were investigated by Benmokrane et al. (2015) their results are demonstrated in Table 3.

Table 3: Mechanical properties of FRP (Benmokrane, Elgabbas et al. 2015)

Bar Type	**Flexural Strength**	**Modulus of Elasticity**	**Max. Outer Fiber Strain**
Units	(MPa)	(GPa)	(%)
Glass/Vinyl ester	1265 ± 40	60 ± 1	2.1
Basalt/Vinyl ester	1555 ± 123	62 ± 1	2.5
Basalt/Epoxy	1501 ± 176	41 ± 2	3.6

All the various FRP bars in Table 3 exhibit substantial flexural strength as concrete reinforcement, and other engineering applications. However, accelerated aging has big impact on B/V and B/E which reduced the flexural capacity of the specimens by 37% and 39 % respectively after 5000 hours where G/V lost only 7% of the strength. The durability of G/V can be attributed to its excellent fiber-resin bond and low moisture uptake in comparison to B/V and B/E (Benmokrane et al. 2015).

To overcome these shortcomings and mechanical weaknesses that limit the usage of the material (Lau 2013), hybridization of fibers was conducted. The hybridization processes can be conducted in various ways, but the most common configurations are interlayer where the fibers are stacked layer by layer, intralayer where the fibers are woven together yarn by yarn, and intrayarn or fiber by fiber (Swolfs, Gorbatikh, and Verpoest 2014).

These composites are designed to enhance the mechanical, thermal, and damping properties in comparison to typical non-hybrid FRP which have abrupt catastrophic failure as shown in Figure 6 (a) (Sathishkumar, Naveen, and Satheeshkumar 2014; Lau 2013). Typical Hybrid composites have characteristic load drops, shown in Figure 6 (b), which can be transformed into a more steady failure called pseudo-ductility as shown in Figure 6 (c).

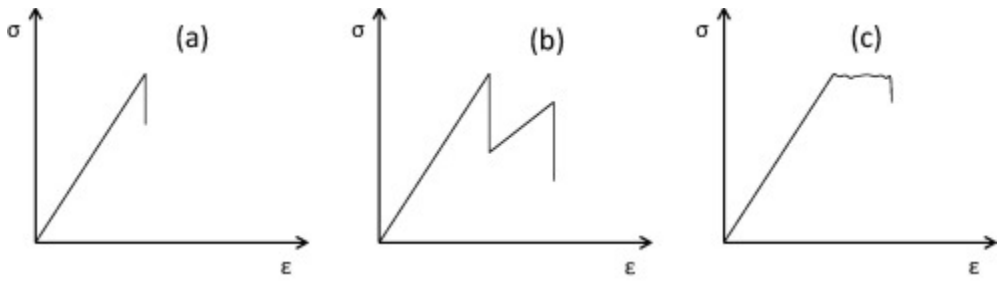

Figure 7: Schematic stress–strain diagrams for (a) non-hybrid composites, (b) typical hybrid composites, and (c) pseudo-ductile hybrid composites (Swolfs, Gorbatikh, and Verpoest 2014)

2.3 3D Printed FRP Composites

Additive manufacturing, also known as 3D printing technology, has been used to manufacture FRP composites. The conventional FRP composites manufacturing is costly, time intensive, and limits design modifications (Pervaiz et al. 2021; Tse, Kapila, and Barton 2016). In 3D printing, the manufacturing is automated and does not require cutting and molding of the material. The process is faster and products with complex shapes and precise dimensions can be produced. Additionally,

the 3D printing process is cost-effective and reduces carbon dioxide emission which has positive impact on the environment (Salmi 2021; Pervaiz et al. 2021; Tse, Kapila, and Barton 2016).

A comparative study of conventional FRP and 3D printed FRP studied specific mechanical properties like tensile strength, elastic modulus, and fatigue life. The researchers discovered the 3D printed composites can be designed to demonstrate higher strength than the conventional composites; however, the fiber orientation significantly impacts the mechanical properties (Agarwal et al. 2018). Similarly, the effect of reinforcement pattern, distribution, print orientation, and fiber percentage on compressive and flexural properties of 3D printed polyamide 6 (PA6) reinforced with continuous carbon fiber was studied. It was found that concentric reinforcement and 0° degree fiber orientation maximized the flexural response (Araya-Calvo et al. 2018). Additionally, increasing the fiber volume in the 3D printed FRP increases stiffness and ultimate strength (Melenka et al. 2016). These improvements highlight the potential of FRP and how 3D printing technology by design can be utilized to enhance the mechanical properties of FRP. In addition to enhancements, 3D printing technology has also been used to transform failure modes of FRP. 3D printing technology has unlimited potential for future smart manufacturing. Similarly, the global growth projection of the additive manufacturing of composites is estimated to be $10 billion by 2028 as shown in Figure 7.

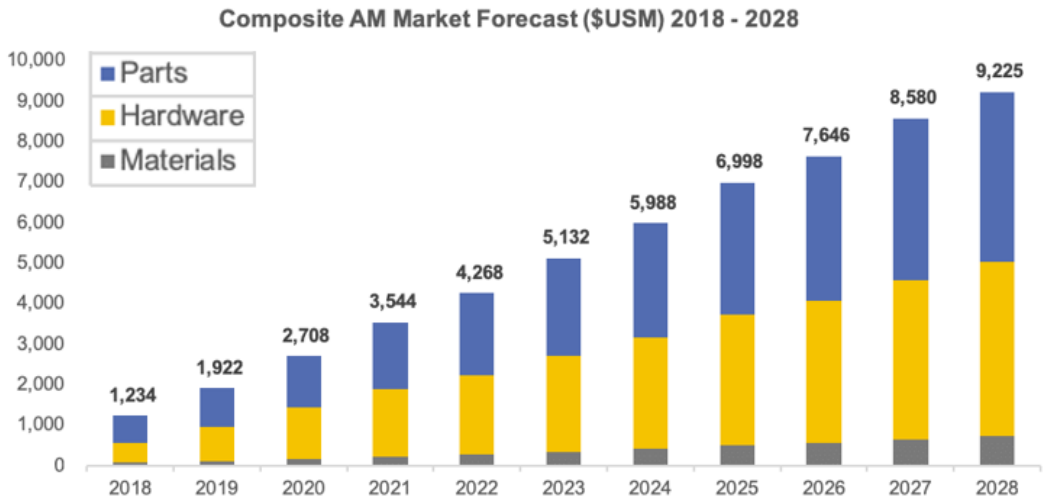

Figure 8: Composite Additive Manufacturing market forecast (Pervaiz et al. 2021)

2.4 3D Printed FRP for Construction

3D printing technology can also be used to optimize the fiber stacking and orientation which significantly influences FRP behavior because of its mechanical orthotropy (Vemuganti, Soliman, and Reda Taha 2020).

A recent study demonstrated FRP pseudo ductility through design of only glass and not hybrid FRP composites by using 3D printing (Vemuganti, Soliman, and Reda Taha 2020; Dickson et al. 2017). As Figure 8 (a) shows, 3D printing technology can be used with a cloud-based software and G code, a simple programming language for Computer Numerical Control machines, to print continuous fibers at different orientations.

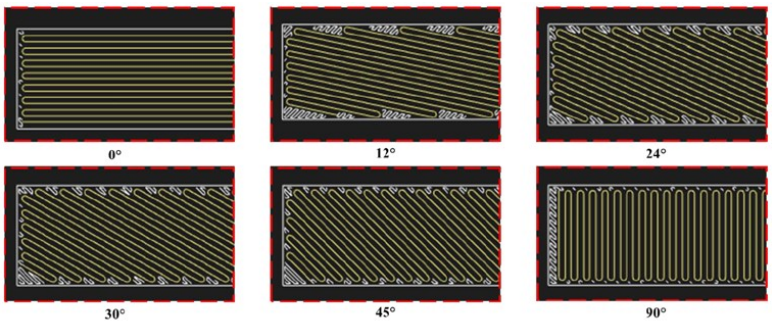

(a)

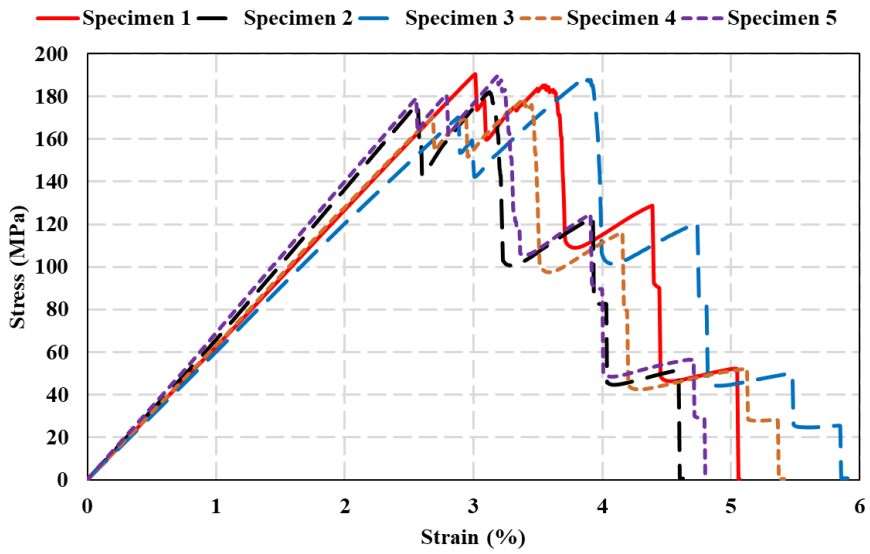

(b)

Figure 9: (a) Example fiber orientations printed using a continuous fiber 3D printer (b) experimental behavior of one design of 3D printed ductile FRP (Vemuganti, Soliman et al. 2020)

This process is continuous fiber 3D printing which is currently available technology. Using the discrete fiber orientations integrated with fiber stacking sequence, the resulting 3D printed GFRP specimens were designed to fail in a gradual mechanism. The layers are designed in consideration of their axial stiffness which was achieved by stacking the fibers based on the orientation and sequence. This precise organization of the fibers ensures appropriate load sharing ratios among the layers. The load sharing ratio determined in Equation (1) assures progressive load transfer and the 'fail-safe' desired properties of the pseudo-ductile composite.

$$\text{Load sharing ratios} = \frac{\left(\frac{EA}{L}\right)_i}{\sum_{i=1}^{N}\left(\frac{EA}{L}\right)_i}, \qquad \textbf{(1)}$$

Where L is the constant length among all layers, E is the modulus of the material, A is the cross-sectional area, N is the total number of layers, EA is the axial stiffness, and i is the layer number.

2.5 FRP- Concrete Behavior

Typically, Portland cement-based concrete has been used in literature for understanding the influence of FRP. FRP behavior and its performance in other types of concrete is highly unexplored. In terms of bond with reinforcement, polymers are known to have higher bond strength with other materials compared to cement due to lack of saturation in the latter. Polymer concrete (PolC) is a composite material which results from the combination of aggregate and polymer binder (Bulut and Şahin 2017). The composite was introduced in the late 1950s and expanded in the 1970s as an alternative to Portland cement concrete in certain applications (Bedi, Chandra, and Singh 2013). Initially, PolC was used for cladding building, however, it was later used for repair due to its ability to cure fast, high strength, durability, and excellent bond to Portland cement concrete, and steel reinforcement (Bedi, Chandra, and Singh 2014b). The PolC composites are categorized in three types: 1) polymer concrete; 2) polymer cement concrete and 3) polymer impregnated concrete (Bărbuţă, Harja, and Baran 2010). The applications of polymer concrete varied over time, covering building surfaces, repairing damaged structures like bridges, and using as precast components. The polymer concrete composites have superior mechanical strength, fast curing, and durability which reduced the need for maintenance repairs (Gorninski, Dal Molin, and Kazmierczak 2004). The modern PolC is efficiently used in precast for buildings, bridge panels, hazardous waste containers, and machine bases (Abdel-Fattah and El-Hawary 1999). The rapid setting property is an asset in the production process since the precast concrete can be placed and demolded in a couple of hours (Gorninski, Dal Molin, and Kazmierczak 2004). Simpler applications like coatings and repairs can be completed and have the structures ready for use within the same day. In comparison to Portland cement concrete, PolC has high corrosion resistance, and impermeability to water and salts (Abdel-Fattah and El-Hawary 1999). Therefore,

it can be use in areas with high moisture content and under water structures. The flexural strength of different types of concrete varies due to their mix properties and additives. The PolC flexural strength increased 5 to 10 times with textile reinforcement depending on the reinforcement location (Murcia et al. 2022). Reinforcing steel fibers increase the flexural strength of PolC by 40%, however, the longer fibers show better mechanical improvement (Bedi, Chandra, and Singh 2014a).

Chapter 3: Materials and Methods

In this chapter, the experimental methodology and materials used in this study are discussed. The testing matrix, FRP fabrication, concrete mixing and casting, and the various test setups and testing methods are explained.

3.1 Test Matrix

A total of 24 beams with the dimensions 12 in by 2 in by 2 in (304.8 mm by 50.8 mm by 50.8 mm) were tested in three-point bending for flexural behavior analysis. The beams were classified in two different types of concrete with four different types of reinforcement. The breakdown test matrix with descriptions is given in Table 4. The manufacturing of different types of reinforcement are described in the following sections.

Table 4: Test Matrix

[1]VAHT - Vacuum Assisted Hand-layup Technique, [2]GFRP – Glass Fiber Reinforced Polymers

Types of Concrete	No. of Beams	Type of Reinforcement
Portland Cement Concrete (PCC)	3	Non-Reinforced
	3	VAHT[1] Unidirectional GFRP[2] (High Strength)
	3	3D Printed Unidirectional GFRP[2] (High Strength)
	3	Multidirectional 3D Printed GFRP[2] for Construction
Polymer Concrete (PolC)	3	Non-Reinforced
	3	VAHT[1] Unidirectional GFRP[2] (High Strength)
	3	3D Printed Unidirectional GFRP[2] (High Strength)
	3	Multidirectional 3D printed GFRP for construction

3.2 Vacuum Assisted Hand-layup Technique (VAHT) for Fabrication

Composite processing can be divided into thermoset composite processing and thermoplastic composite processing based on the type of polymer used to bind the fibers. The thermoset resin or epoxy has high strength, modulus, durability, and demonstrates thermal and chemical resistance (Saba et al. 2016). As a result of its chemical composition, the thermoset composites cannot be reversed, reformed or reshaped after the polymerization process is completed(Saba et al. 2016)

(Asim et al. 2017). The most common processing methods for thermoset composites are hand lay-up, filament winding, compression mold, pultrusion, and injection molding (Asim et al. 2017), the vacuum assisted hand lay-up technique (VAHT) was used to cast unidirectional GFRP.

Casting VAHT GFRP can be considered two major parts, material preparation and fabrication. In this study, the breather cloth, porous plastic peel ply, and peel ply were cut into 21 in by 21 in (533.4 mm by 533.4 mm) dimension, where the release film was 23 in by 23 in (584.2 mm by 584.2 mm) and the 0.04 in (1 mm) thick unidirectional glass fiber was 20 in by 20 in (508 mm by 508 mm).

A steel plate of 24 in by 24 in (609.6 mm by 609.6 mm) was taped on a table with a flat surface to ensure that casting surface is leveled and reduce deficiencies. The plate was covered with the release film and taped down to the table to prevent movement.

TYFO® S Saturant Epoxy 100 parts of Component A and 42 parts of Component B by volume were used. 150 mL of component A and 63 mL of component B was measured out and the two components were mixed with mixing sticks at least for 30 seconds to create a homogenous mix prior to casting. The peel ply was then placed on the release film and small amount of the epoxy mix was applied which creates adhesion and prevents the pieces from sliding off. The GFRP layer was laid, and an adequate amount of the epoxy resin was added. A hand roller was used to evenly distribute the epoxy and fully seep in the GFRP fiber. Subsequently, the VAHT GFRP layers are placed in the sequence shown in Figure 9.

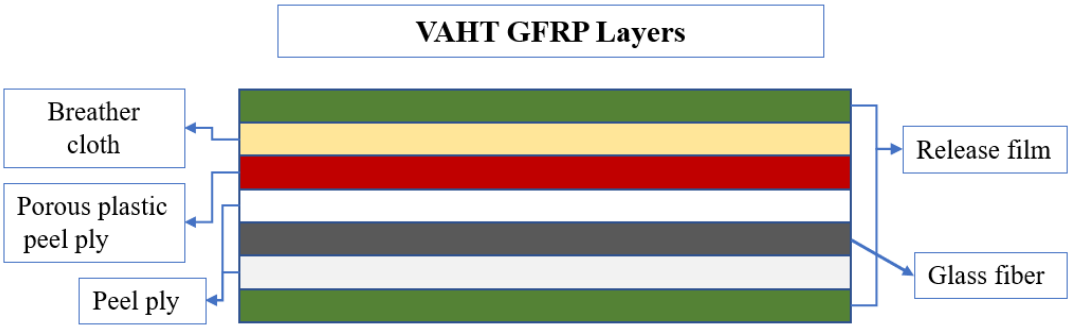

Figure 10: Schematic representation of VAHT layers

Failure to fully saturate the fiber creates inconsistency and reduces the strength of the material. Similarly, oversaturating the material affects the composite mechanical properties and contributes to inconsistent fiber volume fraction. Therefore, a vacuum pump was connected to the setup to suction out the excess matrix as shown in Figure 10 and ran for minimum six hours.

(a)

(b)

Figure 11: (a) VAHT setup (b) VAHT Unidirectional GFRP (High Strength)

To fabricate the conventional VAHT GFRP, 20 in by 20 in by 0.04 in (508 mm by 508 mm by 1 mm) was casted following the process described in the methods. The plate was air cured for 24 hours and heat cured another 48 hours. At the end of the curing process, the plate was sliced into the reinforcement size 12.6 in by 0.6 in by 0.04 in (320 mm by 15 mm by 1 mm) along the fiber

direction, as shown in Figure 10 (b). These unidirectional VAHT coupons were later utilized as concrete reinforcement.

3.3 3D Printing Method for Fabrication

Thermoplastic polymers are gaining popularity for their high toughness and post curing processing possibilities (Balasubramanian 2014). 3D Printing uses thermoplastic composite processing, and this study used a thermoplastic nylon filament. The GFRP coupons were designed using CAD software and Eiger 3D Printing software to determine the specific angles the GFRP was casted. A Markforged® 3D printer (shown in Figure 11 (a)) was used to print with continuous glass fiber and thermoplastic nylon filament as shown in Figure 11 (b).

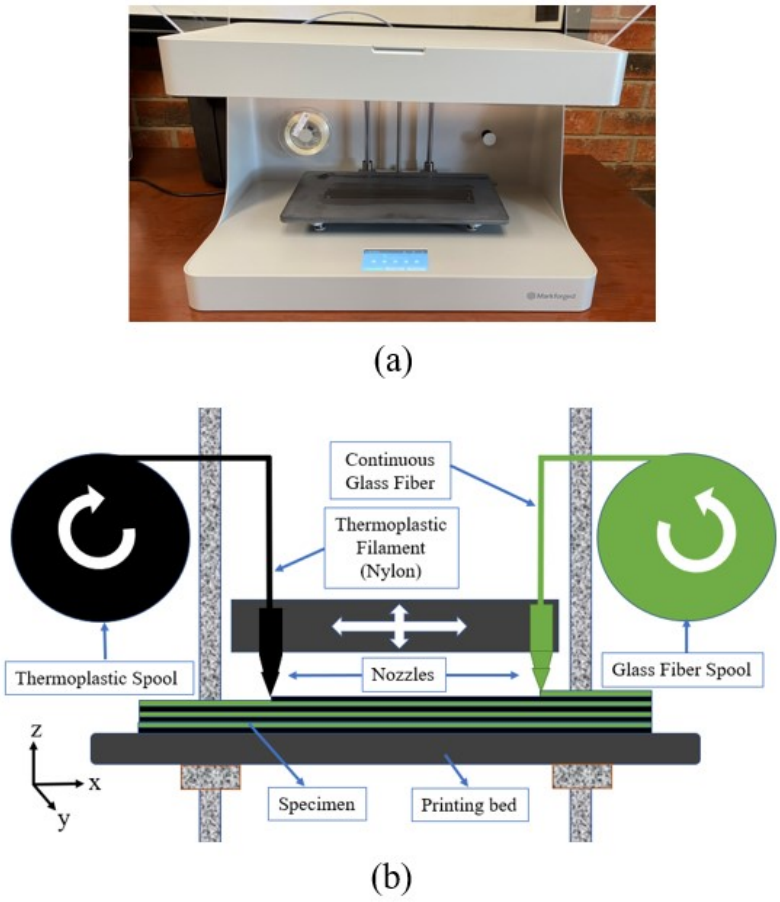

Figure 12: (a) Markforged 3D Printer (b) 3D Printer Setup

For this study, two different 3D printed GFRP reinforcements were investigated: a) unidirectional 3D printed GFRP and b) multidirectional 3D printed GFRP. The unidirectional 3D printed GFRP with dimensions 12.6 in by 0.6 in by 0.04 in (320 mm by 5 mm by 1 mm) was printed with all the fibers in the 0° direction from the horizontal plane as shown in Figure 12.

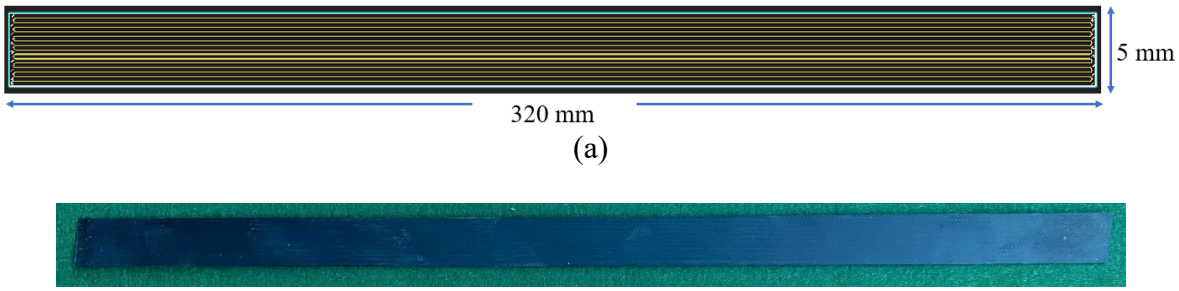

(a)

(b)

Figure 13: (a) 3D printed Unidirectional GFRP Schematic and (b) 3D printed unidirectional coupon GFRP (High Strength)

The multidirectional FRP composite that represents the FRP for construction was made up of 7 fully de-bonded layers as opposed to one continuous layer. The design was systematical where the first layer (red) contained one floor sub-layer of onyx which is a fusion of engineering nylon and chopped carbon fibers ("Introducing Our New Markforged Material: Onyx") followed by four sub-layers of ±30° followed other four sub-layers of ±24° and roof sub-layer of onyx. The second layer (yellow) contained 8 sub-layers of ±24° with a base nylon layer 'floor layer' and cover layer 'roof layer' of onyx. The third layer (black) had two sub-layers of ±24° followed by two sub-layers of ±12° with a base nylon layer 'floor layer' and cover layer 'roof layer' of onyx as well. Lastly, the fourth (white) and middle layer had 8 sub-layers of ±12° with a base nylon layer 'floor layer' and cover layer 'roof layer' of onyx. The symmetrical design and fiber orientations for the design is shown in Figure 13 (a) and (b).

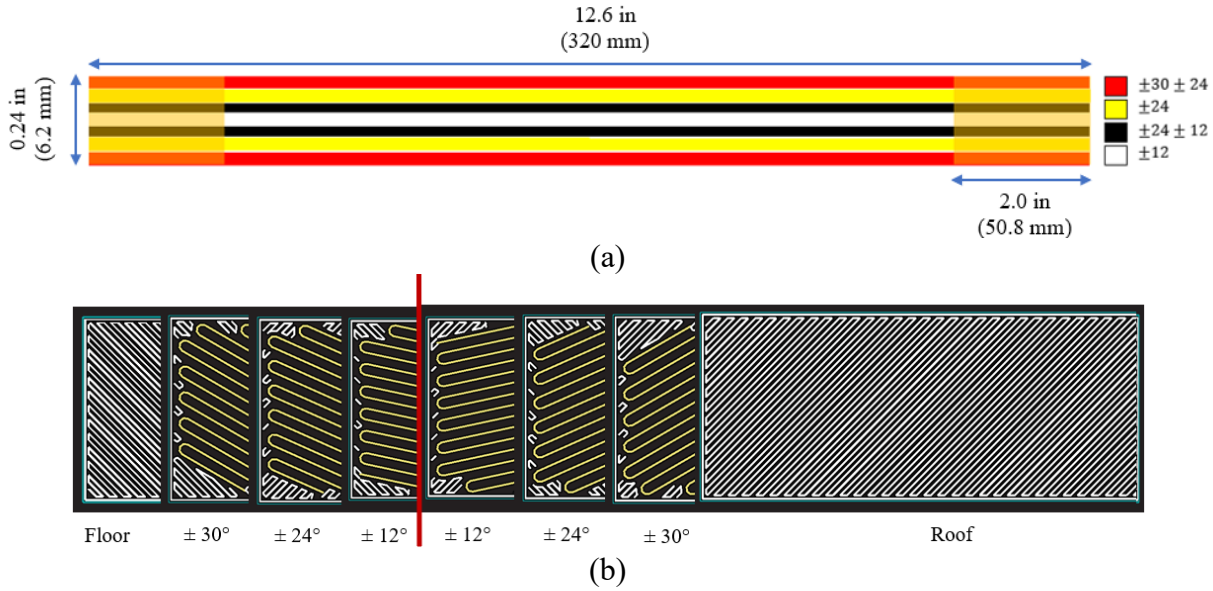

Figure 14: (a) The multidirectional 3D printed design (b) Orientations of the layers

The layers of the multidirectional design were then carefully combined in the correct order and bonded together for 2.0 in (50.8 mm) from each end. TYFO® S Saturant Epoxy was used to bond the end of the specimens. The dimensions of the completed ductile design were 12.6 in by 0.24 in (320 mm by 6.2 mm) as shown in Figure 13. The completed 3D printed multidirectional GFRP is shown in Figure 14.

Figure 15 : 3D printed multidirectional coupon GFRP (High Strength)

3.4 Volume Fraction Test

Fiber reinforced polymers have two main components: the fiber, and the matrix. The volume of fiber in a composite plays a significant role and affects the mechanical properties of the composite.

A higher fiber to matrix ratio corresponds to higher strength for those particular materials (You et al. 2015).

The GFRP VAHT and the 3D printed GFRP used in the study composites have different fiber to matrix ratios which was predicted to impact the mechanical properties of the reinforcement. The volume fraction was determined in accordance with ASTM D3171 Procedure G ('D3171 Standard Test Methods for Constituent Content of Composite Materials' 2015) to burn off the matrix with a furnace. The fiber volume fraction was determined using the following equations:

$$\textit{Fiber Volume Fraction} \qquad V_r = \left[\frac{M_f}{M_i}\right] \times \left[\frac{\rho_r}{\rho_c}\right] \times [100] \qquad \textbf{(2)}$$

Where M_i = initial mass of the composite specimen before digestion or combustion, g, M_f = final mass of the composite specimen after digestion or combustion, g, ρ_r = density of the reinforcement, g/cm^3 and ρ_c = density of the specimen, g/cm^3.

$$\textit{Specimen Density} \qquad \rho_c = \left[\frac{M}{A \times h \times 1000}\right] \qquad \textbf{(3)}$$

Where M = mass of the specimen, g; A = cross-sectional area of the specimen, m^2; and h = thickness of the specimen, mm.

A Compact Split Tube Furnace with Vacuum Flanges and maximum temperature of 1200 °C was used to combust the matrix of the GFRP. Three specimens of VAHT GFRP and three specimens of 3D Printed GFRP with the dimension 1.2 in by 1.2 in by 0.06 in (30 mm by 30 mm by 1 mm) shown in Figure 15 were used. The 3D Printed multidirectional GFRP fiber volume was not determined since it has different thickness than the unidirectional specimens.

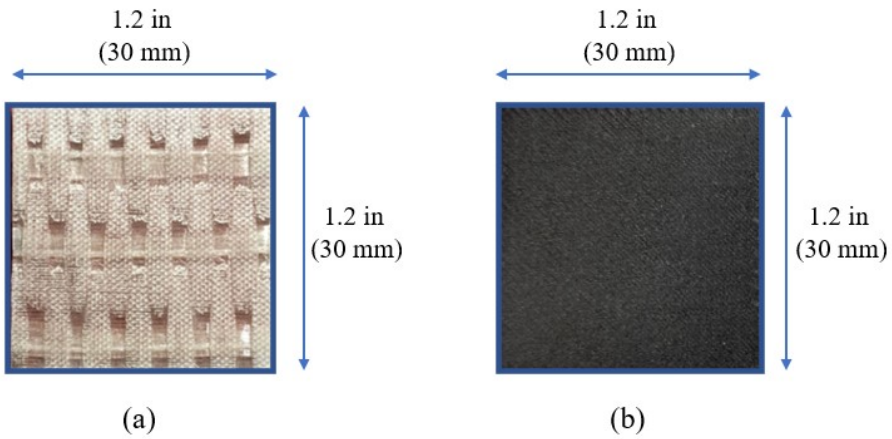

Figure 16: (a) VAHT unidirectional GFRP and (b) 3D Printed unidirectional GFRP

For the VAHT GFRP, TYFO® S Saturant Epoxy was used and TYFO® SHE -51A glass fiber. According to FYFE specifications, the densities of the fiber, component A, component B, and Mixed were listed as 2.55 g/cm^3, 1.16 g/cm^3, 0.95 g/cm^3, 1.11 g/cm^3, respectively.

Similarly, the 3D printed GFRP densities can be found in the specification sheets from Markforged® and are listed as follows: the continuous fiber and the onyx have densities of 1.5 g/cm^3 and 1.2 g/cm^3. The continuous fiber for the Markfogred printers contains both the thermoplastic nylon and the glass fibers. However, the specifications do not state the density of the glass fiber itself. Glass fibers have a medium density of 2.5 g/cm^3 and the medium density was chosen to calculate the volume fraction.

3.5 Tensile Testing Method

A tensile test was conducted to determine the tensile strength, the strain, and Young's Modulus of the material. Three VAHT GFRP specimens of 9.5 in by 1.0 in (242 mm by 25.4 mm) were tabbed with 1.5 in by 1 in (38.1mm by 25.4mm) 45° bidirectional carbon fiber reinforced polymer,

(CFRP) as shown in Figure 16. Using the CFRP tabs increased the strength of the ends and reduced the risk of grip failure.

The coupons were then tested on an MTS 810 Frame, shown in Figure 16 with 55-kip capacity at a consistent rate of 1 mm/min in accordance with ASTM D3039 ('D3039/D3039M Standard Test Method for Tensile Properties of Polymer Matrix Composite Materials' 2017). Strain gauge extensometer with a gauge length of 1 inch (25.4 mm) was placed at the center of the specimens to measure the strain in the coupons as shown in Figure 16. The tensile strength was determined with equation (4)

$$\sigma_c = \left[\frac{P}{A}\right] \quad \textbf{(4)}$$

Where σ_c = stress of the specimen, g; A = cross-sectional area of the specimen, m^2; and P = the load applied, N.

The multidirectional 3D printed GFRP specimens tensile testing was conducted similarly in a previous study in the literature review. The data of the study conducted at the University of New Mexico was available, and with consent from the author's that data was used in this study instead of repeating the same experiment.

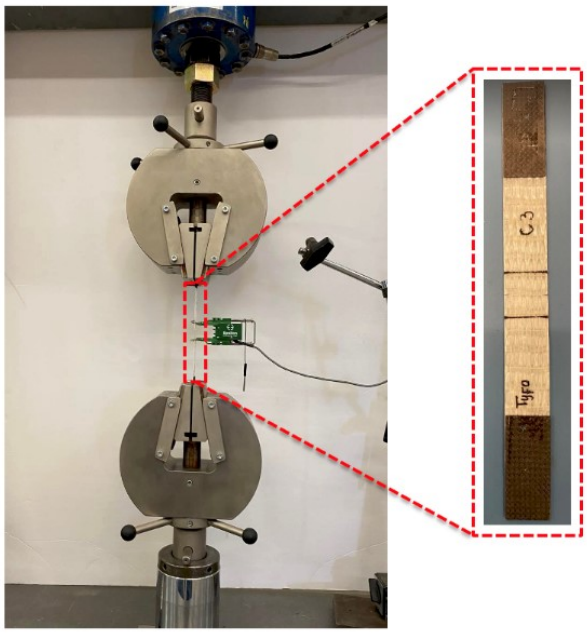

Figure 17: Tensile Testing Setup showing a VAHT unidirectional GFRP

3.6 Portland Cement Concrete

The Portland cement concrete contain type I/II Portland cement, water, fine aggregate, and superplasticizer. The materials were mixed in the proportions stated on Table 5 with a water to cement ratio of 0.3. MasterGlenium 7920 superplasticizer was used in this study, 738 cc per 100 kg of cementitious material which is with the recommended dosage of 130 cc to 780 cc per 100 kg for cementitious materials.

Table 5: PCC material

Material	Units	PCC
Superplasticizer		9.1
Water	$\frac{kg}{m^3}$	352.7
Portland Cement		1175.3
Aggregate		2350.6

The nominal maximum size of the fine aggregate used in this mix was 2.36 mm for both the Portland cement concrete and polymer concrete. The well-graded fine aggregate was selected in

regard to the specimen's small size. Figure 17 shows the size distribution of the fine aggregate for Portland cement concrete.

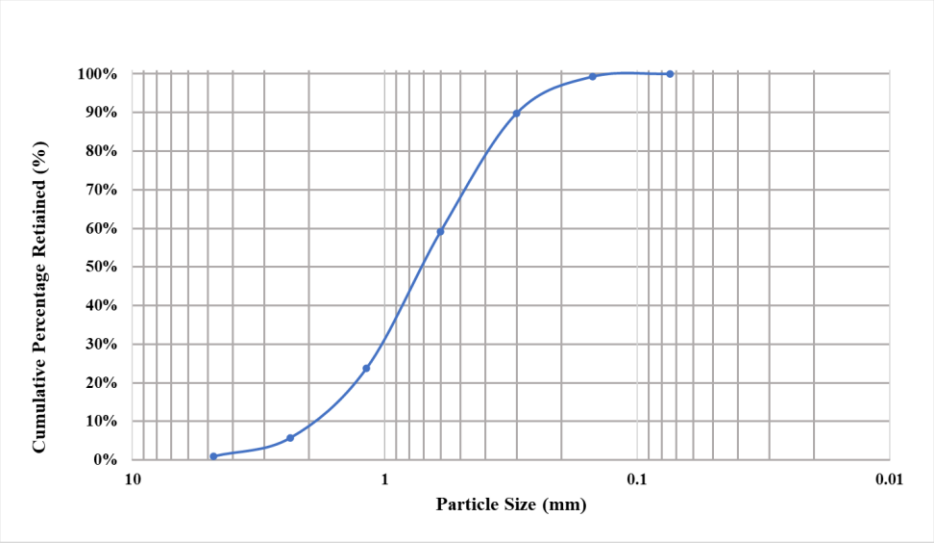

Figure 18: Fine aggregate for Portland cement concrete

The superplasticizer was added to the water and mixed well by hand prior to the casting process. Dry materials were placed in the mixer then mixed together to improve the material distribution. The water and superplasticizer mix were then added incrementally and the mixing continued for 3-5 minutes.

Figure 19: Portland cement concrete mixing process

The concrete was casted following the ASTM C192 ('C192/C192M Standard Practice for Making and Curing Concrete Test Specimens in the Laboratory' 2018) procedure and the specimens were placed in a climate-controlled room at 22 °C to cure. After 24 hours, the specimens were demolded and submerged in water continuing to cure for the following 14 days.

3.7 Polymer Concrete

The primary components of the polymer concrete (PolC) used in this design mix were T-17 Polymer Concrete Liquid Component and T-17 Polymer Concrete Powder Component (Transpo Industries). The mix design ratio of T-17 Liquid T-17 Powder component in this study is 1:8, respectively shown in Table 6 (Murcia et al. 2022). The specimens for this study are relatively small; hence, only fine aggregate with nominal maximum size of 2.36 mm was used for the concrete mix.

Figure 20: Polymer concrete mixing process

The composite was mixed for 3 minutes using a mechanical drill with mixing paddle and a bucket until a homogenous mixture was obtained shown in Figure 19. Since polymer concrete is rapid setting material, the concrete specimens were cast within 3-5 minutes to avoid material hardening.

The cast beams were cured for 24 hours before demolding them and for 7-days in room conditions prior to testing.

Table 6 : Polymer concrete (PolC) mix design (Murcia et al. 2022)

Material	**Units**	**PC**
Aggregate	$\frac{kg}{m^3}$	2002
Polymer Resin		251

3.8 Compressive Strength Test method

Determining the compressive strength of concrete shows the quality of the material and its strength to withstand compressive forces. In this study, cylinders of 4 in by 8 in (101.6 mm by 203.2 mm) were used to conduct the compressive strength of PCC following ASTM C39-17b ("C39/C39M Standard Test Method for Compressive Strength of Cylindrical Concrete Specimens" 2018) and PolC following ASTM C579 ("C579 Standard Test Methods for Compressive Strength of Chemical-Resistant Mortars, Grouts, Monolithic Surfacings, and Polymer Concretes" 2018). The cylinders are tested using Forney L.P. Standard Frame (F) compression testing machine with a capacity of 1500 kN, Figure 20.

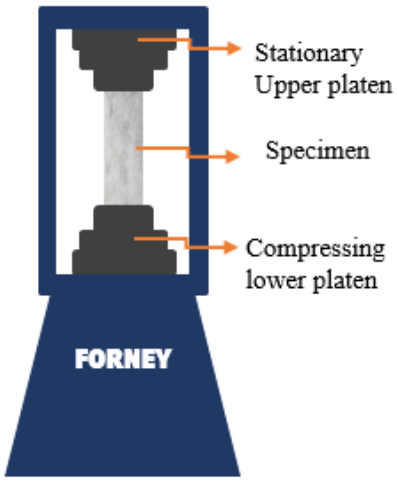

Figure 21: Compression Testing Machine Schematic

After 14 days of water curing, the PCC specimens were tested at a loading ramp rate of 35 psi/sec (0.24 MPa/sec) following ASTM C39-17b ("C39/C39M Standard Test Method for Compressive Strength of Cylindrical Concrete Specimens" 2018) and 100 psi/sec (0.7 MPa/sec) for PolC specimens after 7 days of curing in agreement with ASTM C579 ("C579 Standard Test Methods for Compressive Strength of Chemical-Resistant Mortars, Grouts, Monolithic Surfacings, and Polymer Concretes" 2018). To ensure equal load distribution, silicone caps were used on the cylinders, and the peak load of each cylinder was recorded. The compressive strength equation below from the ASTM C39/C39M-20 ("C39/C39M Standard Test Method for Compressive Strength of Cylindrical Concrete Specimens" 2018) was utilized to calculate the maximum compressive strength ("C39/C39M Standard Test Method for Compressive Strength of Cylindrical Concrete Specimens" 2018).

$$\textit{Compression Strength} \quad f_c = \frac{4\,P_{max}}{\pi D^2} \qquad \textbf{(5)}$$

Where f_c is the compressive strength , P_{max} is the maximum load, and D is the average measured diameter of cylinders.

3.9 Modulus of Rupture Test Method

Modulus of rupture tests were performed on 12 in. by 3 in. by 3 in. (304.8 mm by 76.2 mm by 76.2 mm) beams using four-point bending test as shown in Figure 21.

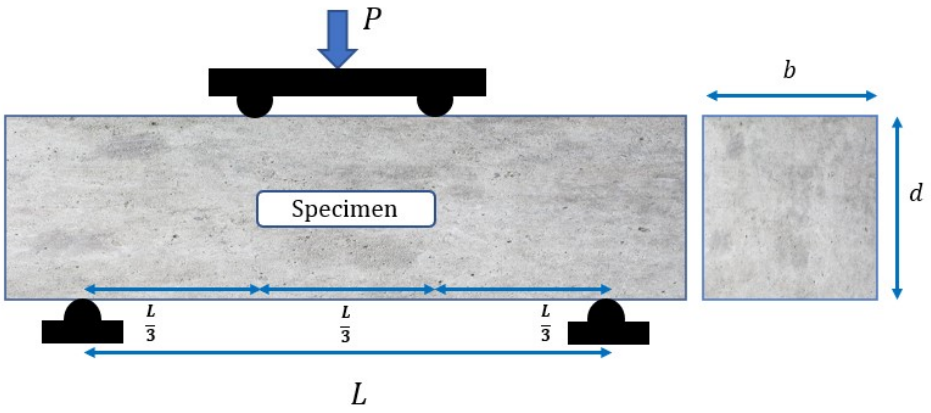

Figure 22: Schematic representation of four-point bending setup

Similar to the compression test, the Forney compression machine was used to test beams after 14 and 7 days of curing, respectively, in accordance with the ASTM C78 ("C78/C78M Standard Test Method for Flexural Strength of Concrete (Using Simple Beam with Third-Point Loading)" 2018) for PCC and ASTM C580 ("C580 Standard Test Method for Flexural Strength and Modulus of Elasticity of Chemical-Resistant Mortars, Grouts, Monolithic Surfacings, and Polymer Concretes" 2018) for PolC. The specimen is loaded at ramp rate of 2.083 psi/sec for PCC and 3 psi/sec (0.0207 MPa/sec) for PolC. For failures within the middle third of the span length, the modulus of rupture is computed using equation 6 ("C78/C78M Standard Test Method for Flexural Strength of Concrete (Using Simple Beam with Third-Point Loading)" 2018).

$$\textit{Modulus of Rupture,} \quad MOR = \frac{PL}{bh^2} \qquad \textbf{(6)}$$

Where MO*R* is the modulus of rupture, *P* is the maximum load, *L* is the span length, *b* is width, and *h* is depth of the beams.

3.10 Flexural Strength Test Method

In this study, there was a size limitation because the 3D printer used could print reinforcements with maximum length of 12.6 in (320 mm), therefore, appropriate molds was designed and

fabricated. The dimensions of the beams were determined using ACI 318-19 to confirm normal beams requirements were met. In chapter 9 section 9.1.1, the ACI 318-19 defines deep beam where the clear span should not exceed four times of the overall depth of the beam as shown in Figure 22.

9.9—Deep beams

9.9.1 *General*

9.9.1.1 Deep beams are members that are loaded on one face and supported on the opposite face such that strut-like compression elements can develop between the loads and supports and that satisfy (a) or (b):

(a) Clear span does not exceed four times the overall member depth ***h***

(b) Concentrated loads exist within a distance **2*h*** from the face of the support

Figure 23: ACI 318-19 deep beam requirements (Committee 2019)

To ensure the beams dimensions were out to the deep beam range, the clear span was calculated as four time larger than the height. The final design had dimensions of 12 in by 2.0 in by 2.0 in (304.8 mm by 50.8 mm by 50.8 mm) shown in Figure 23.

Figure 24: (a) The length (b) cross-section dimensions

Due to the small size of the beams, the reinforcement location and placement is very essential, therefore, the molds were designed to have very precise grooves or cutout. There were multiple designs considered and tested, however, the most efficient and precise design was using 3D

printers to print the sections the reinforcement would be placed and plywood for the other sections of the mold shown in Figure 24.

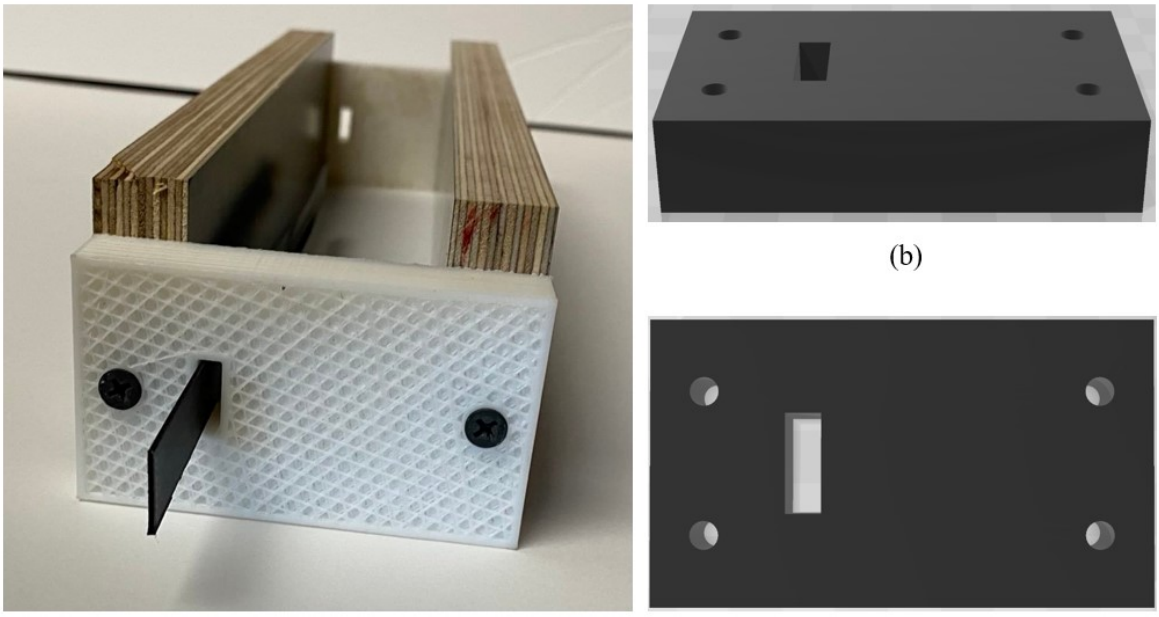

Figure 25: 3D printed mold sections

The molds with the reinforcement are shown, unidirectional VAHT GFRP in Figure 25 (a) and (b), and multidirectional 3D printed GFRP in Figure 25 (c) and (d). These beams were cast sideways to eliminate the possibility of the reinforcement bending during casting. In application, the reinforcement would be bigger and stiffer which would eliminate this limitation.

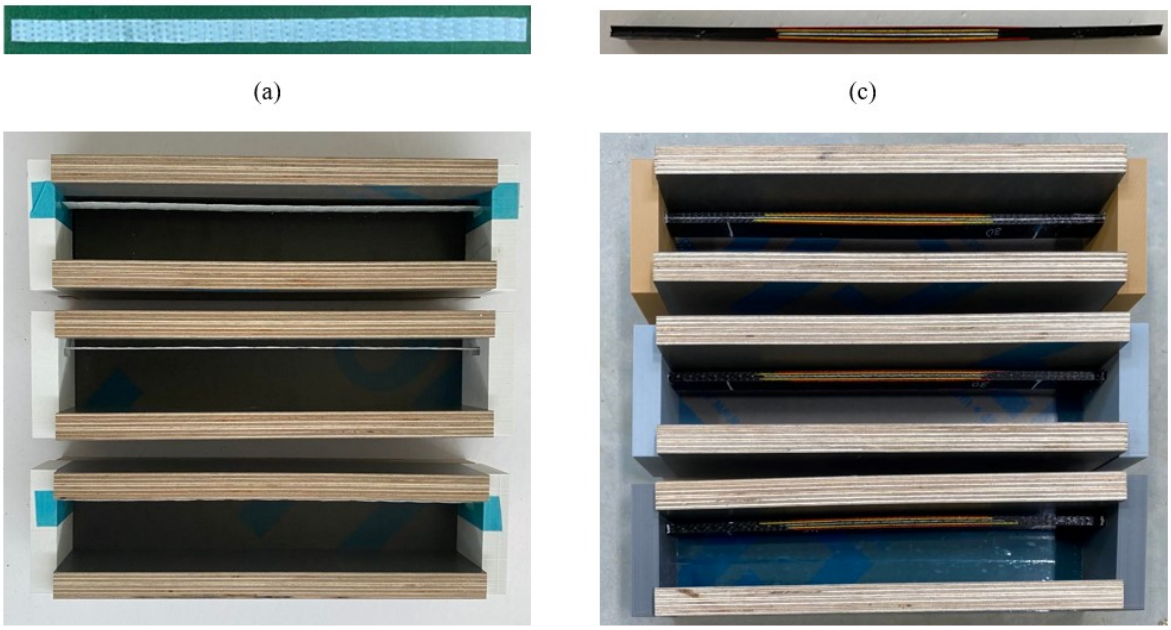

Figure 26: Molds with the reinforcements

The flexural test was conducted using the ASTM C580-18 ("C580 Standard Test Method for Flexural Strength and Modulus of Elasticity of Chemical-Resistant Mortars, Grouts, Monolithic Surfacings, and Polymer Concretes" 2018) guidelines for three-point bending test for both the PolC and PCC. According to previous studies, the PolC reaches about 75% of the ultimate strength within the first 24 hours of curing and almost full strength within seven days (Murcia et al. 2022). Therefore, all the testing was conducted after seven days of curing for PolC and 14 days for PCC. As result of the required beam size, a new testing setup was designed as the schematic in Figure 26 and Figure 27 displays.

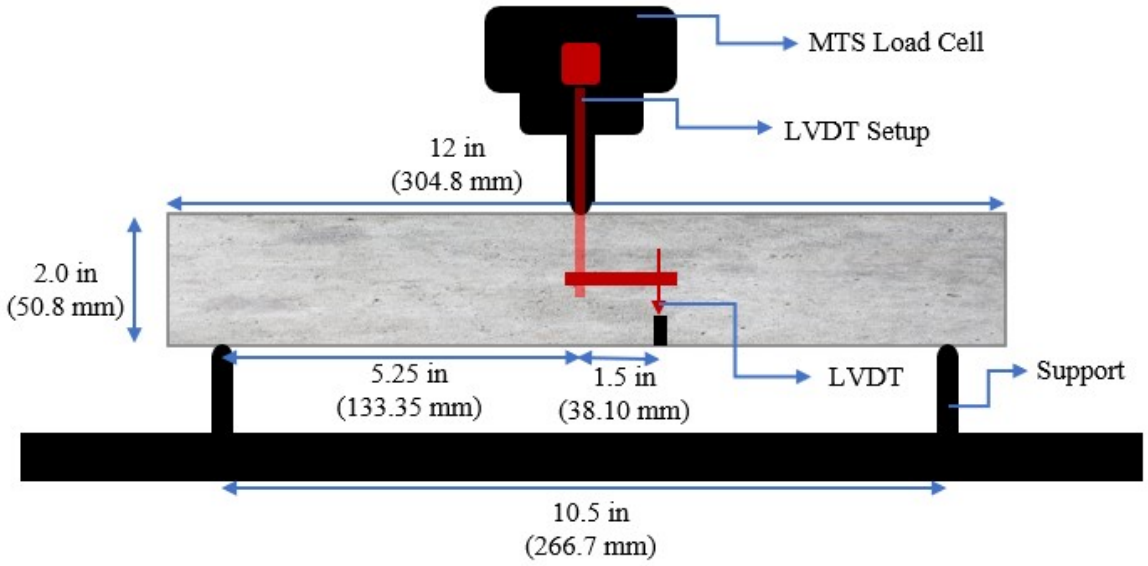

Figure 27: The schematic flexural three-point bending testing setup

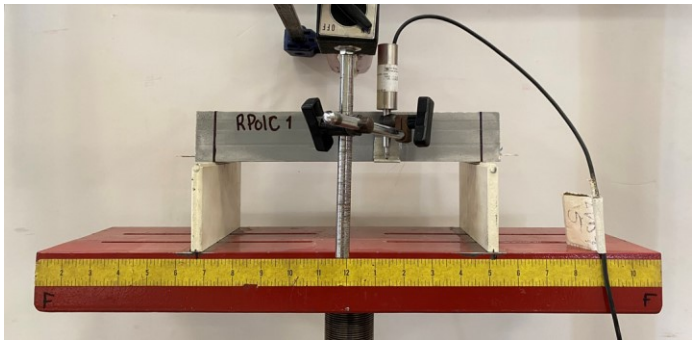

Figure 28:The flexural three-point bending testing

The setup had a clear span from support to support of 10.5 in (266.7 mm), and 5.25 in (133.35 mm) from center to support. An external linear variable differential transducer (LVDT) was incorporated and placed 1.5 in (38.10 mm) away from the center of the beam. The purpose of the LVDT offset was to ensure the possible rapid failures did not damage the device.

All the beams were tested in accordance with ASTM C580-18 ("C580 Standard Test Method for Flexural Strength and Modulus of Elasticity of Chemical-Resistant Mortars, Grouts, Monolithic Surfacings, and Polymer Concretes" 2018). The beams were loaded at a ramp rate of 1 mm/min.

An MTS 810 Frame with 55-kip capacity was utilized for this test and the machine displacement, loading from the load cell, and the time was recorded. An LVDT was integrated with the MTS to collect actual beam deflection as shown in Figure 27.

The collected data was studied and analyzed further to understand the flexural behavior of non-reinforced and reinforced specimens. The load versus displacement data was then used to analyze the flexural behavior of the beams, maximum moment, maximum deflection, maximum toughness, moment curvature, and elasticity index were calculated and analyzed for all types of reinforcements and concrete combinations.

3.11 Microscopic Analysis Method

To understand the failure of different reinforcements in the concretes and to obtain better observations, microscopic images were captured after failure of the beams subjected to flexural testing. Keyence VHX-7000 ultramicroscope, shown in Figure 28, at the Samuel Roberts Noble Microscopy Lab (SRMNL) in The University of Oklahoma was used to conduct the microscopic analysis. The microscope is fully automated and can capture high-resolution images.

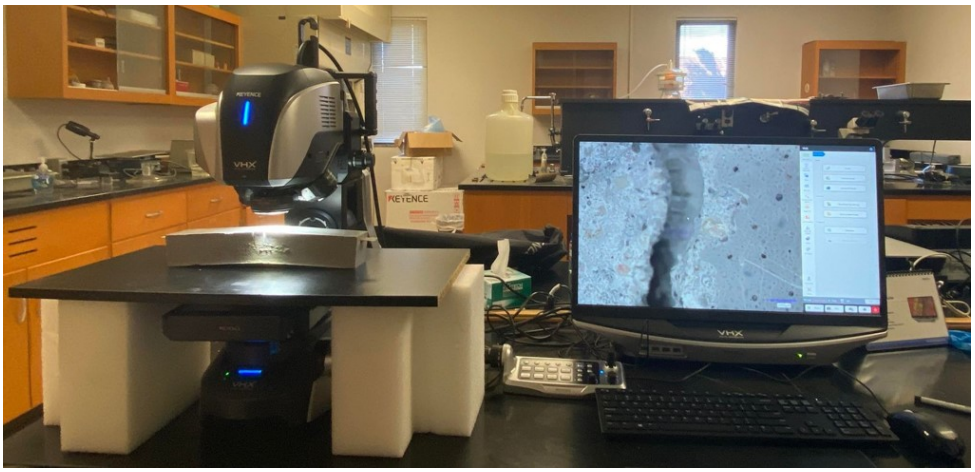

Figure 29: Keyence VHX-7000 ultramicroscope

3.12 Predicted Beam Capacity

The theoretical predicted moment capacity of all types of the beams is presented in this section. All the beams were tested using the three-point bending test, and ACI 440.R-14 was used to determine the moment capacity of the beams. More detailed calculations are presented in Appendix A.

3.12.1 Equilibrium Condition

A loaded simply supported beams experiences compression where the load is applied and tension on the opposite side. The equilibrium condition assumes the compression forces are equal to the tension forces. Since concrete tensile strength is much lower than its compressive strength, the tensile forces consider in the equation come from the reinforcement which is the GFRP in this study.

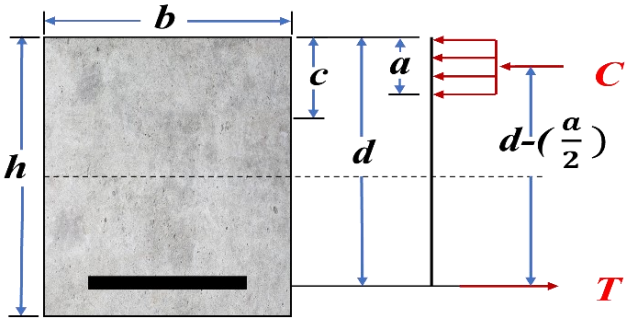

$$C := T \tag{7}$$

C = Compression force

T = tension force

$$C := \alpha_1 \cdot f'_c \cdot \beta_1 \cdot c \cdot b \tag{8}$$

$$T := A_f \cdot f_f \tag{9}$$

$$\rho_f := \frac{A_f}{b \cdot d} \quad \textbf{(10)}$$

Where:

ρ_f = fiber reinforced polymer reinforcement ratio

A_f = Area of FRP reinforcement (mm^2)

f_f = stress in FRP reinforcement in tension (MPa)

α_1= ratio of average stress of equivalent rectangular (Whitney stress block)

d = depth (mm)

b = width (mm)

c= depth of compression zone (mm)

$$\beta_1 := \max\left((0.85) - 0.05 \cdot \left(\frac{f'_c - 28}{7}\right), 0.65\right) \quad \textbf{(11)}$$

Where:

f'_c= specified compressive strength of concrete

According to ACI 440.1R-15:2.1, "β_1 = factor taken as 0.85 for concrete strength fc' up to and including 4000 psi (28 MPa). For strength above 4000 psi (28 MPa), this factor is reduced continuously at a rate of 0.05 per each 1000 psi (7 MPa) of strength in excess of 4000 psi (28 MPa), but is not taken less than 0.65"

For a balanced condition, the reinforcement ratio can be determined using equation 12. The reinforcement ratio at a balanced condition was then compared with the reinforcement ratio based on the geometer of the section as shown in equation 11. If $\rho_{.f.bal}$ is less than $\rho_{.f,}$ the beam fails in tension, and if greater fails in compression.

$$\rho_{f.bal} := \alpha_1 \cdot \beta_1 \cdot \frac{f'_c}{f_{fu}} \cdot \left(\frac{\varepsilon_{cu}}{\varepsilon_{cu} + \varepsilon_{fu}} \right) \quad \textbf{(12)}$$

Where:

f_{fu} = ultimate tensile strength of GFRP

ε_{fu} = ultimate strain in GFRP in tension

ε_{cu} = ultimate strain in concrete in compression

3.12.2 FRP Reinforcement Stress

$$f_f := \frac{\alpha_1 \cdot f'_c \cdot \beta_1 \cdot b}{A_f} \cdot c \quad \textbf{(13)}$$

Where:

f_f = stress in FRP reinforcement in tension

$$a := \frac{A_f \cdot f_f}{0.85 \cdot f'_c \cdot b} \quad \textbf{(14)}$$

3.12.3 Nominal Moment Capacity

$$M_n := A_f \cdot f_f \cdot \left(d - \frac{a}{2} \right) \quad \textbf{(15)}$$

Chapter 4: Results and Discussions

4.1 Volume Fraction Results

A Maximum of three specimens with dimensions of 1.2 in by 1.2 in (30 mm by 30 mm) was used to determine the fiber volume fraction following ASTM D3171 guidance for each type. The average fiber volume fraction of the conventional VAHT unidirectional GFRP was 42.5% ± 0.4% with coefficient of variation of 0.4%. For the 3D printed unidirectional GFRP, the average fiber volume fraction was 24.3% ± 0.1% as shown in Table7. Figure 29 (a) and (b) shows the Conventional VAHT unidirectional GFRR and 3D Printed unidirectional GFRP after the matrix was burnt off with the furnace.

Table 7: The experimental fiber volume fraction results

Fiber Volume Fraction	1	2	3	Average	STDEV	COV
VAHT	42.5%	42.9%	42.1%	42.5%	0.40%	0.94%
3D Printed	24.3%	24.2%	24.3%	24.3%	0.06%	0.24%

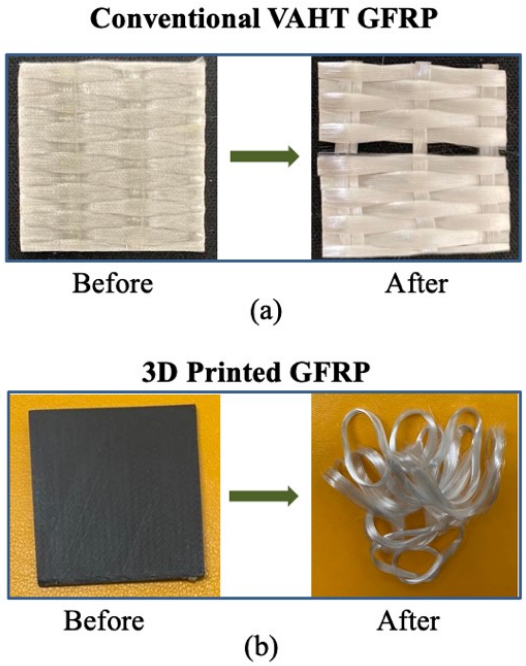

Figure 30: Before and after burning the matrix from the fibers

The 3D Printed unidirectional GFRP contained three different materials; Nylon, chopped fiber, and continuous fiber unlike the Conventional VAHT unidirectional GFRP which contained only two materials; epoxy and fiber. Therefore, the onyx volume fraction should be considered to determine the fiber volume fraction. A detailed calculation and process for determining the fiber volume fraction can be found in Appendix B.

4.2 Tensile Testing Results

4.2.1 VAHT Unidirectional GFRP Results

Three unidirectional VAHT coupons were tested to determine the tensile strength of the VAHT unidirectional GFRP. The tested specimens had broom failures as shown in Figure 31. During the test, the most outer parts of the coupon started to fail, and the rest of the fiber started brooming or broom like tension failure. The results of the tested specimens are shown in Figure 31 and Table 8.

Figure 31: Failed VAHT unidirectional GFRP

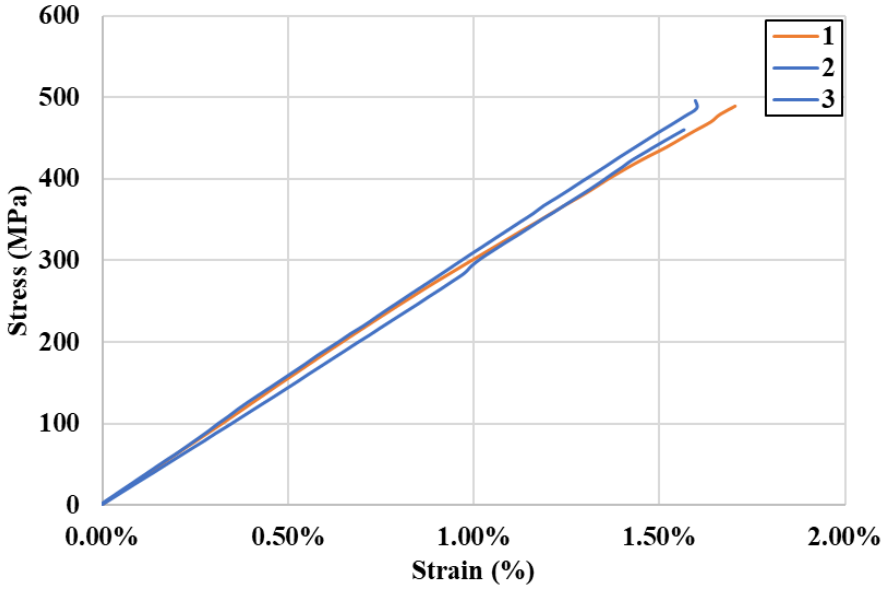

Figure 32: VAHT unidirectional GFRP Results

Table 8: Experimental result of the VAHT tensile test

Properties	Units	Specimens			Average	STDEV	COV
		1	2	3			
Strength	MPa	523.9	529.1	526.3	526.4	2.6	0.50%
Modulus	GPa	28.3	29.95	29.36	29.2	0.84	2.90%
Strain	%	1.81%	1.67%	1.93%	1.80%	0.13%	7.20%

The maximum load, stress, strain, and modulus calculated from the slope of the stress-strain curve are presented in Table 8. The mean of tensile strength was 526.3 MPa ± 2.6 MPa, and modulus, E, of 29.2 GPa ± 0.84 GPa.

4.2.2 3D Printed Unidirectional GFRP Results

The tensile test was repeated for the 3D printed unidirectional GFRP, and a failed specimen is shown in Figure 32, and results are shown in Figure 33. Similar broom like failure mode was observed for the 3D printed unidirectional GFRP as shown in Figure 32.

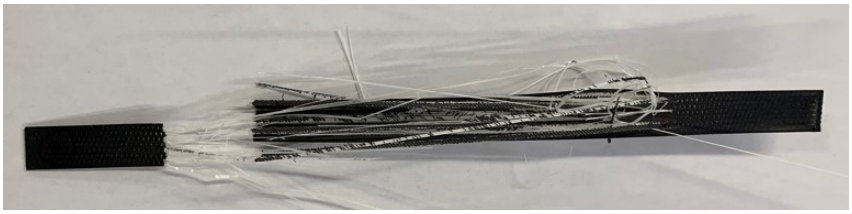

Figure 33: Failed 3D printed unidirectional GFRP specimen

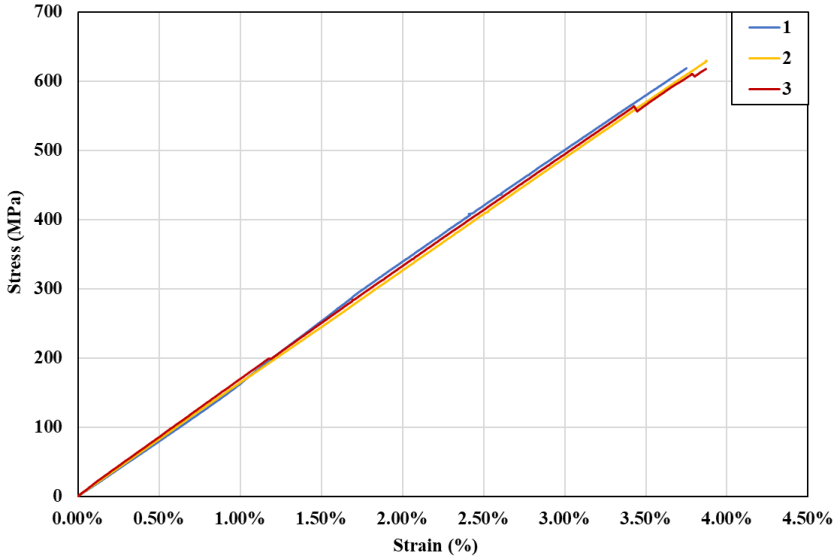

Figure 34: 3D printed unidirectional GFRP results

Table 9: Experimental result of the 3D printed tensile test

Properties	Units	Specimens			Average	STDEV	COV
		1	2	3			
Strength	MPa	625.00	630.00	617.00	624.00	6.56	1.05%
Modulus	GPa	16.67	16.39	16.75	16.60	0.19	1.14%
Strain	%	3.75%	3.86%	3.98%	3.86%	0.12%	2.98%

The stress, strain and modulus are presented in Table 9. The mean of tensile strength is 624.0MPa ± 6.56 MPa, and modulus, E, of 16.6 GPa ± 0.19 GPa. The 3D printed demonstrates higher stress and strain and lower modulus compared to the VAHT.

4.3 Compression Test Results

A total of 12 cylinders, 6 PCC and 6 PolC, were tested to determine the compressive strength of the two different types of concrete with respective to ASTM C39 and ASTM C579 ("C579 Standard Test Methods for Compressive Strength of Chemical-Resistant Mortars, Grouts, Monolithic Surfacings, and Polymer Concretes" 2018). The Figure below shows the testing process, and the different modes of failures.

(a) (b) (c) (d)

Figure 35:Compression Test (a) PCC Loaded Specimen (b) PCC Failed Specimen (c) PolC Loaded Specimen (d) PolC Failed Specimen

The average compressive strength of PCC and PolC were 67.4 and 59.9 MPa, respectively. All tests had a coefficient of variation of two percent which highlights the consistency of the results for both PCC and PolC, Table 10 and Table 11.

A previous study tested five cylinders of 4 in by 8 in (50.8 mm by 101.6 mm) for PCC and PolC compressive strength and concluded the mean compressive strength for PCC and PolC was 68.9 ± 5.1 MPa and 53.9 ± 5.8 MPa (Murcia et al. 2022). Therefore, the compressive strength determined in preliminary PolC compressive strength testing falls within the range of the literature values.

Table 10: Compression Test Results PCC

Properties	Units	PCC Specimens					Mean	STDEV	COV
		1	2	3	4	5			
Peak Load	**kN**	544.4	537.8	548.9	561.3	540.0	546.5	9.3	2%
Max. Stress	**MPa**	67.2	66.3	67.7	69.2	66.6	67.4	1.1	2%

Table 11: Compression Test Results PolC

Properties	Units	PolC Specimens					Mean	STDEV	COV
		1	2	3	4	5			
Peak Load	**kN**	495.6	484.8	488.2	484.7	474.4	485.5	7.6	2%
Max. Stress	**MPa**	61.1	59.8	60.2	59.8	58.5	59.9	0.9	2%

4.4 Modulus of Rupture Results

The modulus of rupture was determined by testing five beams for each concrete using the four-point bending test. Similar to the compression test, Forney machine was used for the MOR test, and following figure shows the test setup, and failed specimens.

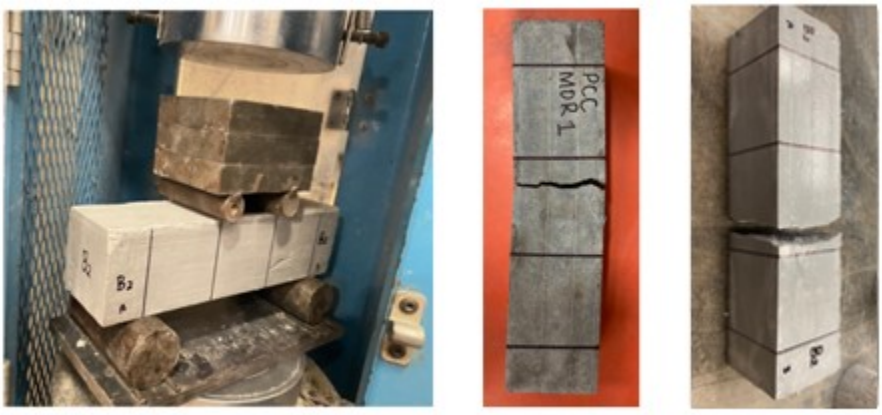

Figure 36:(a) MOR Test (b) PCC failed specimen (c) PolC failed specimen

The average MOR stresses for PCC and PolC were 7.8 MPa and 23.7 MPa as listed in Table 12 and Table 13. The coefficient of variation for PCC was 1% and was 3% for PolC which demonstrated the consistency of the testing. Three beams each were tested and reported in Table 12 and Table 13.

Table 12: Modulus of Rupture Test Results PCC

Properties	Units	PCC Specimens			Mean	STDEV	COV
		1	2	3			
Peak Load	**kN**	10.7	11.0	10.9	10.9	0.15	1%
Max. Stress	**MPa**	7.69	7.9	7.82	7.8	0.11	1%

Table 13: Modulus of Rupture Test Results PolC

Properties	Units	PolC Specimens			Mean	STDEV	COV
		1	2	3			
Peak Load	**kN**	33.6	33.6	34.7	33.9	0.62	2%
Max. Stress	**MPa**	24.48	23.11	23.4	23.7	0.72	3%

Based on the compressive strength and Modulus of Rupture results, two concrete mixes with similar strengths were achieved. The tensile strength of polymer concrete measured in using modulus of rupture is about 3 times greater than Portland cement concrete which indicates a mix design similar to indicated in literature (Murcia et al. 2022).

4.5 Flexural Strength

4.5.1 Portland Cement Concrete (PCC)

A total of 24 PCC beams were casted and tested. The test was conducted using three point bending test to determine the flexural capacity and response of the beams. These beams were broken into four different groups of three: 1) non-reinforced control beams, 2) VAHT unidirectional GFRP reinforced beams, 3) 3D printed unidirectional GFRP reinforced beams, and 4) 3D printed

multidirectional GFRP reinforced beams. This section presents the results of the experimental tests conducted.

4.5.1.1 PCC Non-Reinforced Beams

Three non-reinforced control PCC beams were tested and reported. The beams were loaded to their maximum capacity, and beams suddenly failed at peak load. A single crack was formed near the midspan of the beam corresponding to the point load. The average maximum load for all the beams was 2.47kN ± 0.14kN which is corresponding to the load that the crack appeared. The midspan crack in the beams is shown in Figure 36.

(a)

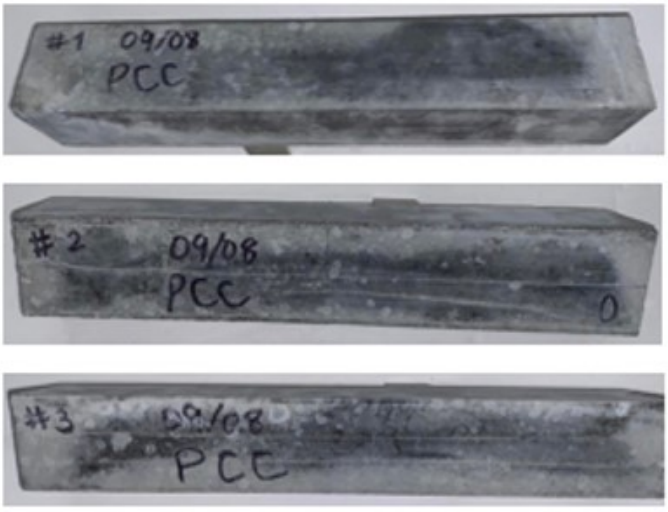

(b)

Figure 37: (a) Zoomed crack at bottom view (b) Failure modes of the Non-Reinforced PCC Beams

Table 14: Experimental results for Non-reinforced PCC

Properties	Specimens				Average	STDEV	COV
	Units	1	2	3			
Peak Load	kN	2.4	2.6	2.4	2.5	0.14	6%
Max. Moment	kN • m	0.2	0.2	0.2	0.2	0.01	6%
Max. Deflection	mm	0.2	0.4	0.3	0.3	0.08	27%

The maximum loads, moments, and deflection of non-reinforced PCC control beams are presented in Table 12. The average load, moment, and deflection are 2.5 kN ± 0.14 kN, 0.2 kN • m ± 0.01 kN • m, and 0.5 mm ± 0.08 mm respectively. The coefficient of variation of load and moment have 6% variation which shows consistency.

The test durations for the non-reinforced control PCC beams were between 30 seconds to 60 seconds. To measure the correct deflection of the beams, and external LVDT was used. Therefore, there was a limited time for data collection which increased the coefficient of variation up to 27%. The deflection variation can be observed in load deflection curve in Figure 37.

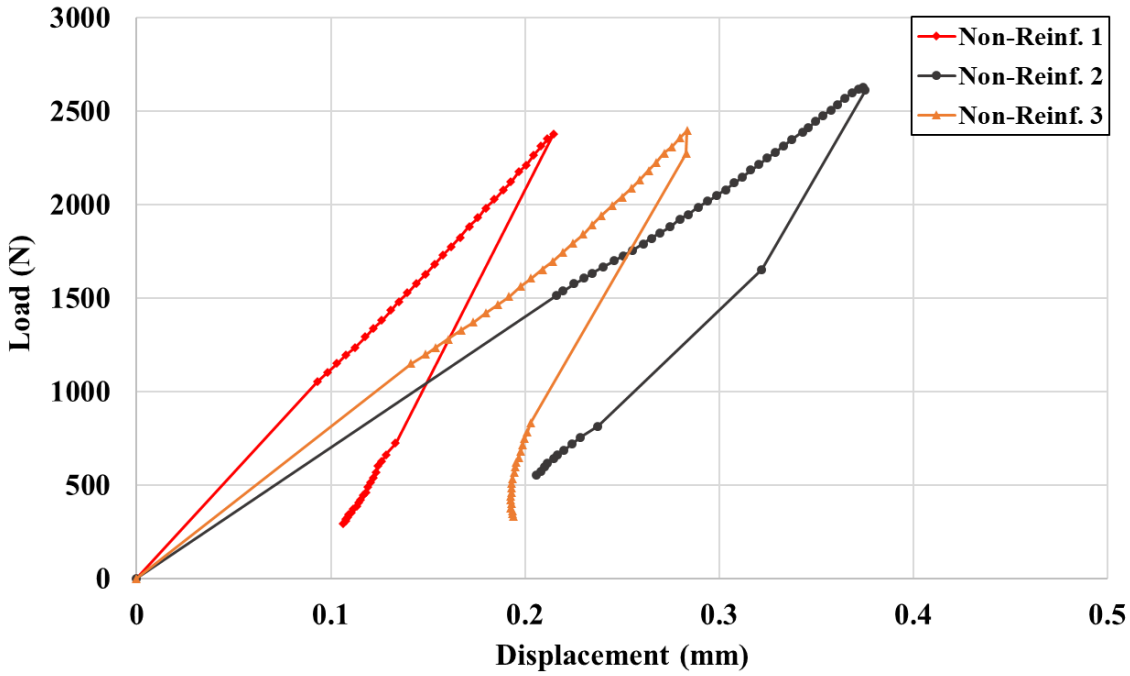

Figure 38: Load deflection relationship of non-reinforced control PCC

4.5.1.2 PCC Beams Reinforced with VAHT Unidirectional GFRP

Three PCC beams reinforced with VAHT unidirectional GFRP were tested and reported. The first cracks of the beams formed similar distance away from midspan on both sides and propagated towards the point of loading. These cracks were observed when the load reached 2.4 kN to 2.75 kN and were followed by a load drop. The failure modes of the VAHT unidirectional GFRP reinforced PCC beams are shown in Figure 38.

(a)

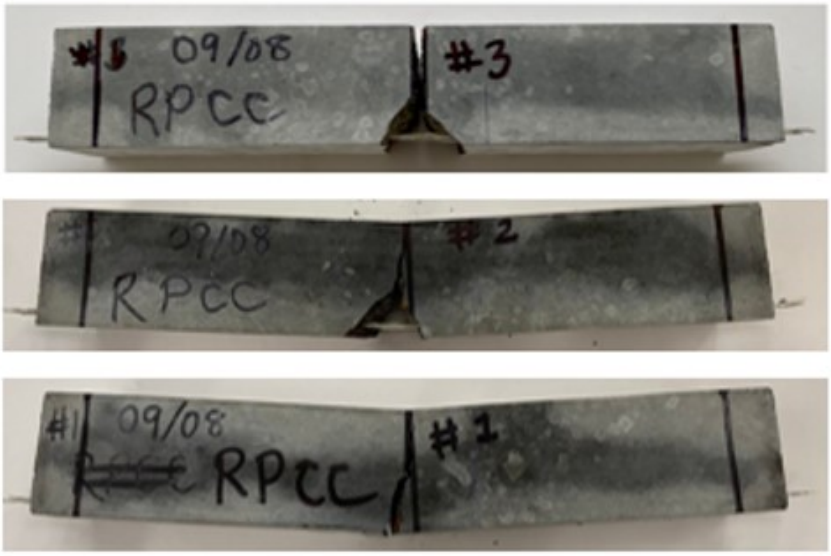

(b)

Figure 39: (a) Zoomed crack at bottom view (b) Failure modes of the VAHT unidirectional GFRP reinforced PCC beams

Table 15: Experimental results for VAHT unidirectional GFRP reinforced PCC

Properties	**Specimens**				**Average**	**STDEV**	**COV**
	Units	**1**	**2**	**3**			
Peak Load	kN	4.7	4.4	4.4	4.5	0.20	4%
Max. Moment	kN • m	0.3	0.3	0.3	0.3	0.01	4%
Max. Deflection	mm	2.7	3.0	2.9	2.9	0.13	4%

In Table 13, the maximum loads, moments, and deflection of VAHT unidirectional GFRP reinforced PCC beams are presented. The average load, moment, and deflection are 4.5 kN ± 0.20

kN, 0.3 kN • m ± 0.l0 kN • m, and 2.9 mm ± 0.13 mm respectively. The data collected had very high consistency with 4% of coefficient of variation for all three parameters.

The load response of the PCC beams reinforced with VAHT unidirectional GFRP is presented in Figure 39. The peak flexural response for the VAHT unidirectional GFRP reinforced PCC beams was 4.5 kN.

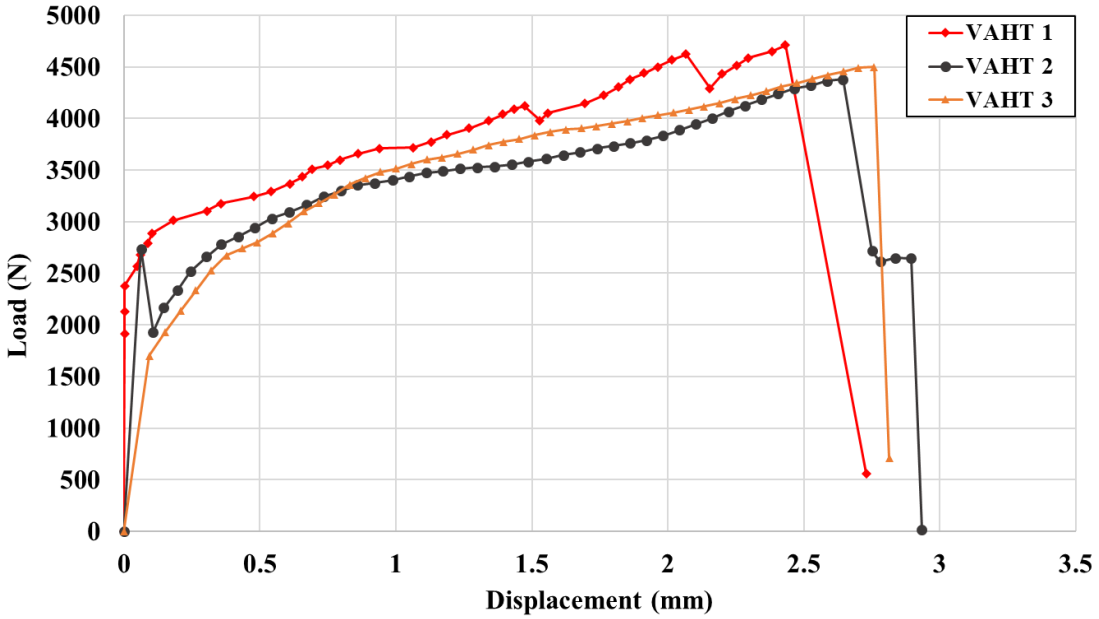

Figure 40: The flexural response of PCC beams reinforced with VAHT unidirectional GFRP

4.5.1.3 PCC Beams Reinforced with 3D Printed Unidirectional GFRP

Three PCC beams reinforced with 3D printed unidirectional GFRP were tested to determine the flexural capacity and response of the beams. Similar to the PCC beams reinforced with VAHT unidirectional GFRP, cracks were observed at midspan corresponding to a loading of 2.5 kN to 3.0 kN where the concrete failed, and the load dropped by 45%. The load was then carried by the reinforcement until the reinforcement debonded of a corresponding load of 2.5 kN to 3.5 kN. The

failure modes of the PCC beams reinforced with 3D printed unidirectional GFRP are shown in Figure 40.

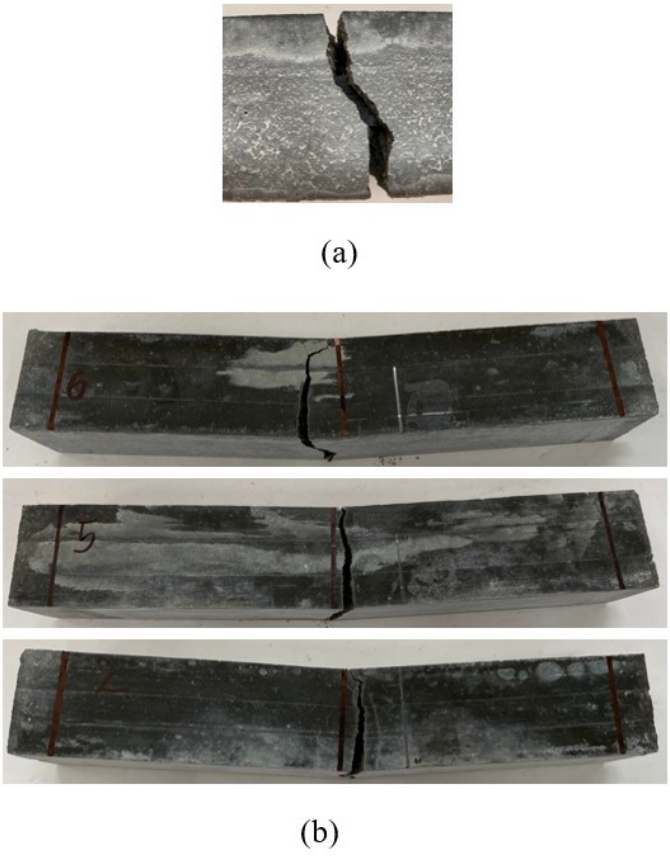

(a)

(b)

Figure 41: (a) Zoomed crack at bottom view (b) Failure modes of the 3D printed unidirectional GFRP reinforced PCC beams

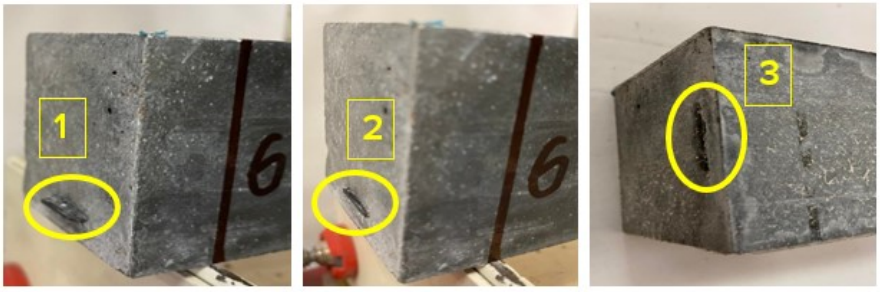

Figure 42: Debonding phases

During the test, a series of photos were taken to show the stages of the reinforcement debonding as shown in Figure 4. At the end of the test, the reinforcement overhanging section fully slipped in the beam for all three tested beams.

Table 16:Experimental results for 3D printed unidirectional GFRP reinforced PCC

Properties	**Specimens**				**Average**	**STDEV**	**COV**
	Units	**1**	**2**	**3**			
Peak Load	kN	3.0	2.7	3.0	2.9	0.19	7%
Max. Moment	kN • m	0.2	0.2	0.2	0.2	0.01	7%
Max. Deflection	mm	4.2	4.3	3.9	4.1	0.22	5%

The experimental results of the load, moment, and deflection parameters of PCC beams reinforced with 3D printed unidirectional GFRP are presented in Table 14. The average load, moment, and deflection are 2.9 kN ± 0.19 kN, 0.2 kN • m ± 0.01 kN • m, and 4.1 mm ± 0.22 mm respectively. The flexural response of the PCC beams reinforced with 3D printed unidirectional GFRP is presented in Figure 42.

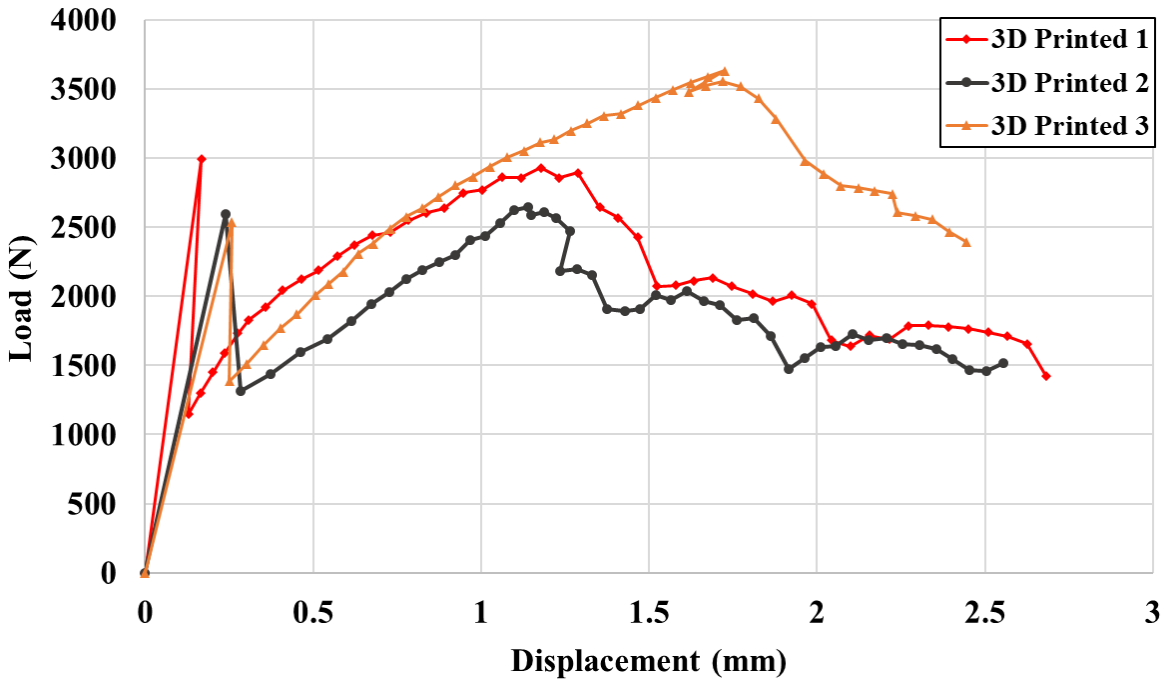

Figure 43: The flexural response of PCC beams reinforced with 3D printed unidirectional GFRP

4.5.1.4 PCC Beams Reinforced with 3D Printed Ductile GFRP

Three PCC beams reinforced with 3D printed multidirectional GFRP were tested. The failure modes of the VAHT unidirectional GFRP reinforced PCC beams are shown in Figure 43.

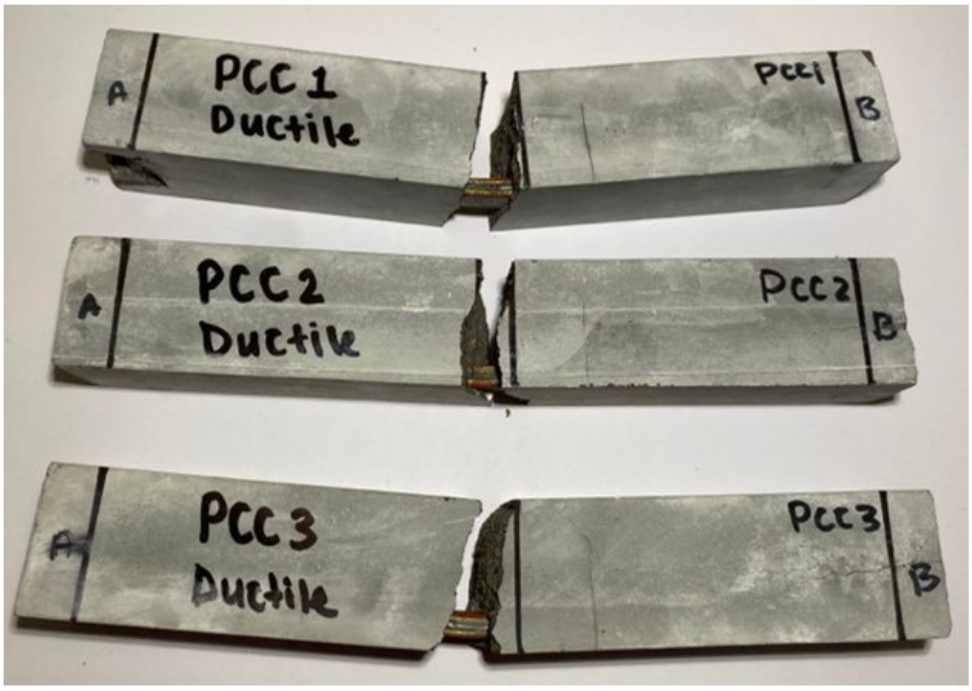

(a)

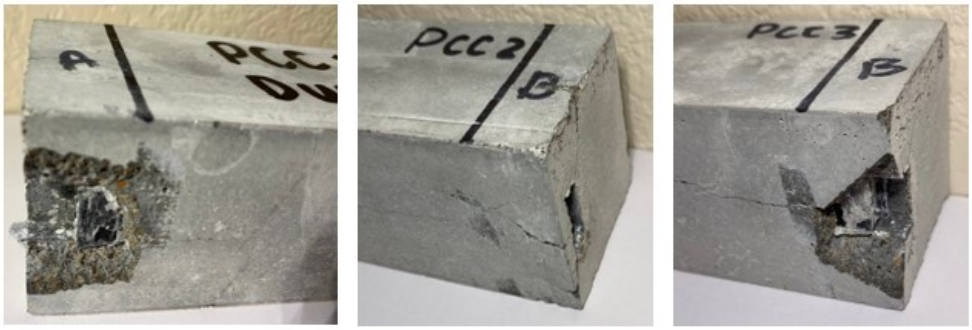

(b)

Figure 44: (a) Failure modes of the 3D printed multidirectional GFRP reinforced PCC beams (b) Debonded reinforcement

The first cracks in the beams formed at midspan at 2.6 kN to 3.0 kN with a sudden load drop as show in Figure 43. Following the load drop, the beams continued to load showing linear elastic behavior until the peak load was reached. The linearity was very different from the behavior that was observed in the VAHT unidirectional GFRP and 3D printed unidirectional GFRP.

After the beam reached maximum loading, the reinforcement started debonding, and the specimens failed on bond failure.

Table 17: Experimental results for 3D printed multidirectional GFRP reinforced PCC

Properties	Specimens				Average	STDEV	COV
	Units	1	2	3			
Peak Load	kN	4.0	3.5	3.8	3.8	0.26	7%
Max. Moment	kN.m	0.3	0.2	0.3	0.3	0.02	7%
Max. Deflection	mm	8.5	6.3	7.0	7.3	1.09	15%

The experimental results of the load, moment, and deflection parameters of PCC beams reinforced with 3D printed multidirectional GFRP are presented in Table 15. The average load, moment, and deflection are 3.8 kN ± 0.26 kN, 0.3 kN • m ± 0.02 kN • m, and 7.3 mm ± 1.09 mm respectively. The specimens experienced debonding therefore the deflection of the specimen cannot be determined with the present data. The flexural response of the PCC beams reinforced with 3D printed multidirectional GFRP is presented in Figure 44.

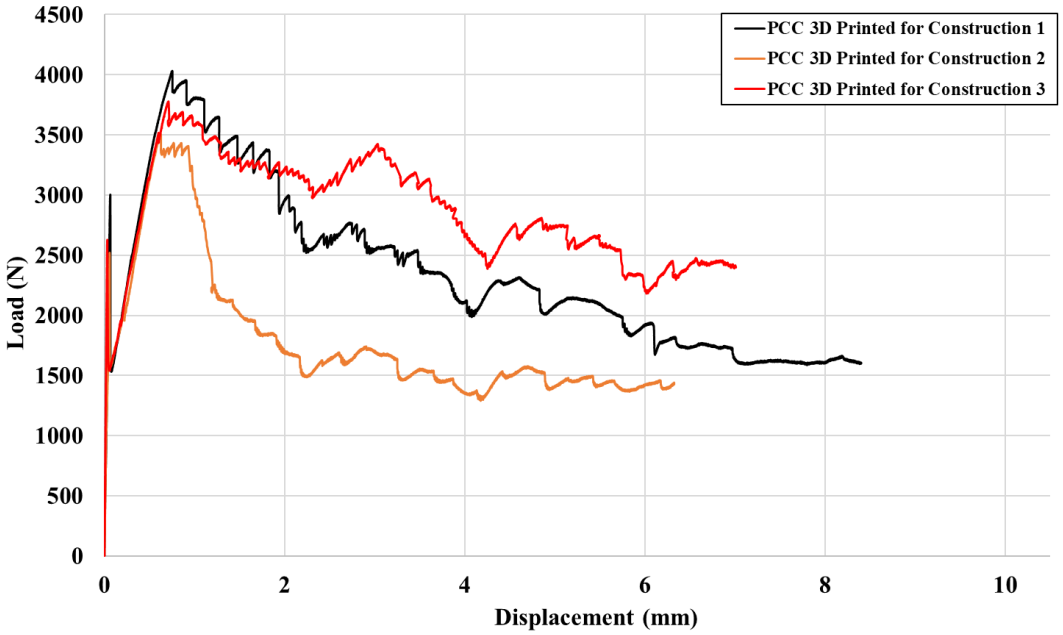

Figure 45: The flexural response of PCC beams reinforced with 3D printed multidirectional GFRP

4.5.2 Polymer Concrete (PolC)

4.5.2.1 Non-Reinforced PolC

To create a baseline for the flexural capacity of PolC, three non-reinforced control beams were tested. Unlike the PCC, multiple small cracks, Figure 45 (a), formed at midspan of the beam followed by a larger crack, Figure 45 (b), near midspan.

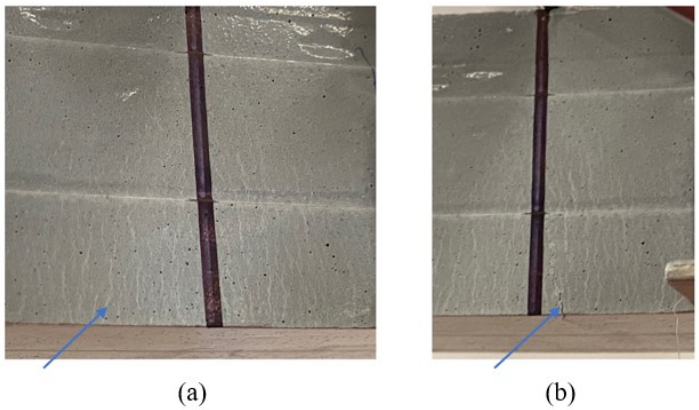

Figure 46: (a) Multiple small cracks (b) larger cracks

The smaller cracks appeared at a larger range, 1.5kN to 2.5kN, of the load for specimens where the first larger cracks were observed at 3.0 kN to 3.5 kN, however, there was no sudden failure or load drop observed as the flexural response in Figure 47 shows. The crack widened as the load increased until the beams ultimately failed. Figure 46 shows the failure mode of the beams.

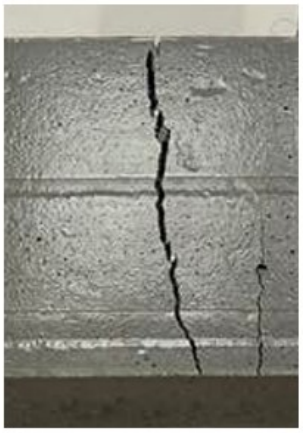

(a)

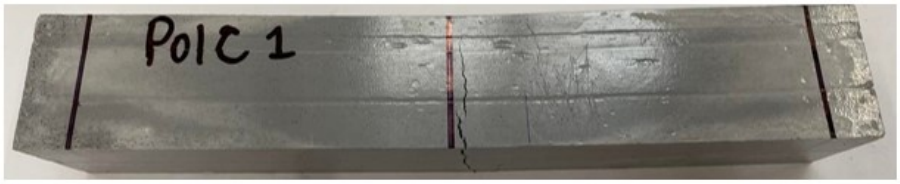

(b)

Figure 47: (a) Zoomed crack at bottom view (b) Failure modes of the Non-Reinforced PolC Beams

Table 18: Experimental results for Non-reinforced PolC

Properties	**Non-reinforced PolC**				**Average**	**STDEV**	**COV**
	Units	**1**	**2**	**3**			
Peak Load	kN	3.5	3.7	3.7	3.6	0.11	3%
Max. Moment	kN • m	0.2	0.2	0.2	0.2	0.01	3%
Max. Deflection	mm	1.9	2.3	1.8	2.0	0.24	12%

The experimental results of the load, moment, and deflection with the mean, standard deviation and coefficient of variation are presented in Table 16. The average maximum load these beams could carry was 3.6 kN ± 0.24 kN. After the ultimate load was reached, the cracks became wider, and the load started to drop. The beams experienced large deformations as the load decrease until

the load practically reached zero. The flexural response of the non-reinforced control PolC beams is presented in Figure 47.

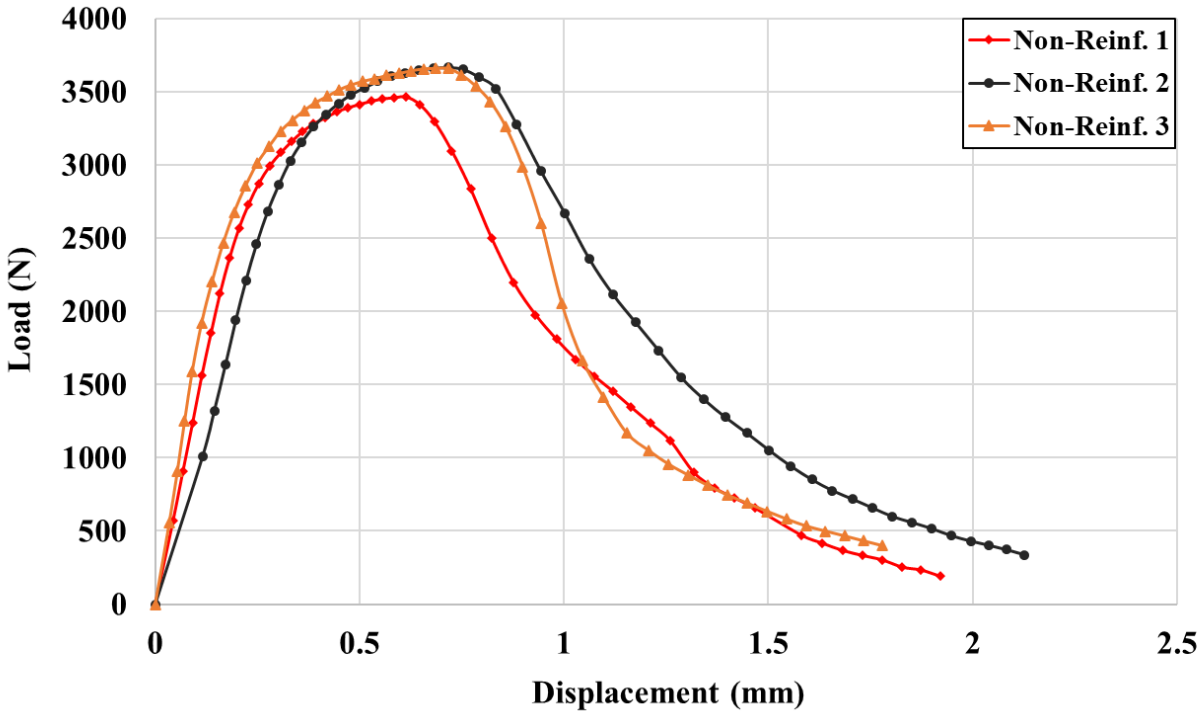

Figure 48: Flexural response of the non-reinforced control PolC beams

4.5.2.2 PolC Beams Reinforced with VAHT Unidirectional GFRP

A total number of three PolC beams reinforced with VAHT unidirectional GFRP were tested. Similar to the non-reinforced PolC, small cracks were observed in the midspan area of the beams. As the beams were loaded, larger cracks formed an opposite side of bottom of the beam and propagated to the middle. Even though the cracks were observed before the ultimate load was reached, the beams did not fail or show a load drop until the beam reach the ultimate capacity. The failure modes of the VAHT unidirectional GFRP reinforced PolC beams are shown in Figure 48.

(a)

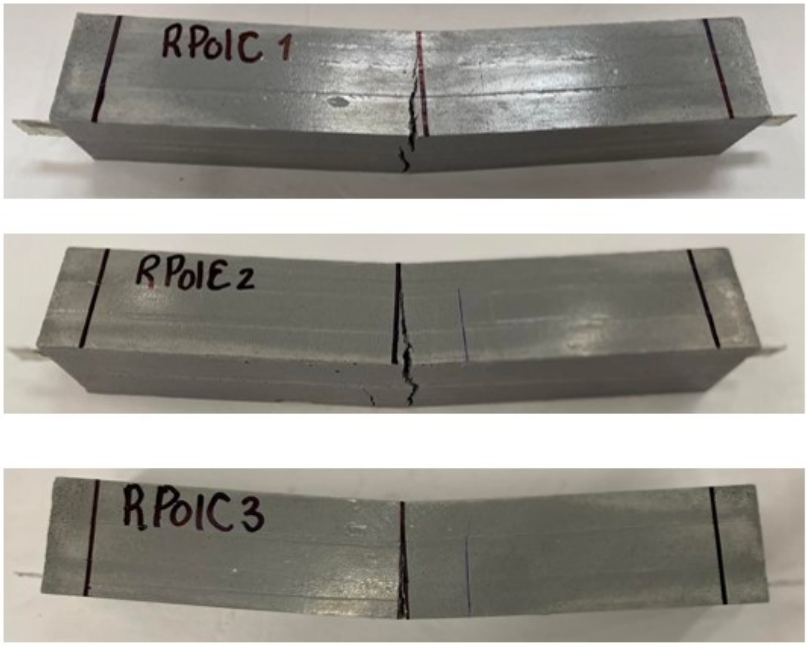

(b)

Figure 49: (a) Zoomed crack at bottom view (b) Failure modes of the VAHT unidirectional GFRP reinforced PolC beams

Table 19: Experimental results for VAHT unidirectional GFRP reinforced PolC

Properties	**VAHT PolC**				**Average**	**STDEV**	**COV**
	Units	**1**	**2**	**3**			
Peak Load	kN	6.9	7.5	7.8	7.4	0.45	6%
Max. Moment	kN • m	0.5	0.5	0.5	0.5	0.03	6%
Max. Deflection	mm	4.3	3.8	3.6	3.9	0.34	9%

The experimental results for VAHT unidirectional GFRP reinforced PolC are given in Table 17.

Maximum average load for VAHT unidirectional GFRP reinforced PolC is 7.4kN ± 0.45 kN where

the moment and deflection are 0.5 kN • m ± 0.03 kN • m and 3.9 mm ± 0.34 mm correspondingly. The flexural response of the VAHT unidirectional GFRP reinforced PolC beams is presented in Figure 49.

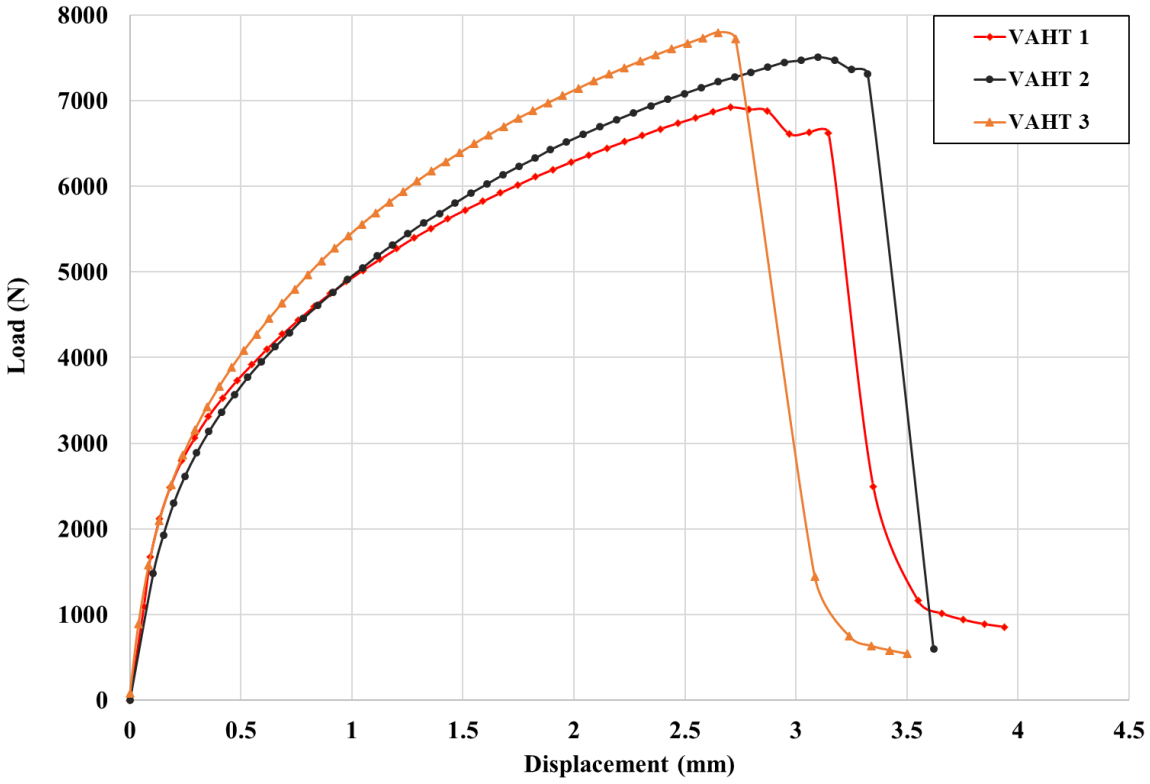

Figure 50: Flexural response of the VAHT unidirectional GFRP reinforced PolC beams

4.5.2.3 PolC Beams Reinforced with 3D Printed Unidirectional GFRP

Three PolC beams reinforced with 3D printed unidirectional GFRP were tested, and failure modes, experimental results, and flexural responses are presented below. In consistent with other PolC beam types, the beams started with minor cracks at the midspan and transitioned to larger cracks. The failure mode of the PolC beams reinforced with 3D printed unidirectional GFRP beams are shown in Figure 50.

(a)

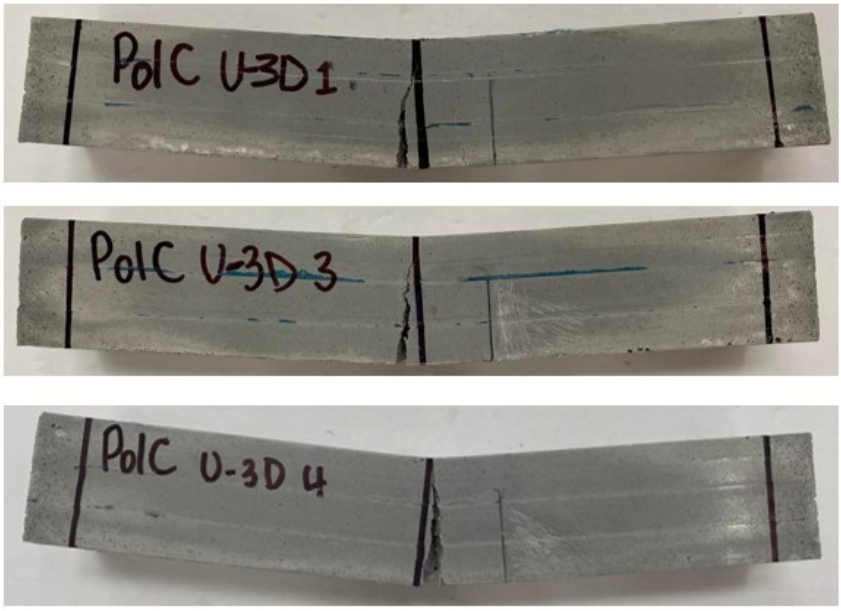

(b)

Figure 51: (a) Zoomed crack at bottom view (b) Failure modes of the 3D printed unidirectional GFRP reinforced PolC beams

The experimental results of PolC beams reinforced with 3D printed unidirectional GFRP are given in Table 18. Maximum average load is 6.8kN ± 0.68 kN where the moment and deflection are 0.5 kN • m ± 0.05 kN • m and 3.6 mm ± 0.28 mm correspondingly.

Table 20: Experimental results for 3D printed unidirectional GFRP reinforced PolC beams

Properties	3D Printed PolC				Average	STDEV	COV
	Units	1	2	3			
Peak Load	kN	7.0	7.4	6.1	6.8	0.68	10%
Max. Moment	kN • m	0.5	0.5	0.4	0.5	0.05	10%
Max. Deflection	mm	3.3	3.7	3.8	3.6	0.28	8%

The VAHT unidirectional GFRP reinforced PolC beams did not show any clear transition where the concrete failed, and the load was transferred to the reinforcement. However, the PolC beams reinforced with 3D printed unidirectional GFRP demonstrates that transition as shown in Figure 51.

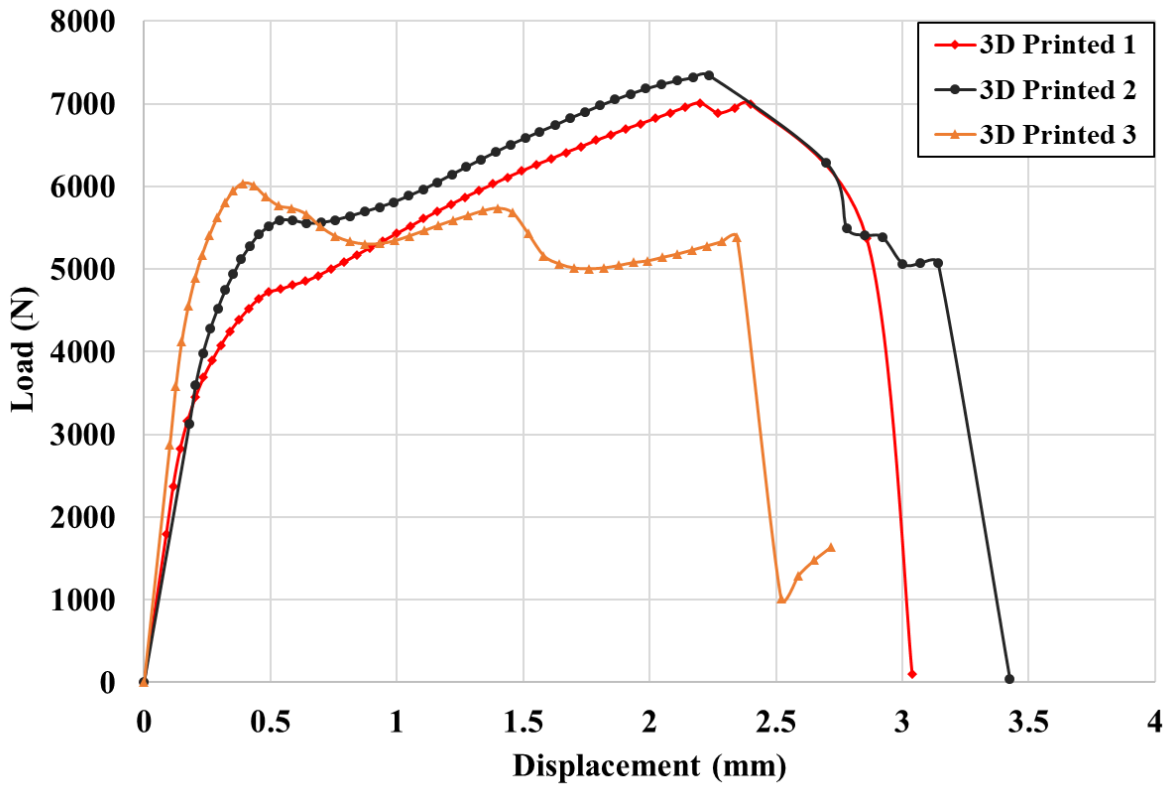

Figure 52: Flexural response of the 3D printed unidirectional GFRP reinforced PolC beams

4.5.2.4 PolC Beams Reinforced with 3D printed multidirectional GFRP

Three beams reinforced with designed ductile 3D printed reinforcements were tested for flexural behavior. The specimens cracked at midspan, and the load dropped significantly following the crack. For all the other PolC specimens that was tested in this study, none of them shows that brittle behavior. The failure modes of these beams are shown in Figure 52.

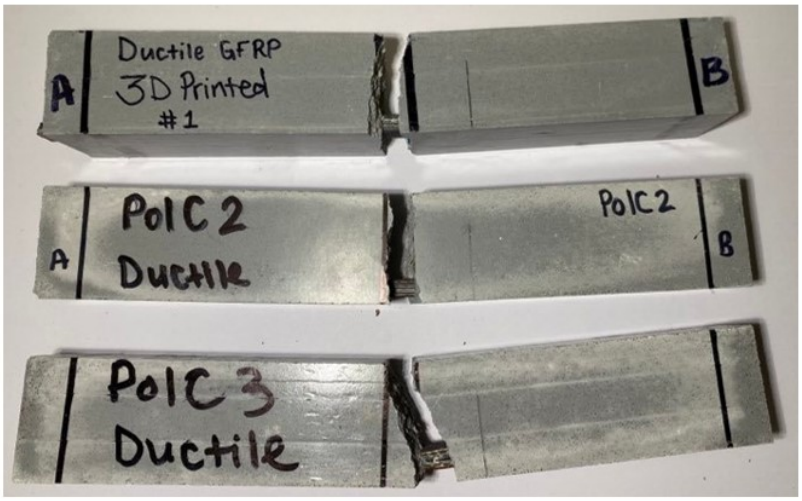

(a)

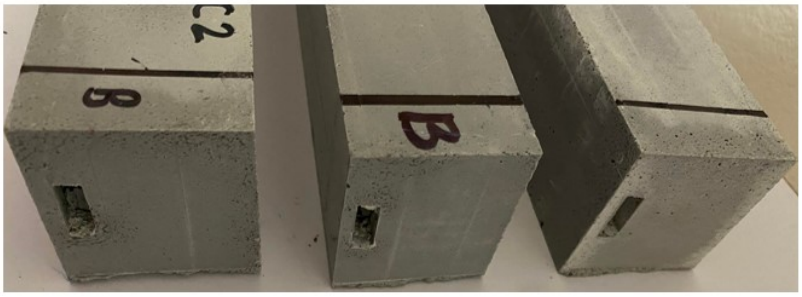

(b)

Figure 53: (a) Failure modes of the 3D printed multidirectional GFRP reinforced PolC beams (b) Debonded reinforcement

Even though the PolC has better engagement with the reinforcement than PCC, the PolC reinforced with 3D printed multidirectional GFRP debonded from the reinforcement. Since the chemical properties are unchanged and the parameters different from the 3D printed unidirectional were size and fiber orientation, the size is proven to play a role in bond engagement.

Table 21: Experimental results for 3D printed multidirectional GFRP reinforced PolC

Properties	Specimens				Average	STDEV	COV
	Units	1	2	3			
Peak Load	kN	5.9	8.1	7.1	7.0	1.09	16%
Max. Moment	kN.m	0.4	0.5	0.5	0.5	0.07	16%
Max. Deflection	mm	8.9	4.5	10.3	7.9	3.02	38%

The experimental results of the load, moment, and deflection parameters of PolC beams reinforced with 3D printed multidirectional GFRP are presented in Table 19. The average load, moment, and deflection are 7.0 kN ± 1.09 kN, 0.5 kN • m ± 0.07 kN • m, and 7.9 mm ± 3.02 mm respectively. The specimens experienced debonding therefore the deflection of the specimen cannot be determined with the present data. The flexural response of the PolC beams reinforced 3D printed multidirectional GFRP is presented in Figure 53.

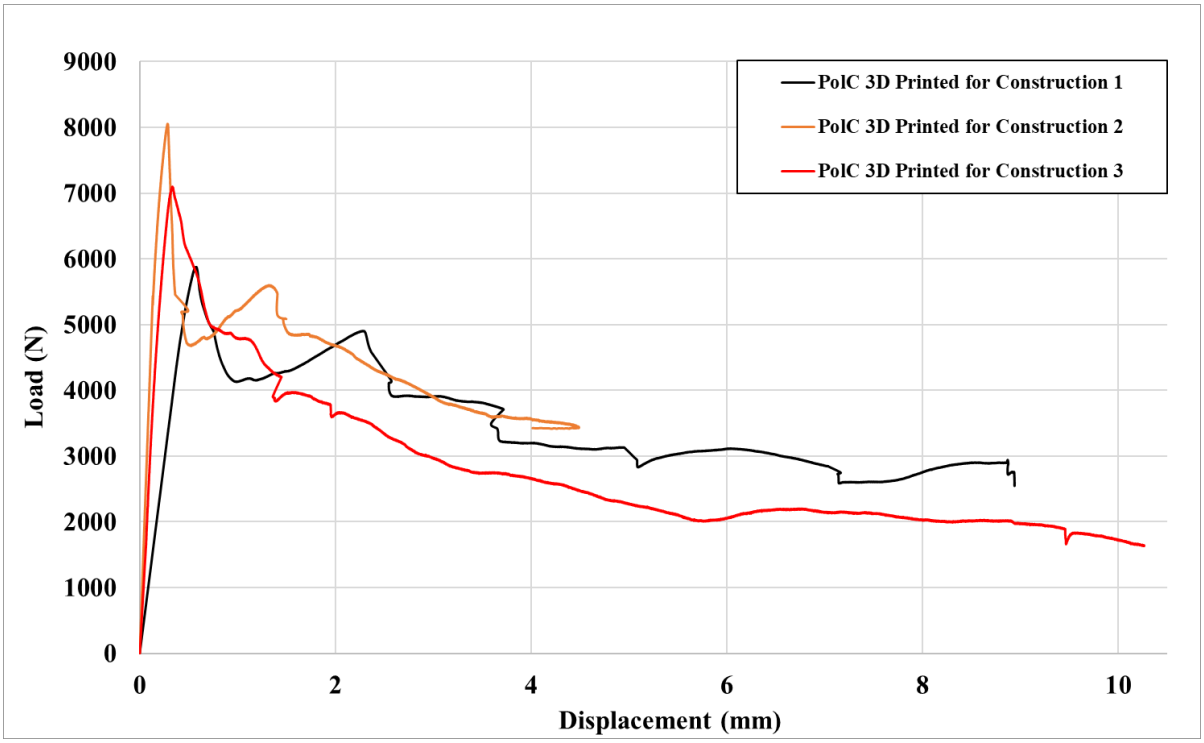

Figure 54: Flexural response of PolC beams reinforced with 3D printed multidirectional GFRP for construction

Chapter 5: Comparisons and Discussion

The PCC and PolC beams with the same reinforcement type are compared and analyzed to determine the performance of the different types of reinforcements. These are the four different groups reinforcement: 1) non-reinforced, 2) VAHT unidirectional GFRP, 3) 3D printed unidirectional GFRP, 4) 3D printed multidirectional GFRP.

5.1.1.1 Non-Reinforced Beams

The flexural capacity of the types of concrete were tested in accordance with the ASTM C580. Determining the flexural strength of the non-reinforced concrete beams was essential to establish the baseline capacity of each type of concrete. Therefore, three PCC beams and three PolC beams were tested, and the result of these tests are shown in Figure 54.

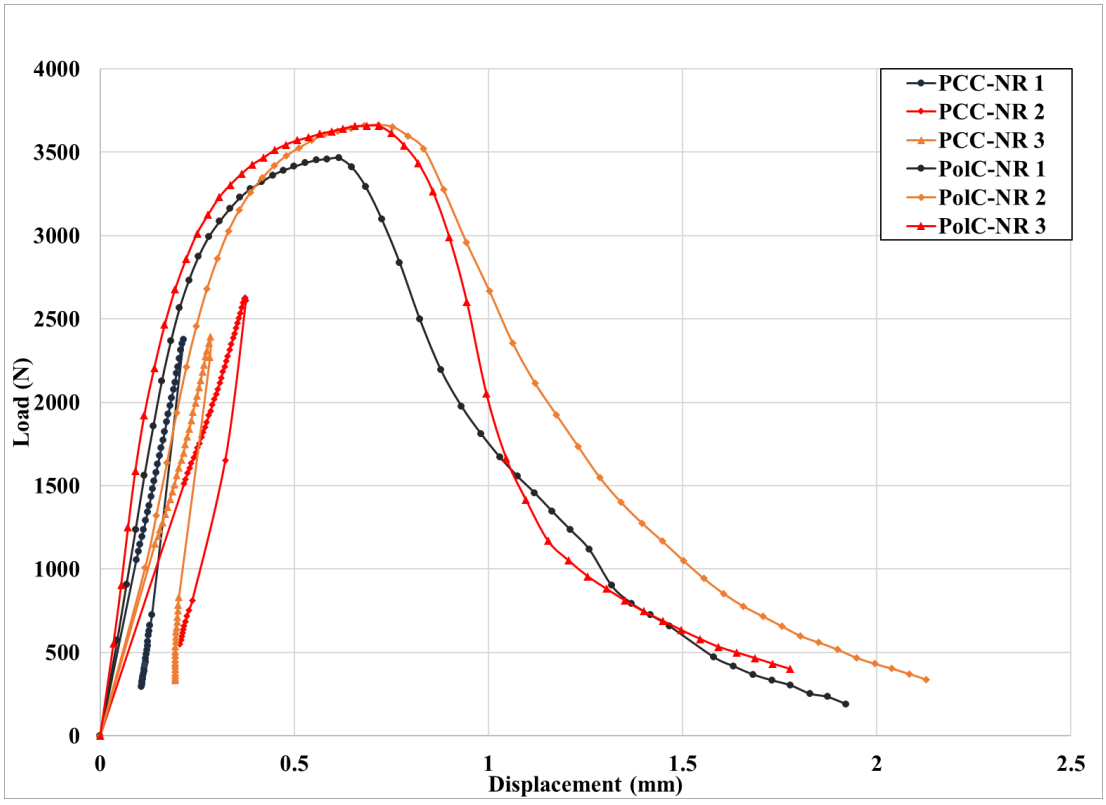

Figure 55: Load vs Displacement response of Non-Reinforced (NR) PCC and Pol C beams under flexure

The flexural capacity of the PCC and PolC depicted for the non-reinforced are vastly different. The PCC has a linear elastic behavior due to the brittle behavior of the concrete and immediate failure after the first crack formed. In comparison, the PolC demonstrated non-linear elastic or semi-ductile failure which attributed to higher tensile strength of the PolC. After the peak load was reached, the PolC specimens did not failure immediately; however, the specimen showed a large deflection, over 2 mm, and the load slowly dropped. The PolC had 44% higher strength than the PCC as shown in Figure 54.

5.1.1.2 VAHT Unidirectional GFRP Reinforced Beams

VAHT unidirectional GFRP with dimensions of 1 mm by 15 mm was used to reinforced both the PCC and PolC specimens. Similar to the non-reinforced beams, three PCC beams and three PolC beams were tested, and the flexural response observed are shown in Figure 55.

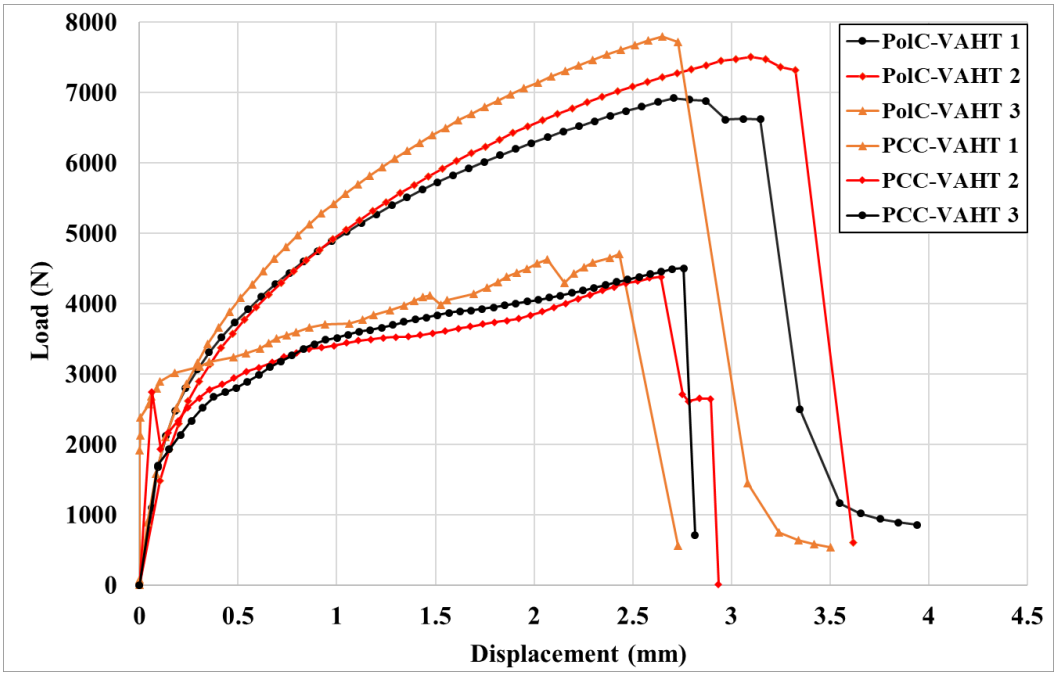

Figure 56: Load vs Displacement response of VAHT unidirectional GRFP reinforced PCC and Pol C beams under flexure

The PCC first drop indicates the concrete crack, then the behavior of the specimen transitions to a nonlinear behavior as the tensile loads transferred to the reinforcement. The second drop of the PCC happened as the crack of the specimen widened, and the last and third drop was observed as the specimen failed completely.

Unlike the PCC, the PolC specimens did not show any load drops until the specimens fully failed. The specimens maintained the nonlinear elastic behavior and progressive load capacity increase even though cracks were observed around 3.0 kN to 3.5 kN and the cracks widened as the load increased until the beams failed. The deflection observed in these specimens was significantly higher than the PCC deflection and the PolC specimens' capacity was twice as the PCC as shown in Figure 55.

5.1.1.3 3D Printed Unidirectional GFRP Reinforced Concretes

The unidirectional 3D printed GFRP reinforcement had the same dimensions as the VAHT GFRP. The major difference of the two reinforcements was that 3D printed coupons had smoother surface in comparison to the VAHT. The Figure 56 below shows the load versus deflection behavior of the PCC and PolC specimens.

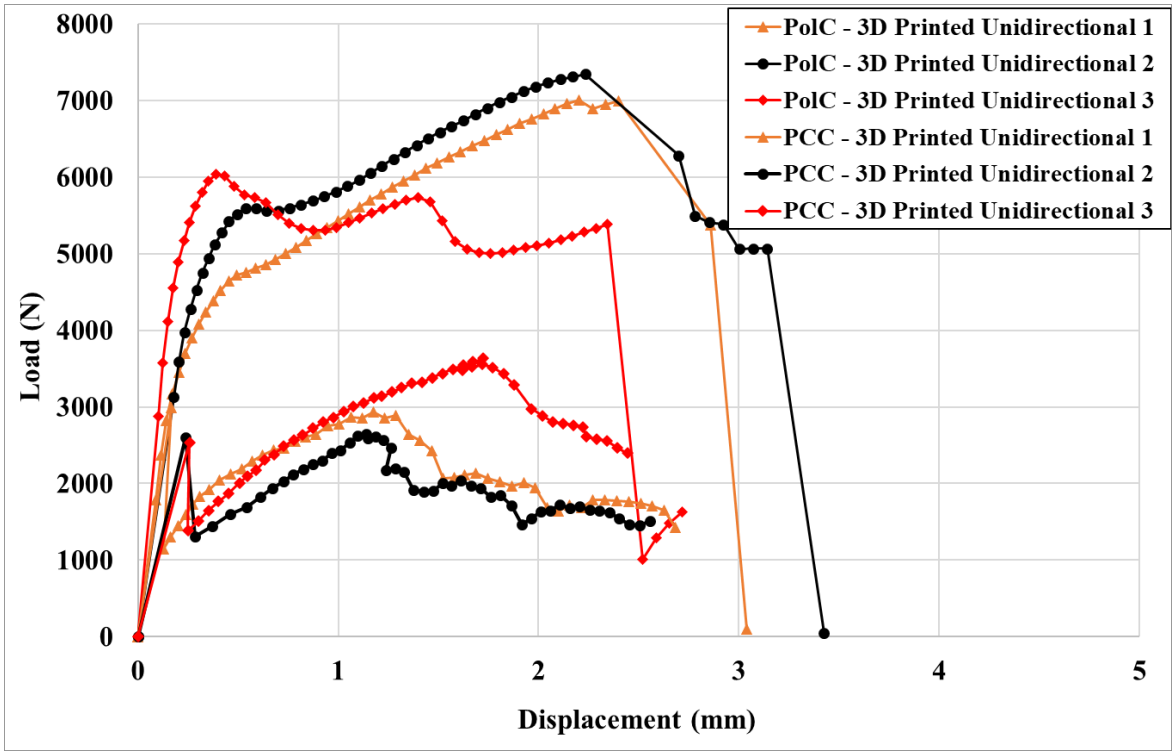

Figure 57: Load vs Displacement response of 3D printed unidirectional GRFP reinforced PCC and Pol C beams under flexure

The initial behavior of the PCC did not change for either reinforcement, the linear elastic to failure was still being observed for all three different types of PCC specimens. As noticed in the VAHT GFRP reinforcement, the first load drop happened as the concrete cracked. The load gradually increased until the second drop where slip of the reinforcement was detected. There was no significant load increase after the slip, and the reinforcement displayed a continuous slipping which resulted in a large deflection. In contrast, the PolC specimens did not experience any reinforcement slipping throughout the testing, and the load capacity increased by 150% compared to the control beams.

5.2 Multidirectional 3D printed GFRP for construction

The PCC and PolC reinforced with multidirectional 3D printed GFRP for construction results are shown in Figure 57. The PCC demonstrates higher stiffness and the PolC has larger flexural response.

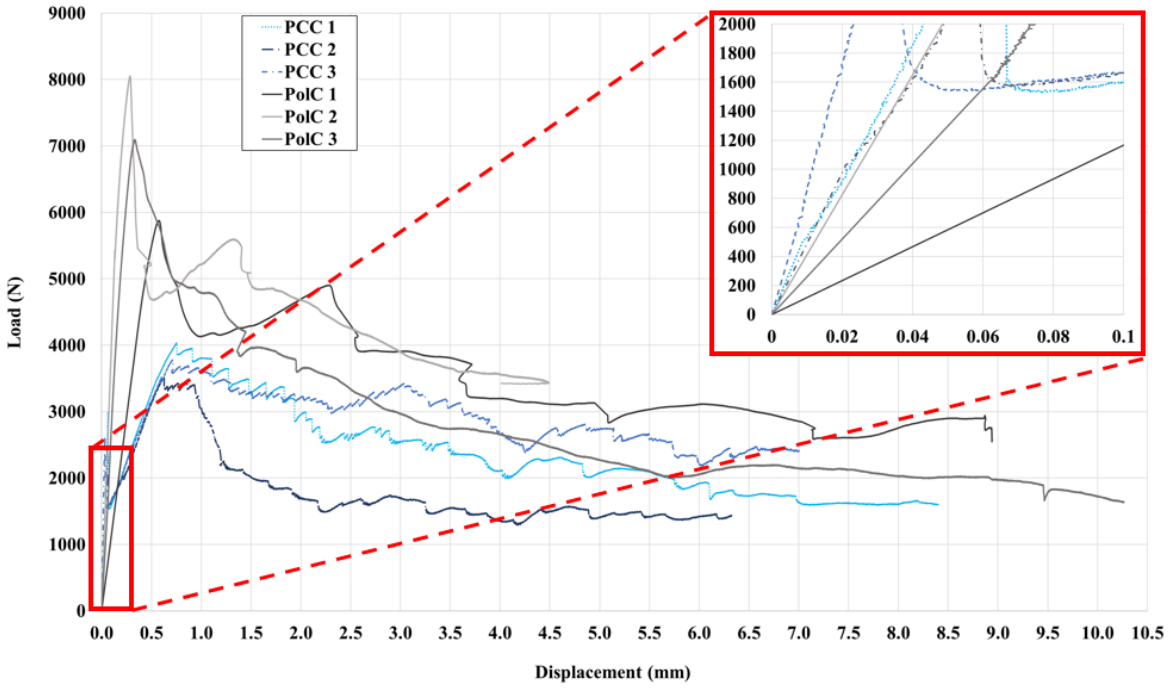

Figure 58: PCC and PolC reinforced with 3D printed multidirectional GFRP for Construction

5.2.1 PCC Reinforced with VAHT and 3D Printed Unidirectional GFRP

The flexural response of the different reinforcements in PCC is presented in Figure 58. The PCC specimens show higher stiffness with VAHT unidirectional GFRP reinforcement. It was determined that the VAHT unidirectional GFRP has higher fiber volume fraction than 3D Printed unidirectional GFRP which contributed to the high stiffness demonstrated in the flexural response curve shown in Figure 58.

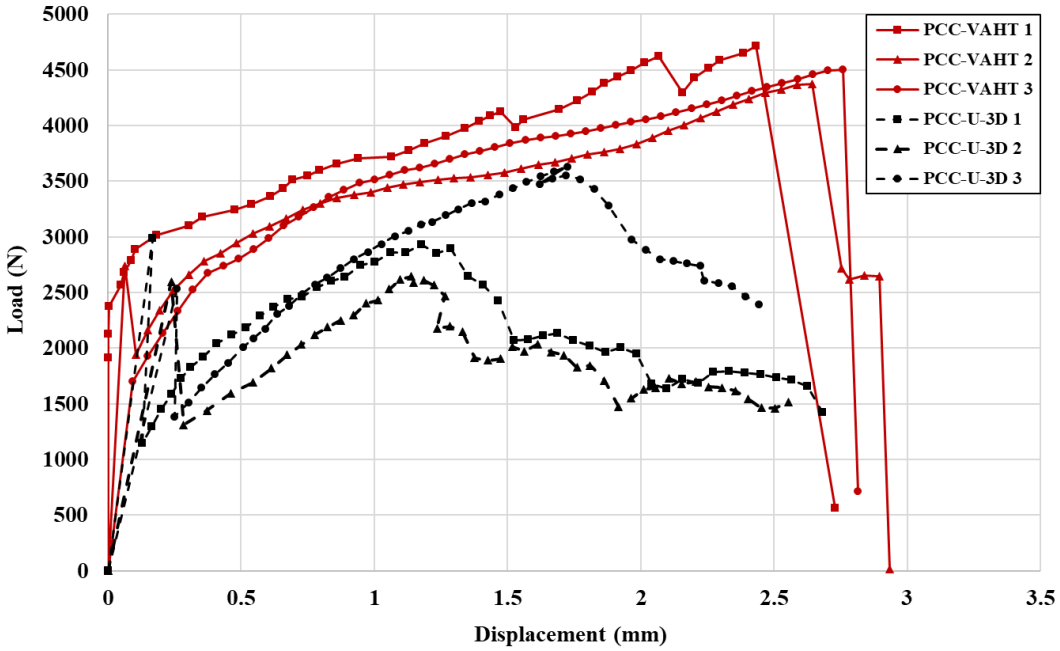

Figure 59: Flexural response of VAHT and 3D Printed Unidirectional GFRP in PCC

There was debonding failure for the PCC specimens reinforced with 3D Printed unidirectional GFRP. Therefore, the full flexural response of the reinforcement remains unknown and the reinforcement with the larger flexural response cannot be determined.

The debonding failure highlighted that there was a poor engagement between the reinforcement, and the concrete. Even though both reinforcements are polymer based, the VAHT showed better engagement with the PCC and there was no debonding failure. An essential physical difference between VAHT and 3D Printed unidirectional GFRP is the surface roughness. The 3D Printed reinforcements have smoother surface which reduces the frictional forces between the materials which increases the likelihood of debonding failures.

5.2.2 PolC Reinforced with VAHT and 3D Printed Unidirectional GFRP

Figure 59 shows the flexural response of PolC beams reinforced with VAHT and 3D Printed Unidirectional GFRP. The stiffness appears to be very similar for the different reinforcements.

Since both types of reinforcement and concrete are polymer based, it was hypothesized that the polymer – polymer interaction would create better engagement. Therefore, the PolC demonstrated better engagement with both unidirectional reinforcements and no debonding failures were observed.

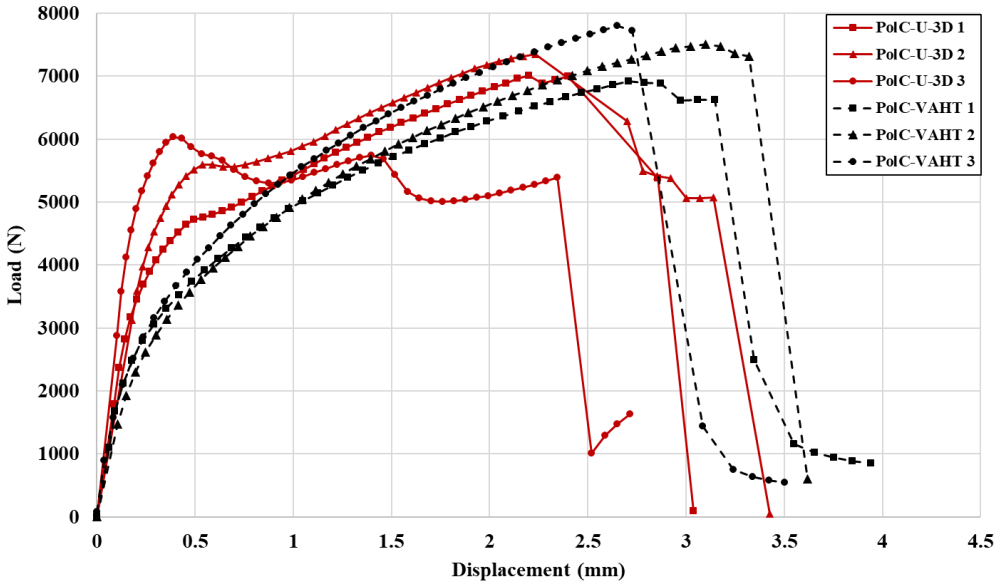

Figure 60: Flexural response of VAHT and 3D Printed Unidirectional GFRP in PolC

The flexural response was very similar in comparison to the PCC since the VAHT unidirectional GFRP beams has only 8.8% higher response. Likewise, the beams deformations are 8% larger with the same reinforcement.

5.3 Flexural Response Comparison of All the Various Specimens

The flexural response of all the different beams with different reinforcements are shown in Figure 59. The overview comparison of the various specimens provides additional insight. The initial portion of the figure is zoomed and shown on top right corner of the figure to highlight the initial behavior of the different specimens.

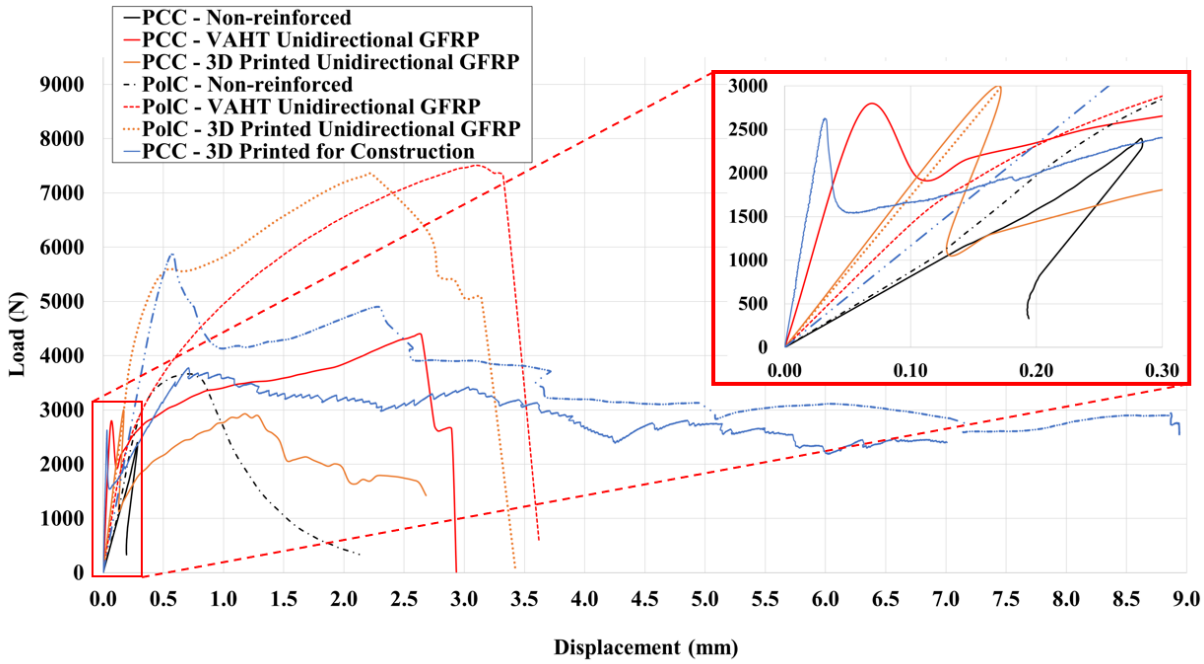

Figure 61: The flexural response of all specimens

As Figure 59 shows, the non-reinforced beams of both concretes have lowest stiffness where the 3D printed for construction exhibits the highest stiffness.

5.3.1.1 Maximum Moment Capacity

The maximum moment capacity calculated from the average of all 3 specimens of the different types of beams are presented in Figure 60. Utilizing reinforcement increased the moment capacity significantly, and generally, the PolC specimens demonstrate higher capacity than their PCC.

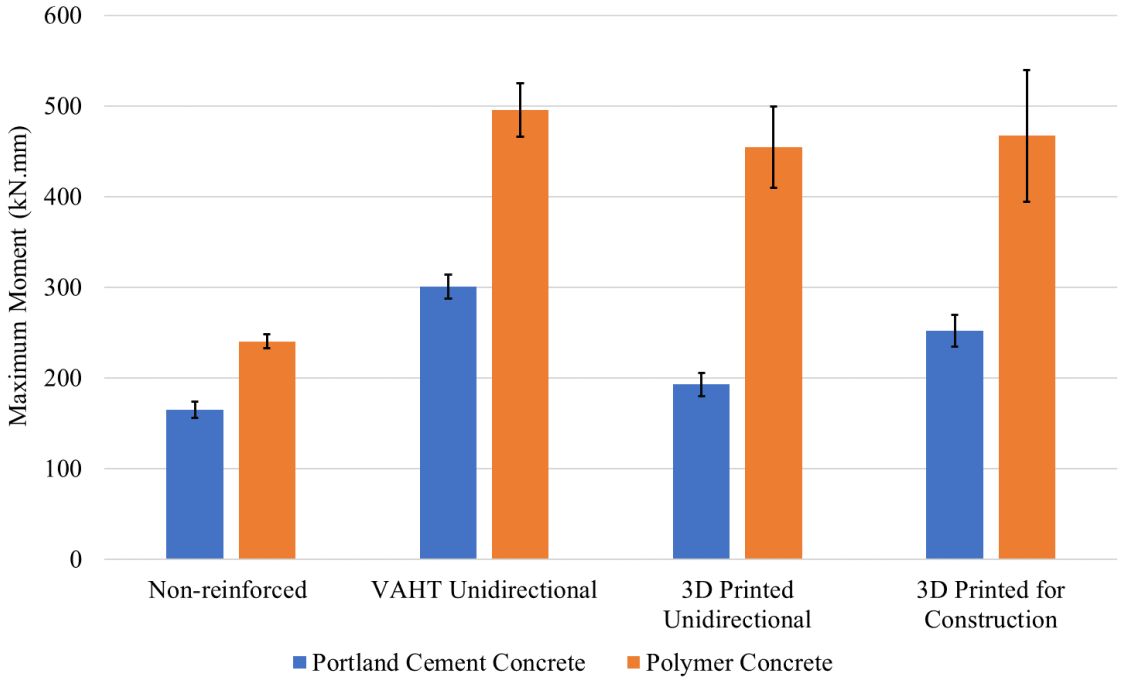

Figure 62: The maximum average moment capacity

For both of concretes, the VAHT unidirectional GFRP shows the most capacity improvement. The capacity increased 80% for PCC and 100.1% for PolC. However, the PCC reinforced with 3D printed unidirectional GFRP experienced bond failure, and the complete moment capacity those beams cannot be determined. The PolC reinforced with 3D printed unidirectional GFRP increased 88 %.

5.3.1.2 Maximum Deflection

Similar to the moment capacity, the beams demonstrated larger deflections with the reinforcements. For PCC, the beams with VAHT unidirectional GFRP show 580% increase in comparison to the non-reinforced. The 3D printed unidirectional GFRP depicts larger deflections however, the increase could be attributed to the bond failure.

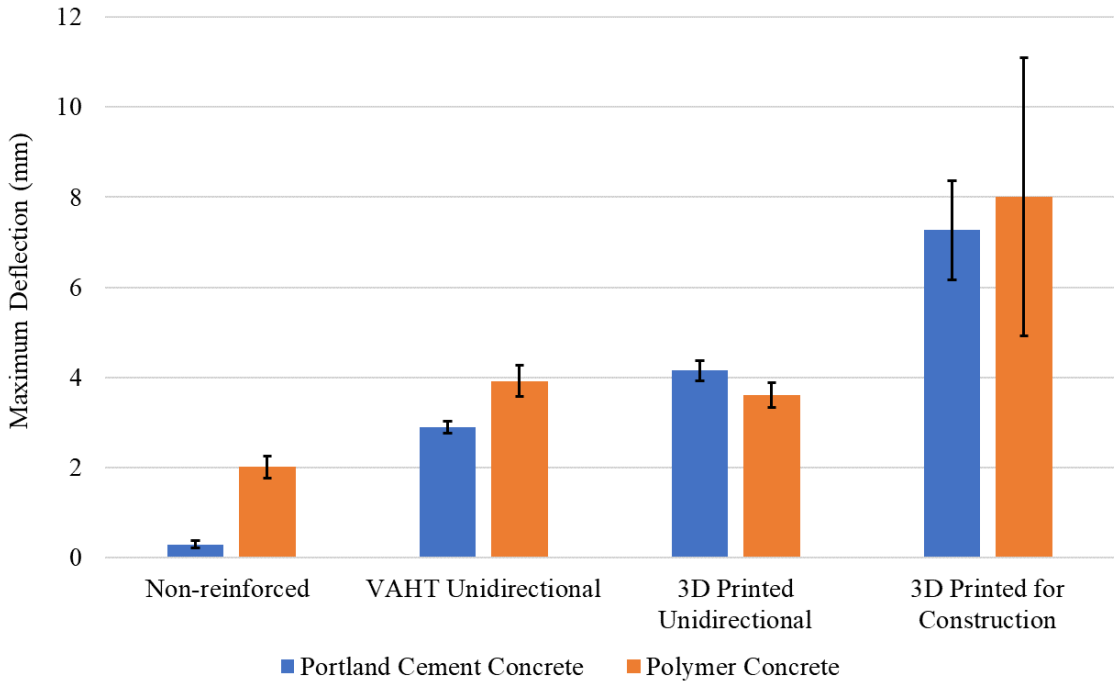

Figure 63: The maximum average deflection

The PolC specimens experienced larger deformations for both non-reinforced and VAHT unidirectional comparing with the PCC tested specimens. Within the PolC specimens, VAHT unidirectional GFRP increased the deflection by 96%, and the 3D printed unidirectional GFRP increase by 83%. There were no bond failures observed in the PolC, but the 3D printed unidirectional GFRP reinforced beams show less deflection than the beams reinforced with VAHT unidirectional GFRP.

5.4 Microscopic Image Analysis

5.5 Portland Cement Concrete Reinforcement Microscopic Analysis

To further investigate the bond engagement of the GFRP reinforcements and concretes, microscope analysis was conducted. There was no saturation observed on the VAHT unidirectional GFRP and 3D printed unidirectional GFRP.

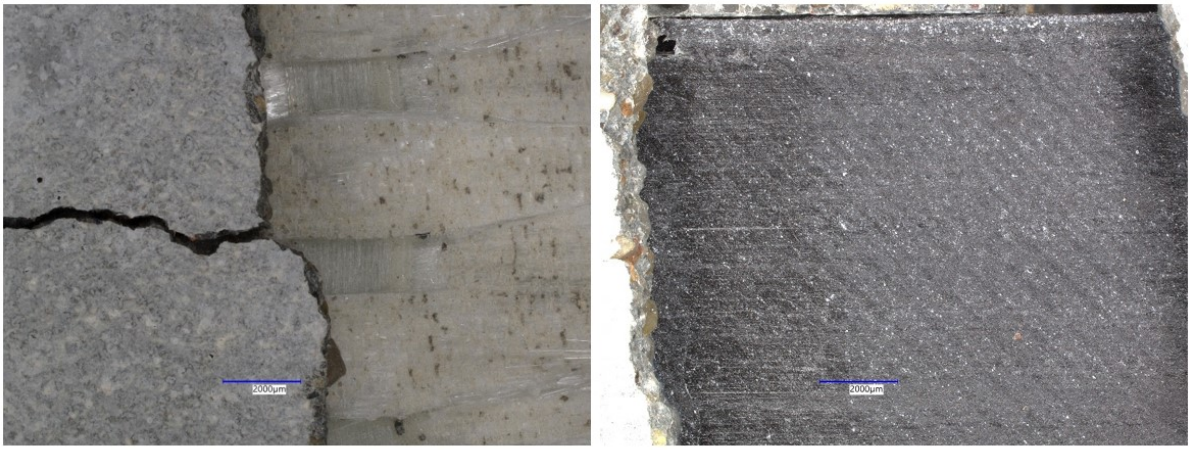

(a) (b)

Figure 64: Microscopic images of PCC reinforced with (a) VAHT GFRP (b) 3D printed GFRP

There was a small fibrous damage on VAHT unidirectional GFRP, and no damage on the 3D printed unidirectional GFRP. As reported earlier, the 3D printed unidirectional GFRP reinforced beams failed due to debonding. The microscopic images in Figure 62 (a) and (b) show the difference of the surface roughness. In addition to the lack of good bond engagement, the 3D printed unidirectional GFRP has smoother surface which could contribute to lower bonding capacity.

5.6 Polymer Concrete Reinforcement Microscopic Analysis

The PolC had better engagement with the reinforcements as predicted. There is a clear saturation with the VAHT unidirectional GFRP where polymer concrete can be observed in the damaged fibers as shown in Figure 63 (a). There are no gaps between the concrete and the reinforcement which highlighted bond connection between the two materials.

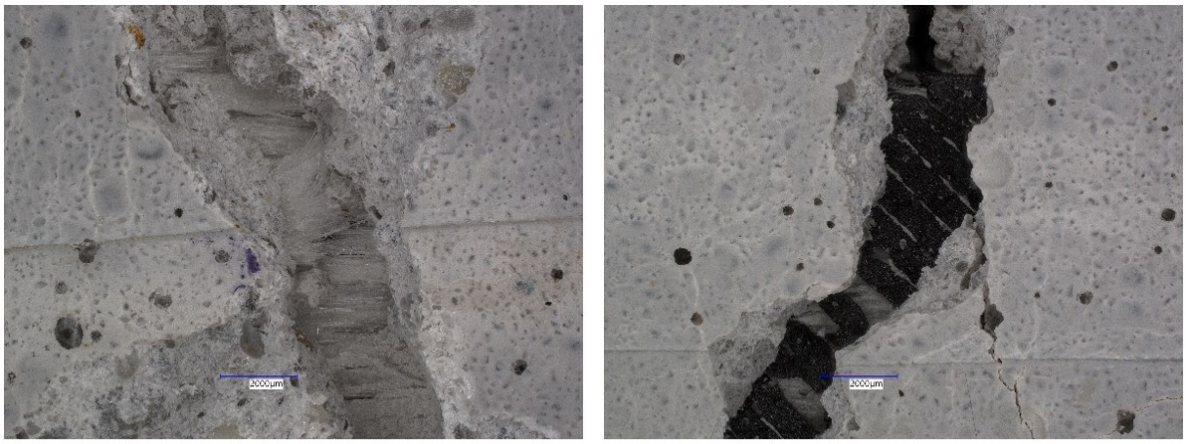

(a) (b)

Figure 65: Microscopic images of PolC reinforced with (a) VAHT unidirectional GFRP (b) 3D printed unidirectional GFRP

Damaged fibers can be observed in both reinforcements. For the 3D printed unidirectional GFRP shown in Figure 63 (b) shows the broken Nylon and batches of broken glass fibers. The higher flexural response and moment capacities in PolC were reached because of the strong bond between the polymer-based materials.

5.7 PCC and PolC Reinforced with multidirectional 3D printed GFRP for construction

The microscopic investigation revealed that PolC can seep in into small gaps. This aids the shear transfer between the debonded layers of the multidirectional FRP. PolC can seep in gaps as small as 106 μm and 94 μm respectively. Figures 64 and 65 show the microscopic results of the 3D printed multidirectional GFRP.

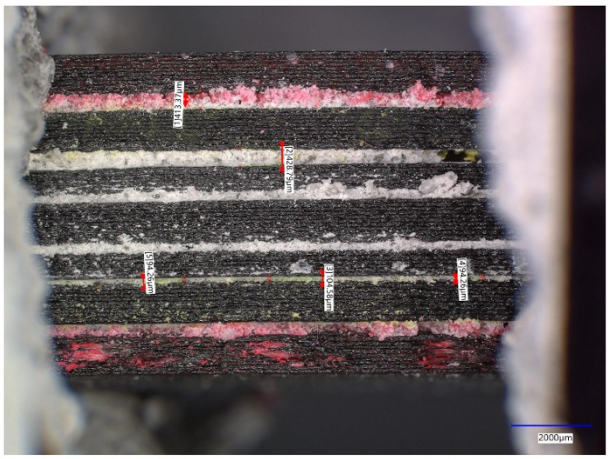

Figure 66: Microscopic image of PolC reinforced with Multidirectional 3D printed GFRP

This is not the case in PCC which can only seep in in larger gaps. This can also explain the changes in flexural response observed in both types of beams.

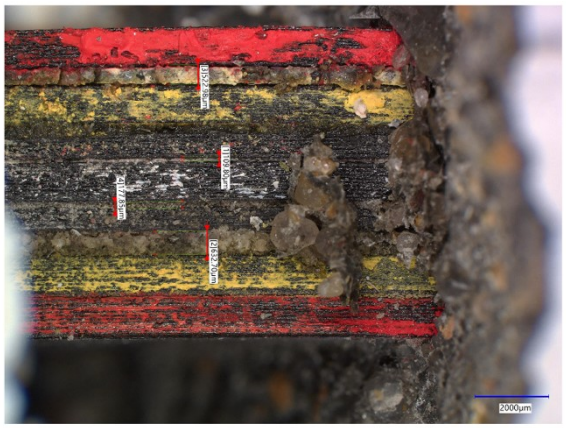

Figure 67: Microscopic image of PCC reinforced with Multidirectional 3D printed GFRP

5.8 Compared Moment Capacities and Failure Modes

The theoretical moment capacities and predicted failure modes were calculated using Mathcad software. The experimental moment capacities were also determined from the collected data and failure modes were analyzed. The comparison between the theoretical and experimental results are shown in Table 20.

Table 22: Theoretical and experimental moment capacities and failure modes of all beams

Types of GFRP Reinforcement	Theoretical Moment Capacity (kN.m)	Theoretical Failure Mode	Experimental Moment Capacity (kN.m)	Experimental Failure Mode
PCC-VAHT Unidirectional	0.13	Tension	0.3	Compression
PCC-3D Printed Unidirectional	0.31	Compression	0.19	Bond
PCC 3D Printed for Construction	0.47	Compression	0.24	Bond
PolC-VAHT Unidirectional	0.13	Tension	0.54	Tension
PolC-3D Printed Unidirectional	0.29	Compression	0.45	Tension
PolC-3D Printed for Construction	0.44	Compression	0.47	Bond

Based on the tensile strength of the reinforcement and compressive strength of the concrete, the moment capacities of the various reinforced beams were calculated. The equations used are developed for Portland cement concrete. These equations do not consider the bond strength between the concrete and reinforcement. For polymer concrete, the equations do not reflect the tensile strength of the concrete which underestimates the expected moment capacity. Besides the limitations listed above, the theoretical moment calculations provide great insight in predicting the moment capacities.

Both PCC and PolC reinforced with VAHT unidirectional GFRP showed a tensile failure; however, PCC failed in compression. The bond engagement of the PCC reinforced with VAHT unidirectional GFRP weaker compared to PolC. Therefore, the reinforcement contribution was limited which led the concrete failure. Due to the weak bond between the PCC and the reinforcements, both 3D printed unidirectional, and 3D printed for construction GFRP reinforced beams experienced bond failure.

Even though 3D printed unidirectional, and 3D printed for construction reinforced PolC beams were predicted to fail in compression, they experience tension and bond failure respectively. The polymer-polymer interaction contributes to the bond strength; however, increasing the thickness of the reinforcement had an impact on the bond strength. Considering limitations, strong conclusions cannot be made based on this comparison.

Chapter 6: Summary, Conclusions, Recommendations, and Future Work

6.1 Summary

In this study, the flexural behavior of concrete reinforced with VAHT unidirectional GFRP, 3D printed unidirectional GFRP, and multidirectional 3D printed GFRP were investigated. The fiber volume fraction of VAHT unidirectional GFRP 43% higher than the 3D printed unidirectional GFRP with the same dimensions.

The PCC and PolC mix were designed to have similar capacities. Compression tests and modulus of rupture tests were used to determine their compressive and tensile strength. Both concretes demonstrated similar capacities for compressive strength. However, polymer concrete had higher tensile strength which was expected since polymer concrete is known for the higher tensile strength. The experimental capacities were than validated with the literature.

The flexural testing followed the mix and reinforcement validation, and the results were analyzed.

6.2 Conclusions

- Mix designs of polymer concrete and cementitious concrete were validate. Tensile strength of polymer concrete was higher than Portland cement concrete
- Since the fiber volume fractions of 3D printed GFRP were lower than conventional GFRP resulting in lower stiffness, there is great scope of improvement of the 3D printing filament to improve fiber content so as to improve mechanical performance.
- 3D printed GFRP showed some fibrous damage in polymer concrete but its engagement in Portland cement concrete was not visible also leading to debonding
- Conventional GFRP also shows partial brooming in polymer concrete but not in cementitious concrete
- Polymer concrete reinforced with both types of FRP showed improved flexural behavior

- All forms of reinforcements improved the moment capacity and flexural capacity of the beams for both PCC and PolC. However, on average, 3D printed GFRP in PolC had improved flexural response compared to the 3D printed GFRP in PCC.
- The PolC had better engagement with VAHT unidirectional GFRP and 3D printed unidirectional GFRP. Both PCC and PolC experienced debonding with the multidirectional 3D printed GFRP for construction. However, damage in the bottom side of the beam was seen in PCC.
- Polymer concrete can seep in in gaps ranging from 94 μm to 534 μm where Portland cement concrete can seep into larger gaps. This can help with engagement of polymer-based reinforcements in polymer concrete when compared to cementitious concretes

6.3 Recommendations for further investigations

To further investigate the polymer concrete-FRP bond,

- Similar work is recommended using strain gauges.
- Reducing the size of the reinforcement for the multidirectional 3D printed GFRP for construction might improve the bond engagement.
- Increasing the length of the reinforcement by overlapping two or more printed specimens however the effects of the overlapping should be carefully considered.

6.4 Future Work into 3D printed FRP composites in concrete

3D printing technology has unlimited potential in many industries including the construction industry. There are ways to 3D print concrete available using cementitious materials, however, the members have limited tensile strength (Al Abadi et al. 2018). These shortcomings can be resolved employing 3D printed reinforcement. Some of the proposed ideas are shown in the Figure 66 obtained from the Institute for Advanced Architecture of Catalonia (IAAC). A 3D printer with

two nozzles, one for printing concrete, and the other for printing the reinforcement working simultaneously. This design would simplify a lot of architectural design issues since printing irregular shapes and complex designs would not be a problem. Attempts to encapsulate reinforced Polylactic acid (PLA) filaments by a cementitious material like clay to test the tools and conditions necessary for simultaneous reinforced concrete printing are in progress. More and more results explaining the behavior of 3D printed FRP in concretes can help customize and optimize designs that are effective for such modern construction methods.

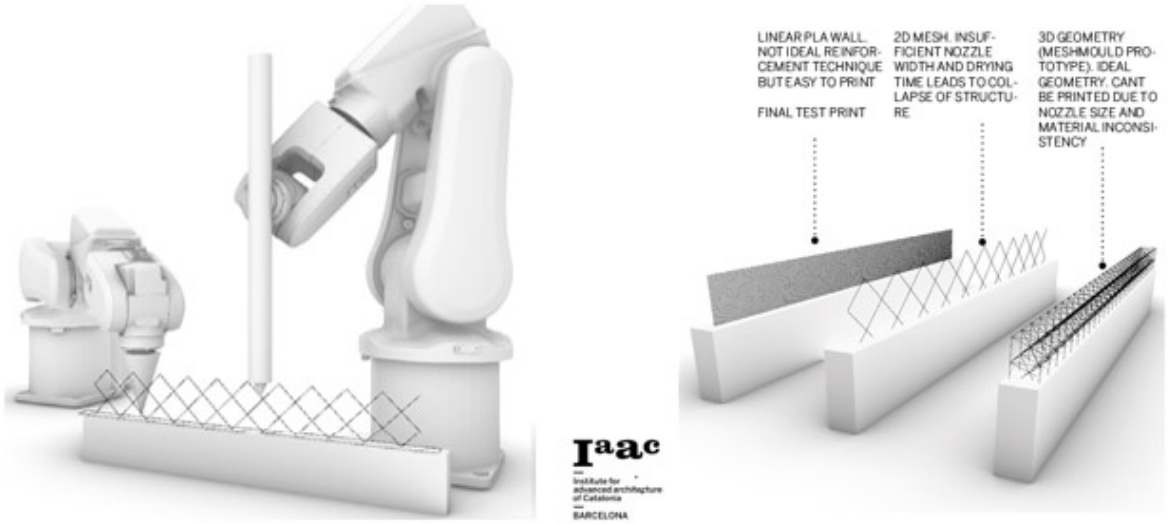

Figure 68: Potential concrete and reinforcement 3D printer (obtained from Institute for Advanced Architecture of Catalonia (IAAC))

Chapter 7: References

Abdel-Fattah, Hisham, and Moetaz M El-Hawary. 1999. 'Flexural behavior of polymer concrete', *Construction and Building Materials*, 13: 253-62.

Agarwal, Kuldeep, Suresh K. Kuchipudi, Benoit Girard, and Matthew Houser. 2018. 'Mechanical properties of fiber reinforced polymer composites: A comparative study of conventional and additive manufacturing methods', *Journal of Composite Materials*, 52: 3173-81.

Al Abadi, Haider, Huu-Tai Thai, Vidal Paton-Cole, and VI Patel. 2018. 'Elastic properties of 3D printed fibre-reinforced structures', *Composite Structures*, 193: 8-18.

Araya-Calvo, Miguel, Ignacio López-Gómez, Nicolette Chamberlain-Simon, José Luis León-Salazar, Teodolito Guillén-Girón, Juan Sebastián Corrales-Cordero, and Olga Sánchez-Brenes. 2018. 'Evaluation of compressive and flexural properties of continuous fiber fabrication additive manufacturing technology', *Additive Manufacturing*, 22: 157-64.

Asim, Mohammad, Mohammad Jawaid, Naheed Saba, Ramengmawii, Mohammad Nasir, and Mohamed Thariq Hameed Sultan. 2017. '1 - Processing of hybrid polymer composites—a review.' in Vijay Kumar Thakur, Manju Kumari Thakur and Raju Kumar Gupta (eds.), *Hybrid Polymer Composite Materials* (Woodhead Publishing).

Bai, Jiping. 2013. *Advanced fibre-reinforced polymer (FRP) composites for structural applications* (Elsevier).

Balasubramanian, M. 2014. *Composite materials and processing* (CRC press Boca Raton).

Bank, Lawrence C. 2006. *Composites for construction: structural design with FRP materials* (John Wiley & Sons).

Bărbuţă, Marinela, Maria Harja, and Irina Baran. 2010. 'Comparison of mechanical properties for polymer concrete with different types of filler', *Journal of Materials in Civil Engineering*, 22: 696-701.

Bedi, Raman, Rakesh Chandra, and S. P. Singh. 2014a. 'Reviewing some properties of polymer concrete', *Indian Concrete Journal*, 88: 47-68.

Bedi, Raman, Rakesh Chandra, and SP Singh. 2013. 'Mechanical properties of polymer concrete', *Journal of Composites*, 2013.

———. 2014b. 'Reviewing some properties of polymer concrete', *Indian Concrete Journal*, 88: 47-68.

Benmokrane, Brahim, Fareed Elgabbas, Ehab Ahmed, and Patrice Cousin. 2015. 'Characterization and Comparative Durability Study of Glass/Vinylester, Basalt/Vinylester, and Basalt/Epoxy FRP Bars', *Journal of Composites for Construction*, 19.

Bulut, H Alperen, and Remzi Şahin. 2017. 'A study on mechanical properties of polymer concrete containing electronic plastic waste', *Composite Structures*, 178: 50-62.

"C39/C39M Standard Test Method for Compressive Strength of Cylindrical Concrete Specimens." In. 2018.

"C78/C78M Standard Test Method for Flexural Strength of Concrete (Using Simple Beam with Third-Point Loading)." In. 2018.

'C192/C192M Standard Practice for Making and Curing Concrete Test Specimens in the Laboratory'. 2018.

"C579 Standard Test Methods for Compressive Strength of Chemical-Resistant Mortars, Grouts, Monolithic Surfacings, and Polymer Concretes." In. 2018.

"C580 Standard Test Method for Flexural Strength and Modulus of Elasticity of Chemical-Resistant Mortars, Grouts, Monolithic Surfacings, and Polymer Concretes." In. 2018.

Committee, A. C. I. 2019. 'Building code requirements for structural concrete (ACI 318-19) : an ACI standard

Commentary on building code requirements for structural concrete (ACI 318R-19) / reported by ACI Committee 318', *ACI standard : commentary on building code requirements for structural concrete (ACI 318R-19)*.

'D3039/D3039M Standard Test Method for Tensile Properties of Polymer Matrix Composite Materials'. 2017.

'D3171 Standard Test Methods for Constituent Content of Composite Materials'. 2015.

Del Giudice, Lorenzo, and Michalis Vassiliou. 2020. 'Mechanical properties of 3D printed material with binder jet technology and potential applications of additive manufacturing in seismic testing of structures', *Additive Manufacturing*, 36.

Dickson, Andrew N, James N Barry, Kevin A McDonnell, and Denis P Dowling. 2017. 'Fabrication of continuous carbon, glass and Kevlar fibre reinforced polymer composites using additive manufacturing', *Additive Manufacturing*, 16: 146-52.

El-Hajjar, R., H. Tan, and K. M. Pillai. 2013. '3 - Advanced processing techniques for composite materials for structural applications.' in Nasim Uddin (ed.), *Developments in Fiber-Reinforced Polymer (FRP) Composites for Civil Engineering* (Woodhead Publishing).

Gorninski, Jane Proszek, Denise C Dal Molin, and Claudio S Kazmierczak. 2004. 'Study of the modulus of elasticity of polymer concrete compounds and comparative assessment of polymer concrete and portland cement concrete', *Cement and concrete research*, 34: 2091-95.

Gowayed, Y. 2013. '1 - Types of fiber and fiber arrangement in fiber-reinforced polymer (FRP) composites.' in Nasim Uddin (ed.), *Developments in Fiber-Reinforced Polymer (FRP) Composites for Civil Engineering* (Woodhead Publishing).

Gunaslan, Sultan Erdemli, Abdulhalim Karasin, and Mehmet Emin Öncü. 2014. "Properties of FRP Materials for Strengthening." In.

"Introducing Our New Markforged Material: Onyx." In. *Markforged* Markforged

Krishna, S. Vamshi, and M. Pradeep Kumar. 2016. "Properties Evaluation of Chopped, Bi-Directional and Uni-Directional Glass Fibre Reinforced Epoxy based Composites." In.

Lau, D. 2013. '8 - Hybrid fiber-reinforced polymer (FRP) composites for structural applications.' in Nasim Uddin (ed.), *Developments in Fiber-Reinforced Polymer (FRP) Composites for Civil Engineering* (Woodhead Publishing).

Melenka, Garrett W., Benjamin K. O. Cheung, Jonathon S. Schofield, Michael R. Dawson, and Jason P. Carey. 2016. 'Evaluation and prediction of the tensile properties of continuous fiber-reinforced 3D printed structures', *Composite Structures*, 153: 866-75.

Murcia, Daniel Heras, Bekir Çomak, Eslam Soliman, and Mahmoud M Reda Taha. 2022. 'Flexural Behavior of a Novel Textile-Reinforced Polymer Concrete', *Polymers*, 14: 176.

Pervaiz, Salman, Taimur Ali Qureshi, Ghanim Kashwani, and Sathish Kannan. 2021. '3D Printing of Fiber-Reinforced Plastic Composites Using Fused Deposition Modeling: A Status Review', *Materials*, 14: 4520.

Saba, Naheed, Mohammad Jawaid, Othman Y Alothman, MT Paridah, and Azman Hassan. 2016. 'Recent advances in epoxy resin, natural fiber-reinforced epoxy composites and their applications', *Journal of Reinforced Plastics and Composites*, 35: 447-70.

Salmi, Mika. 2021. 'Additive manufacturing processes in medical applications', *Materials*, 14: 191.

Sathishkumar, TP, J Naveen, and S Satheeshkumar. 2014. 'Hybrid fiber reinforced polymer composites – a review', *Journal of Reinforced Plastics and Composites*, 33: 454-71.

Sonnenschein, Robert, Katarina Gajdosova, and Ivan Holly. 2016. 'FRP composites and their using in the construction of bridges', *Procedia engineering*, 161: 477-82.

Swolfs, Yentl, Larissa Gorbatikh, and Ignaas Verpoest. 2014. 'Fibre hybridisation in polymer composites: A review', *Composites Part A: Applied Science and Manufacturing*, 67: 181-200.

Tse, LYL, S Kapila, and K Barton. 2016. "Contoured 3D printing of fiber reinforced polymers." In *2016 International Solid Freeform Fabrication Symposium*. University of Texas at Austin.

Vemuganti, Shreya, Eslam Soliman, and Mahmoud Reda Taha. 2020. '3D-printed pseudo ductile fiber-reinforced polymer (FRP) composite using discrete fiber orientations', *Fibers*, 8: 53.

Wu, Zhengyu, Ali M. Memari, and Jose P. Duarte. 2022. 'State of the Art Review of Reinforcement Strategies and Technologies for 3D Printing of Concrete', *Energies*, 15: 360.

You, Young-Jun, Jang-Ho Jay Kim, Sung-Jae Kim, and Young-Hwan Park. 2015. 'Methods to enhance the guaranteed tensile strength of GFRP rebar to 900MPa with general fiber volume fraction', *Construction and Building Materials*, 75: 54-62.

Appendix A

PCC Reinforced with VAHT Unidirectional GFRP

(a) (b)

Section properties

$h := 50.8 \cdot mm$ h = height

$d := 43.3 \cdot mm$ d = depth

$b := 50.8 \cdot mm$ b = width

$L := 304.8 \cdot mm$ L = length

$f'_c := 67.4 \cdot MPa$ f'_c = specified compressive strength of concrete

$\varepsilon_{cu} := 0.003$ ε_{cu} = ultimate strain in concrete

Reinforcement properties

$f_{fu} := 526.4 \cdot MPa$ f_{fu} = design tensile strength of FRP

$E_f := 29.2 \cdot GPa$ E_f = design or guaranteed modulus of elasticity of FRP

$A_f := 15 \cdot mm^2$ A_f = Area of reinforcement

$\varepsilon_{fu} := 0.018$ ε_{fu} = Strain in FRP

Equilibrium Condition

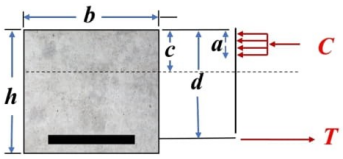

C = Compression force

a = depth of equivalent rectangular stress block

T = tension force

c = distance from extreme compression fiber to the neutral axis

C=T

$\alpha_1 := 0.85$

α_1 = ratio of average stress of equivalent rectangular stress block to fc′

$$\beta_1 := \max\left((0.85) - 0.05 \cdot \left(\frac{f'_c - 28 \cdot MPa}{7\ MPa}\right), 0.65\right)$$

$\beta_1 = 0.65$

Reinforcement ratio - Failure Mode

$$\rho_f := \frac{A_f}{b \cdot d} = 0.007$$

ρ_f = fiber-reinforced polymer reinforcement ratio

ACI 440.1R-15:2.1

β1 = factor taken as 0.85 for concrete strength *fc′* up to and including 4000 psi (28 MPa). For strength above 4000 psi (28 MPa), this factor is reduced continuously at a rate of 0.05 per each 1000 psi (7 MPa) of strength in excess of 4000 psi (28 MPa), but is not taken less than 0.65

$$\rho_{f.bal} := \alpha_1 \cdot \beta_1 \cdot \frac{f'_c}{f_{fu}} \cdot \left(\frac{\varepsilon_{cu}}{\varepsilon_{cu} + \varepsilon_{fu}}\right) = 0.01$$

$\rho_{f.bal}$ = fiber-reinforced polymer reinforcement ratio at a balanced

$Check := \text{if}\left(\rho_f > \rho_{f.bal}, \text{“Compression Failure”}, \text{“Tension Failure”}\right)$

$Check$ = “Tension Failure”

Calculate c_b and assume a c value bigger than c_b

Assume c

$$c_b := \frac{\varepsilon_{cu} \cdot d}{\varepsilon_{cu} + \varepsilon_{fu}} \qquad c < c_b \qquad c_{as1} := 4.501 \cdot mm$$

$$c_b = 6.186\ mm$$

$$\varepsilon_{c1} := \frac{c_{as1}}{d - c_{as1}} \cdot \varepsilon_{fu}$$

$$\varepsilon_{c1} = 0.002$$

Equivalent Stress Blocks

$$E_c := \left((4700) \cdot \sqrt{\frac{f'_c}{MPa}} \right) \cdot MPa \qquad E_c = \left(3.859 \cdot 10^4\right)\ MPa$$

$$\varepsilon'_u := \frac{1.71 \cdot f'_c}{E_c} \qquad \varepsilon'_u = 0.003$$

$$\beta_{1E1} := 2 - \frac{4 \cdot \left(\left(\frac{\varepsilon_{c1}}{\varepsilon'_u} \right) - \operatorname{atan}\left(\frac{\varepsilon_{c1}}{\varepsilon'_u} \right) \right)}{\left(\frac{\varepsilon_{c1}}{\varepsilon'_u} \right) \ln\left(\left(1 + \left(\frac{\varepsilon_{c1}}{\varepsilon'_u} \right)^2 \right) \right)} = 0.721 \qquad \alpha_{1E1} := 0.9 \frac{\ln\left(1 + \left(\frac{\varepsilon_{c1}}{\varepsilon'_u} \right)^2 \right)}{\beta_{1E1} \cdot \left(\frac{\varepsilon_{c1}}{\varepsilon'_u} \right)}$$

$$\beta_{1E1} = 0.721 \qquad \alpha_{1E1} = 0.711$$

Calculate c value

$$C_c := \alpha_{1E1} \cdot \beta_{1E1} \cdot f'_c \cdot c \cdot b \qquad T_f := A_f \cdot f_{fu}$$

$$c_{cal1} := \frac{A_f \cdot f_{fu}}{\alpha_{1E1} \cdot \beta_{1E1} \cdot f'_c \cdot b} \qquad c_{cal1} = 4.502\ mm \qquad c_{as1} < c_{cal}$$

$$Check. := \text{if}\left(c_{as1} - c_{cal1} < 10^{-3} \cdot mm, \text{“OK”}, \text{“Use new assumption”} \right)$$

$$Check. = \text{“OK”}$$

$$\beta_{1E} := \beta_{1E1}$$

$$\alpha_{1E} := \alpha_{1E1}$$

Nominal Moment Capacity

$$Mn := A_f \cdot f_{fu} \cdot \left(d - \frac{\beta_{1E} \cdot c_{cal1}}{2} \right) \qquad \rho_f < \rho_{f.bal} \qquad \phi := 0.55$$

$$Mn = 0.243 \ kip \cdot ft$$

$$Mu := \phi \cdot Mn$$

$$Mu = 0.133 \ kip \cdot ft$$

PCC Reinforced with 3D Printed Unidirectional GFRP

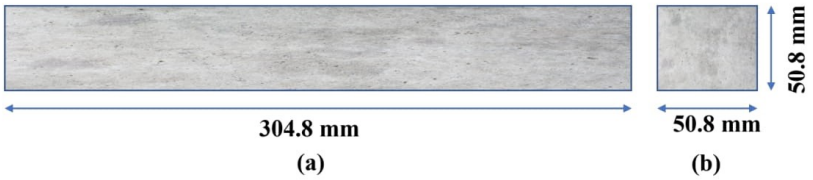

Section properties

$h := 50.8 \cdot mm$	h = height
$d := 43.3 \cdot mm$	d = depth
$b := 50.8 \cdot mm$	b = width
$L := 304.8 \cdot mm$	L = length
$f'_c := 67.4 \cdot MPa$	f'_c = specified compressive strength of concrete
$\varepsilon_{cu} := 0.003$	ε_{cu} = ultimate strain in concrete

Reinforcement properties

$f_{fu} := 624 \cdot MPa$	f_{fu} = design tensile strength of FRP
$E_f := 16.5 \cdot GPa$	E_f = design or guaranteed modulus of elasticity of FRP
$A_f := 15 \cdot mm^2$	A_f = Area of reinforcement
$\varepsilon_{fu} := 0.0367$	ε_f = Strain in FRP

Equilibrium Condition

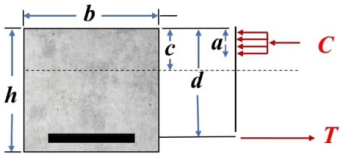

C = Compression force

a = depth of equivalent rectangular stress block

T = tension force

c = distance from extreme compression fiber to the neutral axis

C=T

$\alpha_1 := 0.85$

α_1 = ratio of average stress of equivalent rectangular stress block to fc′

$$\beta_1 := \max\left((0.85) - 0.05 \cdot \left(\frac{f'_c - 28 \cdot MPa}{7\ MPa}\right), 0.65\right)$$

$\beta_1 = 0.65$

Reinforcement ratio - Failure Mode

$$\rho_f := \frac{A_f}{b \cdot d} = 0.007$$

ρ_f = fiber-reinforced polymer reinforcement ratio

ACI 440.1R-15:2.1

β1 = factor taken as 0.85 for concrete strength *fc′* up to and including 4000 psi (28 MPa). For strength above 4000 psi (28 MPa), this factor is reduced continuously at a rate of 0.05 per each 1000 psi (7 MPa) of strength in excess of 4000 psi (28 MPa), but is not taken less than 0.65

$$\rho_{f.bal} := \alpha_1 \cdot \beta_1 \cdot \frac{f'_c}{f_{fu}} \cdot \left(\frac{\varepsilon_{cu}}{\varepsilon_{cu} + \varepsilon_{fu}}\right) = 0.005$$

$\rho_{f.bal}$ = fiber-reinforced polymer reinforcement ratio at a balanced

$Check := \text{if}\left(\rho_f > \rho_{f.bal}, \text{“Compression Failure”}, \text{“Tension Failure”}\right)$

$Check$ = “Compression Failure”

Calculate c

$c < c_b$

$$c := \frac{-A_f \cdot E_f \cdot \varepsilon_{cu} + \sqrt{(A_f \cdot E_f \cdot \varepsilon_{cu})^2 + 4 \cdot \alpha_1 \cdot f'_c \cdot \beta_1 \cdot A_f \cdot E_f \cdot \varepsilon_{cu} \cdot b \cdot d}}{2 \cdot \alpha_1 \cdot f'_c \cdot \beta_1 \cdot b}$$

$c = 3.931\ mm$

FRP Stress

$$f_f := \frac{\alpha_1 \cdot f'_c \cdot \beta_1 \cdot b}{A_f} \cdot c = 495.75\ MPa$$

$f_f = 495.75\ MPa$ f_f = stress in FRP reinforcement in tension

$$a := \frac{A_f \cdot f_f}{0.85 \cdot f'_c \cdot b}$$

$a = 2.555\ mm$

$C := \alpha_1 \cdot f'_c \cdot \beta_1 \cdot c \cdot b$ $C = \langle 7.436 \cdot 10^3 \rangle\ N$

$T := A_f \cdot f_f$ $T = \langle 7.436 \cdot 10^3 \rangle\ N$

Nominal Moment Capacity

$$M_n := A_f \cdot f_f \cdot \left(d - \frac{a}{2}\right)$$ M_n = nominal moment capacity

$M_n = 0.312\ kN \cdot m$

PCC Reinforced with 3D Printed Multidirectional GFRP

(a) (b)

Section properties

$h := 50.8 \cdot mm$	h = height
$d := 43.3 \cdot mm$	d = depth
$b := 50.8 \cdot mm$	b = width
$L := 304.8 \cdot mm$	L = length
$f'_c := 67.4 \cdot MPa$	f'_c = specified compressive strength of concrete
$\varepsilon_{cu} := 0.003$	ε_{cu} = ultimate strain in concrete

Reinforcement properties

$f_{fu} := 146 \cdot MPa$	f_{fu} = design tensile strength of FRP
$E_f := 6.4 \cdot GPa$	E_f = design or guaranteed modulus of elasticity of FRP
$A_f := 93 \cdot mm^2$	A_f = Area of reinforcement
$\varepsilon_{fu} := 0.0367$	ε_f = Strain in FRP

Equilibrium Condition

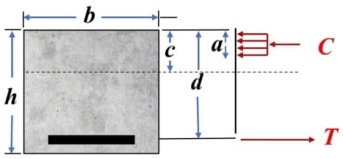

C=T

C = Compression force

a = depth of equivalent rectangular stress block

T = tension force

c = distance from extreme compression fiber to the neutral axis

$\alpha_1 := 0.85$

α_1 = ratio of average stress of equivalent rectangular stress block to fc′

$$\beta_1 := \max\left((0.85) - 0.05 \cdot \left(\frac{f'_c - 28 \cdot MPa}{7\ MPa}\right), 0.65\right)$$

$\beta_1 = 0.65$

Reinforcement ratio - Failure Mode

$$\rho_f := \frac{A_f}{b \cdot d} = 0.042$$

ρ_f = fiber-reinforced polymer reinforcement ratio

ACI 440.1R-15:2.1

β1 = factor taken as 0.85 for concrete strength *fc′* up to and including 4000 psi (28 MPa). For strength above 4000 psi (28 MPa), this factor is reduced continuously at a rate of 0.05 per each 1000 psi (7 MPa) of strength in excess of 4000 psi (28 MPa), but is not taken less than 0.65

$$\rho_{f.bal} := \alpha_1 \cdot \beta_1 \cdot \frac{f'_c}{f_{fu}} \cdot \left(\frac{\varepsilon_{cu}}{\varepsilon_{cu} + \varepsilon_{fu}}\right) = 0.019$$

$\rho_{f.bal}$ = fiber-reinforced polymer reinforcement ratio at a balanced

$Check := \text{if}\left(\rho_f > \rho_{f.bal}, \text{“Compression Failure”}, \text{“Tension Failure”}\right)$

$Check$ = “Compression Failure”

Calculate c

$c < c_b$

$$c := \frac{-A_f \cdot E_f \cdot \varepsilon_{cu} + \sqrt{(A_f \cdot E_f \cdot \varepsilon_{cu})^2 + 4 \cdot \alpha_1 \cdot f'_c \cdot \beta_1 \cdot A_f \cdot E_f \cdot \varepsilon_{cu} \cdot b \cdot d}}{2 \cdot \alpha_1 \cdot f'_c \cdot \beta_1 \cdot b}$$

$c = 5.938\ mm$

FRP Stress

$$f_f := \frac{\alpha_1 \cdot f'_c \cdot \beta_1 \cdot b}{A_f} \cdot c = 120.795\ MPa$$

$f_f = 120.795\ MPa$ f_f = stress in FRP reinforcement in tension

$$a := \frac{A_f \cdot f_f}{0.85 \cdot f'_c \cdot b}$$

$a = 3.86\ mm$

$C := \alpha_1 \cdot f'_c \cdot \beta_1 \cdot c \cdot b$ $C = (1.123 \cdot 10^4)\ N$

$T := A_f \cdot f_f$ $T = (1.123 \cdot 10^4)\ N$

Nominal Moment Capacity

$M_n := A_f \cdot f_f \cdot \left(d - \frac{a}{2}\right)$ M_n = nominal moment capacity

$M_n = 0.465\ kN \cdot m$

PolC Reinforced with VAHT Unidirectional GFRP

(a) (b)

Section properties

$h := 50.8 \cdot mm$ h = height

$d := 43.3 \cdot mm$ d = depth

$b := 50.8 \cdot mm$ b = width

$L := 304.8 \cdot mm$ L = length

$f'_c := 59.9 \cdot MPa$ f'_c = specified compressive strength of concrete

$\varepsilon_{cu} := 0.003$ ε_{cu} = ultimate strain in concrete

Reinforcement properties

$f_{fu} := 526.4 \cdot MPa$ f_{fu} = design tensile strength of FRP

$E_f := 29.2 \cdot GPa$ E_f = design or guaranteed modulus of elasticity of FRP

$A_f := 15 \cdot mm^2$ A_f = Area of reinforcement

$\varepsilon_{fu} := 0.018$ ε_{fu} = Strain in FRP

Equilibrium Condition

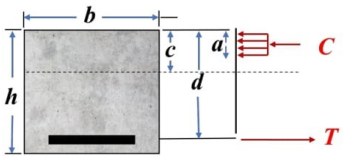

C = Compression force

a = depth of equivalent rectangular stress block

T = tension force

c = distance from extreme compression fiber to the neutral axis

C=T

$\alpha_1 := 0.85$

α_1 = ratio of average stress of equivalent rectangular stress block to fc′

$$\beta_1 := \max\left((0.85) - 0.05 \cdot \left(\frac{f'_c - 28 \cdot MPa}{7\ MPa}\right), 0.65\right)$$

$\beta_1 = 0.65$

Reinforcement ratio - Failure Mode

$$\rho_f := \frac{A_f}{b \cdot d}$$

ρ_f = fiber-reinforced polymer reinforcement ratio

ACI 440.1R-15:2.1

β1 = factor taken as 0.85 for concrete strength *fc′* up to and including 4000 psi (28 MPa). For strength above 4000 psi (28 MPa), this factor is reduced continuously at a rate of 0.05 per each 1000 psi (7 MPa) of strength in excess of 4000 psi (28 MPa), but is not taken less than 0.65

$$\rho_{f.bal} := \alpha_1 \cdot \beta_1 \cdot \frac{f'_c}{f_{fu}} \cdot \left(\frac{\varepsilon_{cu}}{\varepsilon_{cu} + \varepsilon_{fu}}\right) = 0.009$$

$\rho_{f.bal}$ = fiber-reinforced polymer reinforcement ratio at a balanced

$Check := \text{if}\left(\rho_f > \rho_{f.bal}, \text{“Compression Failure”}, \text{“Tension Failure”}\right)$

$Check$ = “Tension Failure”

Calculate c_b and assume a c value bigger than c_b

Assume c

$$c_b := \frac{\varepsilon_{cu} \cdot d}{\varepsilon_{cu} + \varepsilon_{fu}} \qquad c < c_b \qquad c_{as1} := 4.723 \cdot mm$$

$$c_b = 6.186\ mm$$

$$\varepsilon_{c1} := \frac{c_{as1}}{d - c_{as1}} \cdot \varepsilon_{fu}$$

$$\varepsilon_{c1} = 0.002$$

Equivalent Stress Blocks

$$E_c := \left((4700) \cdot \sqrt{\frac{f'_c}{MPa}} \right) \cdot MPa \qquad E_c = \left(3.638 \cdot 10^4\right)\ MPa$$

$$\varepsilon'_u := \frac{1.71 \cdot f'_c}{E_c} \qquad \varepsilon'_u = 0.003$$

$$\beta_{1E1} := 2 - \frac{4 \cdot \left(\left(\frac{\varepsilon_{c1}}{\varepsilon'_u} \right) - \operatorname{atan}\left(\frac{\varepsilon_{c1}}{\varepsilon'_u} \right) \right)}{\left(\frac{\varepsilon_{c1}}{\varepsilon'_u} \right) \ln\left(\left(1 + \left(\frac{\varepsilon_{c1}}{\varepsilon'_u} \right)^2 \right) \right)} = 0.732 \qquad \alpha_{1E1} := 0.9 \frac{\ln\left(1 + \left(\frac{\varepsilon_{c1}}{\varepsilon'_u} \right)^2 \right)}{\beta_{1E1} \cdot \left(\frac{\varepsilon_{c1}}{\varepsilon'_u} \right)}$$

$$\beta_{1E1} = 0.732 \qquad \alpha_{1E1} = 0.751$$

Calculate c value

$$C_c := \alpha_{1E1} \cdot \beta_{1E1} \cdot f'_c \cdot c \cdot b \qquad T_f := A_f \cdot f_{fu}$$

$$c_{cal1} := \frac{A_f \cdot f_{fu}}{\alpha_{1E1} \cdot \beta_{1E1} \cdot f'_c \cdot b} \qquad c_{cal1} = 4.723\ mm \qquad c_{as1} < c_{cal}$$

$$Check. := \text{if}\left(c_{as1} - c_{cal1} < 10^{-3} \cdot mm, \text{“OK”}, \text{“Use new assumption”} \right)$$

$$Check. = \text{“OK”}$$

$$\beta_{1E} := \beta_{1E1}$$

$$\alpha_{1E} := \alpha_{1E1}$$

Nominal Moment Capacity

$$Mn := A_f \cdot f_{fu} \cdot \left(d - \frac{\beta_{1E} \cdot c_{cal1}}{2} \right) \qquad \rho_f < \rho_{f.bal} \qquad \phi := 0.55$$

$$Mn = 0.242 \ kip \cdot ft$$

$$Mu := \phi \cdot Mn$$

$$Mu = 0.133 \ kip \cdot ft$$

PolC Reinforced with 3D Printed Unidirectional GFRP

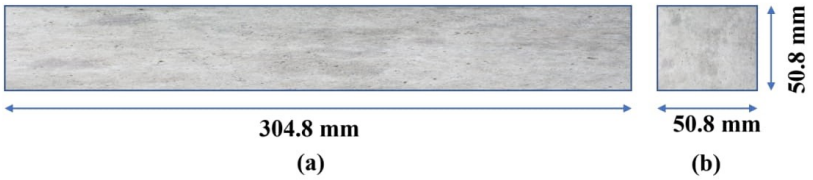

Section properties

$h := 50.8 \cdot mm$	h = height
$d := 43.3 \cdot mm$	d = depth
$b := 50.8 \cdot mm$	b = width
$L := 304.8 \cdot mm$	L = length
$f'_c := 59.9 \cdot MPa$	f'_c = specified compressive strength of concrete
$\varepsilon_{cu} := 0.003$	ε_{cu} = ultimate strain in concrete

Reinforcement properties

$f_{fu} := 526.4 \cdot MPa$	f_{fu} = design tensile strength of FRP
$E_f := 16.5 \cdot GPa$	E_f = design or guaranteed modulus of elasticity of FRP
$A_f := 15 \cdot mm^2$	A_f = Area of reinforcement
$\varepsilon_{fu} := 0.0386$	ε_{fu} = Strain in FRP

Equilibrium Condition

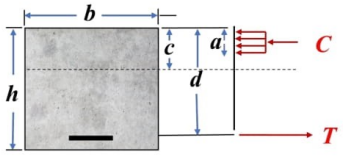

C = Compression force

a = depth of equivalent rectangular stress block

T = tension force

c = distance from extreme compression fiber to the neutral axis

C=T

$\alpha_1 := 0.85$

α_1 = ratio of average stress of equivalent rectangular stress block to fc′

$$\beta_1 := \max\left((0.85) - 0.05 \cdot \left(\frac{f'_c - 28 \cdot MPa}{7\ MPa}\right), 0.65\right)$$

$\beta_1 = 0.65$

Reinforcement ratio - Failure Mode

$$\rho_f := \frac{A_f}{b \cdot d} = 0.007$$

ρ_f = fiber-reinforced polymer reinforcement ratio

ACI 440.1R-15:2.1

β1 = factor taken as 0.85 for concrete strength *fc′* up to and including 4000 psi (28 MPa). For strength above 4000 psi (28 MPa), this factor is reduced continuously at a rate of 0.05 per each 1000 psi (7 MPa) of strength in excess of 4000 psi (28 MPa), but is not taken less than 0.65

$$\rho_{f.bal} := \alpha_1 \cdot \beta_1 \cdot \frac{f'_c}{f_{fu}} \cdot \left(\frac{\varepsilon_{cu}}{\varepsilon_{cu} + \varepsilon_{fu}}\right) = 0.005$$

$\rho_{f.bal}$ = fiber-reinforced polymer reinforcement ratio at a balanced

$Check := \text{if}\left(\rho_f > \rho_{f.bal}, \text{“Compression Failure”}, \text{“Tension Failure”}\right)$

$Check$ = “Compression Failure”

Calculate c

$c < c_b$

$$c := \frac{-A_f \cdot E_f \cdot \varepsilon_{cu} + \sqrt{(A_f \cdot E_f \cdot \varepsilon_{cu})^2 + 4 \cdot \alpha_1 \cdot f'_c \cdot \beta_1 \cdot A_f \cdot E_f \cdot \varepsilon_{cu} \cdot b \cdot d}}{2 \cdot \alpha_1 \cdot f'_c \cdot \beta_1 \cdot b}$$

$c = 4.158\ mm$

FRP Stress

$$f_f := \frac{\alpha_1 \cdot f'_c \cdot \beta_1 \cdot b}{A_f} \cdot c$$

$f_f = 466.006\ MPa$ f_f = stress in FRP reinforcement in tension

$$a := \frac{A_f \cdot f_f}{0.85 \cdot f'_c \cdot b}$$

$a = 2.703\ mm$

$C := \alpha_1 \cdot f'_c \cdot \beta_1 \cdot c \cdot b$ $C = (6.99 \cdot 10^3)\ N$

$T := A_f \cdot f_f$ $T = (6.99 \cdot 10^3)\ N$

Nominal Moment Capacity

$$M_n := A_f \cdot f_f \cdot \left(d - \frac{a}{2}\right)$$ M_n = nominal moment capacity

$M_n = 0.293\ kN \cdot m$

PolC Reinforced with 3D Printed Multidirectional GFRP

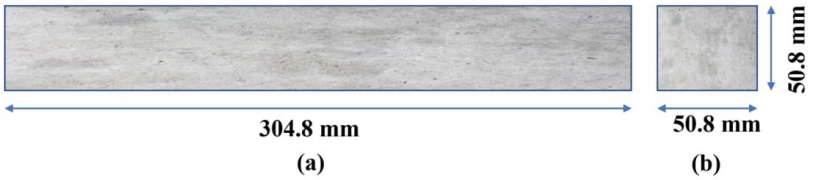

Section properties

$h := 50.8 \cdot mm$	h = height
$d := 43.3 \cdot mm$	d = depth
$b := 50.8 \cdot mm$	b = width
$L := 304.8 \cdot mm$	L = length
$f'_c := 59.9 \cdot MPa$	f'_c = specified compressive strength of concrete
$\varepsilon_{cu} := 0.003$	ε_{cu} = ultimate strain in concrete

Reinforcement properties

$f_{fu} := 526.4 \cdot MPa$	f_{fu} = design tensile strength of FRP
$E_f := 6.4 \cdot GPa$	E_f = design or guaranteed modulus of elasticity of FRP
$A_f := 93 \cdot mm^2$	A_f = Area of reinforcement
$\varepsilon_{fu} := 0.0367$	ε_{fu} = Strain in FRP

Equilibrium Condition

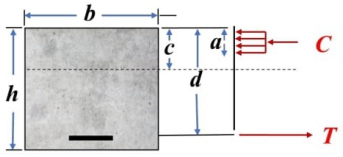

C = Compression force

a = depth of equivalent rectangular stress block

T = tension force

c = distance from extreme compression fiber to the neutral axis

C=T

$\alpha_1 := 0.85$

α_1 = ratio of average stress of equivalent rectangular stress block to fc′

$$\beta_1 := \max\left((0.85) - 0.05 \cdot \left(\frac{f'_c - 28 \cdot MPa}{7\ MPa}\right), 0.65\right)$$

$\beta_1 = 0.65$

Reinforcement ratio - Failure Mode

$$\rho_f := \frac{A_f}{b \cdot d} = 0.042$$

ρ_f = fiber-reinforced polymer reinforcement ratio

ACI 440.1R-15:2.1

β1 = factor taken as 0.85 for concrete strength *fc′* up to and including 4000 psi (28 MPa). For strength above 4000 psi (28 MPa), this factor is reduced continuously at a rate of 0.05 per each 1000 psi (7 MPa) of strength in excess of 4000 psi (28 MPa), but is not taken less than 0.65

$$\rho_{f.bal} := \alpha_1 \cdot \beta_1 \cdot \frac{f'_c}{f_{fu}} \cdot \left(\frac{\varepsilon_{cu}}{\varepsilon_{cu} + \varepsilon_{fu}}\right) = 0.005$$

$\rho_{f.bal}$ = fiber-reinforced polymer reinforcement ratio at a balanced

$Check := \text{if}\left(\rho_f > \rho_{f.bal}, \text{“Compression Failure”}, \text{“Tension Failure”}\right)$

$Check$ = “Compression Failure”

Calculate c

$c < c_b$

$$c := \frac{-A_f \cdot E_f \cdot \varepsilon_{cu} + \sqrt{(A_f \cdot E_f \cdot \varepsilon_{cu})^2 + 4 \cdot \alpha_1 \cdot f'_c \cdot \beta_1 \cdot A_f \cdot E_f \cdot \varepsilon_{cu} \cdot b \cdot d}}{2 \cdot \alpha_1 \cdot f'_c \cdot \beta_1 \cdot b}$$

$c = 6.271\ mm$

FRP Stress

$$f_f := \frac{\alpha_1 \cdot f'_c \cdot \beta_1 \cdot b}{A_f} \cdot c$$

$f_f = 113.368\ MPa$ f_f = stress in FRP reinforcement in tension

$$a := \frac{A_f \cdot f_f}{0.85 \cdot f'_c \cdot b}$$

$a = 4.076\ mm$

$C := \alpha_1 \cdot f'_c \cdot \beta_1 \cdot c \cdot b$ $C = (1.054 \cdot 10^4)\ N$

$T := A_f \cdot f_f$ $T = (1.054 \cdot 10^4)\ N$

Nominal Moment Capacity

$$M_n := A_f \cdot f_f \cdot \left(d - \frac{a}{2}\right)$$ M_n = nominal moment capacity

$M_n = 0.435\ kN \cdot m$

PCC Reinforced with 3D Printed Unidirectional GFRP

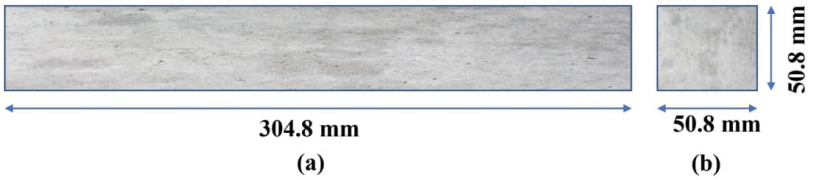

Section properties

$h := 50.8 \cdot mm$	h = height
$d := 43.3 \cdot mm$	d = depth
$b := 50.8 \cdot mm$	b = width
$L := 304.8 \cdot mm$	L = length
$f'_c := 67.4 \cdot MPa$	f'_c = specified compressive strength of concrete
$\varepsilon_{cu} := 0.003$	ε_{cu} = ultimate strain in concrete

Reinforcement properties

$f_{fu} := 624 \cdot MPa$	f_{fu} = design tensile strength of FRP
$E_f := 16.5 \cdot GPa$	E_f = design or guaranteed modulus of elasticity of FRP
$A_f := 15 \cdot mm^2$	A_f = Area of reinforcement
$\varepsilon_{fu} := 0.0367$	ε_f = Strain in FRP

Equilibrium Condition

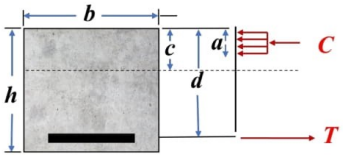

C = Compression force

a = depth of equivalent rectangular stress block

T = tension force

c = distance from extreme compression fiber to the neutral axis

C=T

$\alpha_1 := 0.85$

α_1 = ratio of average stress of equivalent rectangular stress block to fc′

$$\beta_1 := \max\left((0.85) - 0.05 \cdot \left(\frac{f'_c - 28 \cdot MPa}{7\ MPa}\right), 0.65\right)$$

$\beta_1 = 0.65$

Reinforcement ratio - Failure Mode

$$\rho_f := \frac{A_f}{b \cdot d} = 0.007$$

ρ_f = fiber-reinforced polymer reinforcement ratio

ACI 440.1R-15:2.1

β1 = factor taken as 0.85 for concrete strength *fc′* up to and including 4000 psi (28 MPa). For strength above 4000 psi (28 MPa), this factor is reduced continuously at a rate of 0.05 per each 1000 psi (7 MPa) of strength in excess of 4000 psi (28 MPa), but is not taken less than 0.65

$$\rho_{f.bal} := \alpha_1 \cdot \beta_1 \cdot \frac{f'_c}{f_{fu}} \cdot \left(\frac{\varepsilon_{cu}}{\varepsilon_{cu} + \varepsilon_{fu}}\right) = 0.005$$

$\rho_{f.bal}$ = fiber-reinforced polymer reinforcement ratio at a balanced

$Check := \text{if}\left(\rho_f > \rho_{f.bal}, \text{“Compression Failure”}, \text{“Tension Failure”}\right)$

$Check$ = “Compression Failure”

Calculate c

$c < c_b$

$$c := \frac{-A_f \cdot E_f \cdot \varepsilon_{cu} + \sqrt{(A_f \cdot E_f \cdot \varepsilon_{cu})^2 + 4 \cdot \alpha_1 \cdot f'_c \cdot \beta_1 \cdot A_f \cdot E_f \cdot \varepsilon_{cu} \cdot b \cdot d}}{2 \cdot \alpha_1 \cdot f'_c \cdot \beta_1 \cdot b}$$

$c = 3.931\ mm$

FRP Stress

$$f_f := \frac{\alpha_1 \cdot f'_c \cdot \beta_1 \cdot b}{A_f} \cdot c = 495.75\ MPa$$

$f_f = 495.75\ MPa$ f_f = stress in FRP reinforcement in tension

$$a := \frac{A_f \cdot f_f}{0.85 \cdot f'_c \cdot b}$$

$a = 2.555\ mm$

$C := \alpha_1 \cdot f'_c \cdot \beta_1 \cdot c \cdot b$ $C = \langle 7.436 \cdot 10^3 \rangle\ N$

$T := A_f \cdot f_f$ $T = \langle 7.436 \cdot 10^3 \rangle\ N$

Nominal Moment Capacity

$$M_n := A_f \cdot f_f \cdot \left(d - \frac{a}{2}\right)$$ M_n = nominal moment capacity

$M_n = 0.312\ kN \cdot m$

PCC Reinforced with 3D Printed Multidirectional GFRP

(a) (b)

Section properties

$h := 50.8 \cdot mm$	h = height
$d := 43.3 \cdot mm$	d = depth
$b := 50.8 \cdot mm$	b = width
$L := 304.8 \cdot mm$	L = length
$f'_c := 67.4 \cdot MPa$	f'_c = specified compressive strength of concrete
$\varepsilon_{cu} := 0.003$	ε_{cu} = ultimate strain in concrete

Reinforcement properties

$f_{fu} := 146 \cdot MPa$	f_{fu} = design tensile strength of FRP
$E_f := 6.4 \cdot GPa$	E_f = design or guaranteed modulus of elasticity of FRP
$A_f := 93 \cdot mm^2$	A_f = Area of reinforcement
$\varepsilon_{fu} := 0.0367$	ε_f = Strain in FRP

Equilibrium Condition

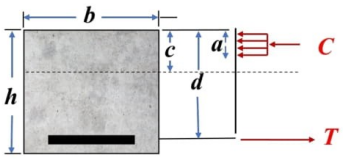

C=T

C = Compression force

a = depth of equivalent rectangular stress block

T = tension force

c = distance from extreme compression fiber to the neutral axis

$\alpha_1 := 0.85$

α_1 = ratio of average stress of equivalent rectangular stress block to fc′

$$\beta_1 := \max\left((0.85) - 0.05 \cdot \left(\frac{f'_c - 28 \cdot MPa}{7\ MPa}\right), 0.65\right)$$

$\beta_1 = 0.65$

Reinforcement ratio - Failure Mode

$$\rho_f := \frac{A_f}{b \cdot d} = 0.042$$

ρ_f = fiber-reinforced polymer reinforcement ratio

ACI 440.1R-15:2.1

β1 = factor taken as 0.85 for concrete strength *fc′* up to and including 4000 psi (28 MPa). For strength above 4000 psi (28 MPa), this factor is reduced continuously at a rate of 0.05 per each 1000 psi (7 MPa) of strength in excess of 4000 psi (28 MPa), but is not taken less than 0.65

$$\rho_{f.bal} := \alpha_1 \cdot \beta_1 \cdot \frac{f'_c}{f_{fu}} \cdot \left(\frac{\varepsilon_{cu}}{\varepsilon_{cu} + \varepsilon_{fu}}\right) = 0.019$$

$\rho_{f.bal}$ = fiber-reinforced polymer reinforcement ratio at a balanced

$Check := \text{if}\left(\rho_f > \rho_{f.bal}, \text{“Compression Failure”}, \text{“Tension Failure”}\right)$

$Check$ = “Compression Failure”

Calculate c

$c < c_b$

$$c := \frac{-A_f \cdot E_f \cdot \varepsilon_{cu} + \sqrt{(A_f \cdot E_f \cdot \varepsilon_{cu})^2 + 4 \cdot \alpha_1 \cdot f'_c \cdot \beta_1 \cdot A_f \cdot E_f \cdot \varepsilon_{cu} \cdot b \cdot d}}{2 \cdot \alpha_1 \cdot f'_c \cdot \beta_1 \cdot b}$$

$c = 5.938\ mm$

FRP Stress

$$f_f := \frac{\alpha_1 \cdot f'_c \cdot \beta_1 \cdot b}{A_f} \cdot c = 120.795\ MPa$$

$f_f = 120.795\ MPa$ f_f = stress in FRP reinforcement in tension

$$a := \frac{A_f \cdot f_f}{0.85 \cdot f'_c \cdot b}$$

$a = 3.86\ mm$

$C := \alpha_1 \cdot f'_c \cdot \beta_1 \cdot c \cdot b$ $C = (1.123 \cdot 10^4)\ N$

$T := A_f \cdot f_f$ $T = (1.123 \cdot 10^4)\ N$

Nominal Moment Capacity

$$M_n := A_f \cdot f_f \cdot \left(d - \frac{a}{2}\right)$$ M_n = nominal moment capacity

$M_n = 0.465\ kN \cdot m$

PolC Reinforced with VAHT Unidirectional GFRP

(a) (b)

Section properties

$h := 50.8 \cdot mm$	h = height
$d := 43.3 \cdot mm$	d = depth
$b := 50.8 \cdot mm$	b = width
$L := 304.8 \cdot mm$	L = length
$f'_c := 59.9 \cdot MPa$	f'_c = specified compressive strength of concrete
$\varepsilon_{cu} := 0.003$	ε_{cu} = ultimate strain in concrete

Reinforcement properties

$f_{fu} := 526.4 \cdot MPa$	f_{fu} = design tensile strength of FRP
$E_f := 29.2 \cdot GPa$	E_f = design or guaranteed modulus of elasticity of FRP
$A_f := 15 \cdot mm^2$	A_f = Area of reinforcement
$\varepsilon_{fu} := 0.018$	ε_{fu} = Strain in FRP

Equilibrium Condition

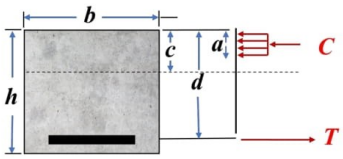

C = Compression force

a = depth of equivalent rectangular stress block

T = tension force

c = distance from extreme compression fiber to the neutral axis

C=T

$\alpha_1 := 0.85$

α_1 = ratio of average stress of equivalent rectangular stress block to fc′

$$\beta_1 := \max\left((0.85) - 0.05 \cdot \left(\frac{f'_c - 28 \cdot MPa}{7\ MPa}\right), 0.65\right)$$

$\beta_1 = 0.65$

Reinforcement ratio - Failure Mode

$$\rho_f := \frac{A_f}{b \cdot d}$$

ρ_f = fiber-reinforced polymer reinforcement ratio

ACI 440.1R-15:2.1

β1 = factor taken as 0.85 for concrete strength *fc′* up to and including 4000 psi (28 MPa). For strength above 4000 psi (28 MPa), this factor is reduced continuously at a rate of 0.05 per each 1000 psi (7 MPa) of strength in excess of 4000 psi (28 MPa), but is not taken less than 0.65

$$\rho_{f.bal} := \alpha_1 \cdot \beta_1 \cdot \frac{f'_c}{f_{fu}} \cdot \left(\frac{\varepsilon_{cu}}{\varepsilon_{cu} + \varepsilon_{fu}}\right) = 0.009$$

$\rho_{f.bal}$ = fiber-reinforced polymer reinforcement ratio at a balanced

$Check := \text{if}\left(\rho_f > \rho_{f.bal}, \text{“Compression Failure”}, \text{“Tension Failure”}\right)$

$Check$ = “Tension Failure”

Calculate c_b and assume a c value bigger than c_b

Assume c

$$c_b := \frac{\varepsilon_{cu} \cdot d}{\varepsilon_{cu} + \varepsilon_{fu}} \qquad c < c_b \qquad c_{as1} := 4.723 \cdot mm$$

$$c_b = 6.186\ mm$$

$$\varepsilon_{c1} := \frac{c_{as1}}{d - c_{as1}} \cdot \varepsilon_{fu}$$

$$\varepsilon_{c1} = 0.002$$

Equivalent Stress Blocks

$$E_c := \left((4700) \cdot \sqrt{\frac{f'_c}{MPa}} \right) \cdot MPa \qquad E_c = \left(3.638 \cdot 10^4\right)\ MPa$$

$$\varepsilon'_u := \frac{1.71 \cdot f'_c}{E_c} \qquad \varepsilon'_u = 0.003$$

$$\beta_{1E1} := 2 - \frac{4 \cdot \left(\left(\frac{\varepsilon_{c1}}{\varepsilon'_u} \right) - \operatorname{atan}\left(\frac{\varepsilon_{c1}}{\varepsilon'_u} \right) \right)}{\left(\frac{\varepsilon_{c1}}{\varepsilon'_u} \right) \ln\left(\left(1 + \left(\frac{\varepsilon_{c1}}{\varepsilon'_u} \right)^2 \right) \right)} = 0.732 \qquad \alpha_{1E1} := 0.9 \frac{\ln\left(1 + \left(\frac{\varepsilon_{c1}}{\varepsilon'_u} \right)^2 \right)}{\beta_{1E1} \cdot \left(\frac{\varepsilon_{c1}}{\varepsilon'_u} \right)}$$

$$\beta_{1E1} = 0.732 \qquad \alpha_{1E1} = 0.751$$

Calculate c value

$$C_c := \alpha_{1E1} \cdot \beta_{1E1} \cdot f'_c \cdot c \cdot b \qquad T_f := A_f \cdot f_{fu}$$

$$c_{cal1} := \frac{A_f \cdot f_{fu}}{\alpha_{1E1} \cdot \beta_{1E1} \cdot f'_c \cdot b} \qquad c_{cal1} = 4.723\ mm \qquad c_{as1} < c_{cal}$$

$$Check. := \text{if}\left(c_{as1} - c_{cal1} < 10^{-3} \cdot mm, \text{“OK”}, \text{“Use new assumption”} \right)$$

$$Check. = \text{“OK”}$$

$$\beta_{1E} := \beta_{1E1}$$

$$\alpha_{1E} := \alpha_{1E1}$$

Nominal Moment Capacity

$$Mn := A_f \cdot f_{fu} \cdot \left(d - \frac{\beta_{1E} \cdot c_{cal1}}{2} \right) \qquad \rho_f < \rho_{f.bal} \qquad \phi := 0.55$$

$$Mn = 0.242 \ kip \cdot ft$$

$$Mu := \phi \cdot Mn$$

$$Mu = 0.133 \ kip \cdot ft$$

PolC Reinforced with 3D Printed Unidirectional GFRP

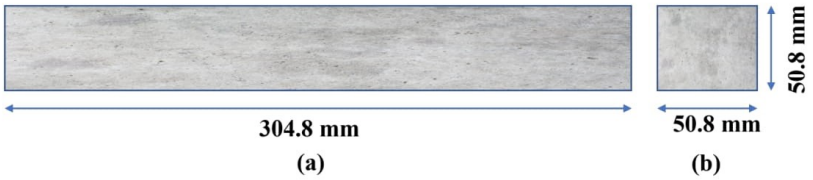

Section properties

$h := 50.8 \cdot mm$	h = height
$d := 43.3 \cdot mm$	d = depth
$b := 50.8 \cdot mm$	b = width
$L := 304.8 \cdot mm$	L = length
$f'_c := 59.9 \cdot MPa$	f'_c = specified compressive strength of concrete
$\varepsilon_{cu} := 0.003$	ε_{cu} = ultimate strain in concrete

Reinforcement properties

$f_{fu} := 526.4 \cdot MPa$	f_{fu} = design tensile strength of FRP
$E_f := 16.5 \cdot GPa$	E_f = design or guaranteed modulus of elasticity of FRP
$A_f := 15 \cdot mm^2$	A_f = Area of reinforcement
$\varepsilon_{fu} := 0.0386$	ε_{fu} = Strain in FRP

Equilibrium Condition

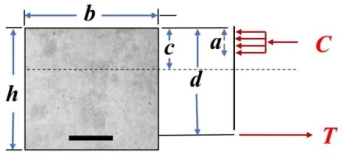

C = Compression force

a = depth of equivalent rectangular stress block

T = tension force

c = distance from extreme compression fiber to the neutral axis

C=T

$\alpha_1 := 0.85$

α_1 = ratio of average stress of equivalent rectangular stress block to fc′

$$\beta_1 := \max\left((0.85) - 0.05 \cdot \left(\frac{f'_c - 28 \cdot MPa}{7\ MPa}\right), 0.65\right)$$

$\beta_1 = 0.65$

Reinforcement ratio - Failure Mode

$$\rho_f := \frac{A_f}{b \cdot d} = 0.007$$

ρ_f = fiber-reinforced polymer reinforcement ratio

ACI 440.1R-15:2.1

β1 = factor taken as 0.85 for concrete strength *fc′* up to and including 4000 psi (28 MPa). For strength above 4000 psi (28 MPa), this factor is reduced continuously at a rate of 0.05 per each 1000 psi (7 MPa) of strength in excess of 4000 psi (28 MPa), but is not taken less than 0.65

$$\rho_{f.bal} := \alpha_1 \cdot \beta_1 \cdot \frac{f'_c}{f_{fu}} \cdot \left(\frac{\varepsilon_{cu}}{\varepsilon_{cu} + \varepsilon_{fu}}\right) = 0.005$$

$\rho_{f.bal}$ = fiber-reinforced polymer reinforcement ratio at a balanced

$Check := \text{if}\left(\rho_f > \rho_{f.bal}, \text{“Compression Failure”}, \text{“Tension Failure”}\right)$

$Check$ = “Compression Failure”

Calculate c

$c < c_b$

$$c := \frac{-A_f \cdot E_f \cdot \varepsilon_{cu} + \sqrt{(A_f \cdot E_f \cdot \varepsilon_{cu})^2 + 4 \cdot \alpha_1 \cdot f'_c \cdot \beta_1 \cdot A_f \cdot E_f \cdot \varepsilon_{cu} \cdot b \cdot d}}{2 \cdot \alpha_1 \cdot f'_c \cdot \beta_1 \cdot b}$$

$c = 4.158\ mm$

FRP Stress

$$f_f := \frac{\alpha_1 \cdot f'_c \cdot \beta_1 \cdot b}{A_f} \cdot c$$

$f_f = 466.006\ MPa$ f_f = stress in FRP reinforcement in tension

$$a := \frac{A_f \cdot f_f}{0.85 \cdot f'_c \cdot b}$$

$a = 2.703\ mm$

$C := \alpha_1 \cdot f'_c \cdot \beta_1 \cdot c \cdot b$ $C = (6.99 \cdot 10^3)\ N$

$T := A_f \cdot f_f$ $T = (6.99 \cdot 10^3)\ N$

Nominal Moment Capacity

$$M_n := A_f \cdot f_f \cdot \left(d - \frac{a}{2}\right)$$ M_n = nominal moment capacity

$M_n = 0.293\ kN \cdot m$

PolC Reinforced with 3D Printed Multidirectional GFRP

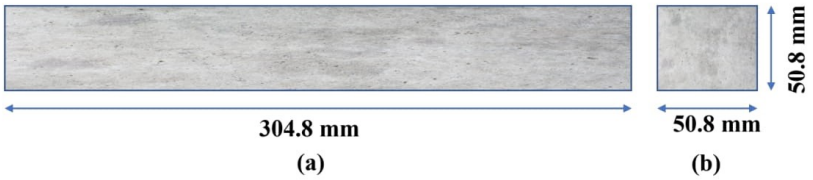

Section properties

$h := 50.8 \cdot mm$	h = height
$d := 43.3 \cdot mm$	d = depth
$b := 50.8 \cdot mm$	b = width
$L := 304.8 \cdot mm$	L = length
$f'_c := 59.9 \cdot MPa$	f'_c = specified compressive strength of concrete
$\varepsilon_{cu} := 0.003$	ε_{cu} = ultimate strain in concrete

Reinforcement properties

$f_{fu} := 526.4 \cdot MPa$	f_{fu} = design tensile strength of FRP
$E_f := 6.4 \cdot GPa$	E_f = design or guaranteed modulus of elasticity of FRP
$A_f := 93 \cdot mm^2$	A_f = Area of reinforcement
$\varepsilon_{fu} := 0.0367$	ε_{fu} = Strain in FRP

Equilibrium Condition

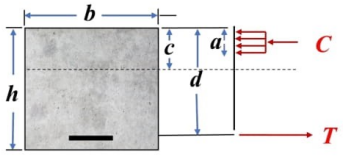

C = Compression force

a = depth of equivalent rectangular stress block

T = tension force

c = distance from extreme compression fiber to the neutral axis

C=T

$\alpha_1 := 0.85$

α_1 = ratio of average stress of equivalent rectangular stress block to fc′

$$\beta_1 := \max\left((0.85) - 0.05 \cdot \left(\frac{f'_c - 28 \cdot MPa}{7\ MPa}\right), 0.65\right)$$

$\beta_1 = 0.65$

Reinforcement ratio - Failure Mode

$$\rho_f := \frac{A_f}{b \cdot d} = 0.042$$

ρ_f = fiber-reinforced polymer reinforcement ratio

ACI 440.1R-15:2.1

β1 = factor taken as 0.85 for concrete strength *fc′* up to and including 4000 psi (28 MPa). For strength above 4000 psi (28 MPa), this factor is reduced continuously at a rate of 0.05 per each 1000 psi (7 MPa) of strength in excess of 4000 psi (28 MPa), but is not taken less than 0.65

$$\rho_{f.bal} := \alpha_1 \cdot \beta_1 \cdot \frac{f'_c}{f_{fu}} \cdot \left(\frac{\varepsilon_{cu}}{\varepsilon_{cu} + \varepsilon_{fu}}\right) = 0.005$$

$\rho_{f.bal}$ = fiber-reinforced polymer reinforcement ratio at a balanced

$Check := \text{if}\left(\rho_f > \rho_{f.bal}, \text{“Compression Failure”}, \text{“Tension Failure”}\right)$

$Check$ = “Compression Failure”

Calculate c

$c < c_b$

$$c := \frac{-A_f \cdot E_f \cdot \varepsilon_{cu} + \sqrt{(A_f \cdot E_f \cdot \varepsilon_{cu})^2 + 4 \cdot \alpha_1 \cdot f'_c \cdot \beta_1 \cdot A_f \cdot E_f \cdot \varepsilon_{cu} \cdot b \cdot d}}{2 \cdot \alpha_1 \cdot f'_c \cdot \beta_1 \cdot b}$$

$c = 6.271\ mm$

FRP Stress

$$f_f := \frac{\alpha_1 \cdot f'_c \cdot \beta_1 \cdot b}{A_f} \cdot c$$

$f_f = 113.368\ MPa$ f_f = stress in FRP reinforcement in tension

$$a := \frac{A_f \cdot f_f}{0.85 \cdot f'_c \cdot b}$$

$a = 4.076\ mm$

$C := \alpha_1 \cdot f'_c \cdot \beta_1 \cdot c \cdot b$ $C = (1.054 \cdot 10^4)\ N$

$T := A_f \cdot f_f$ $T = (1.054 \cdot 10^4)\ N$

Nominal Moment Capacity

$$M_n := A_f \cdot f_f \cdot \left(d - \frac{a}{2}\right)$$ M_n = nominal moment capacity

$M_n = 0.435\ kN \cdot m$

Appendix B

Given :

FYFE Specifications (VAHT)

$\rho_r := 2.55 \cdot \frac{gm}{cm^3}$ ρ_r = density of the reinforcement

$\rho_c := \frac{M}{(A \cdot h \cdot 1000)}$ $\rho_c := \frac{M}{V}$

$w := 30\ mm$
$b := 30\ mm$
$h := 0.1\ cm$
$As := w \cdot b$
$As = (9 \cdot 10^{-4})\ m^2$
$V := 90\ cm^3$

Markford Specifications (3D Printed)

$\rho_f := 2.5 \cdot \frac{gm}{cm^3}$ ρ_f = density of the continuous fiber

$\rho_n := 1.5 \cdot \frac{gm}{cm^3}$ ρ_n = density of the specimen

$\rho_o := 1.2 \cdot \frac{gm}{cm^3}$ ρ_o = density of the onyx

$v := 0.53 \cdot cm^3$ v = volume of the onyx

$n := v \cdot \rho_o$ n = mass of the onyx

Solution

FYFE Specimens

1	*2*	*3*
$M_{f1} := 0.975 \cdot gm$	$M_{f2} := 0.984 \cdot gm$	$M_{f3} := 0.967 \cdot gm$
$M_{i1} := 1.174 \cdot gm$	$M_{i2} := 1.165 \cdot gm$	$M_{i3} := 1.151 \cdot gm$
$\rho_{c1} := \frac{M_{i1}}{V}$	$\rho_{c2} := \frac{M_{i2}}{V}$	$\rho_{c3} := \frac{M_{i3}}{V}$
$\rho_{c1} = 0.013\ \frac{gm}{cm^3}$	$\rho_{c2} = 0.013\ \frac{gm}{cm^3}$	$\rho_{c3} = 0.013\ \frac{gm}{cm^3}$
$V_{r1} := \left(\frac{M_{f1}}{M_{i1}}\right) \cdot \frac{\rho_{c1}}{\rho_r} \cdot 100$	$V_{r2} := \left(\frac{M_{f2}}{M_{i2}}\right) \cdot \frac{\rho_{c2}}{\rho_r} \cdot 100$	$V_{r3} := \left(\frac{M_{f3}}{M_{i3}}\right) \cdot \frac{\rho_{c3}}{\rho_r} \cdot 100$
$V_{r1} = 0.425$	$V_{r2} = 0.429$	$V_{r3} = 0.421$

$V_r := \frac{V_{r1} + V_{r2} + V_{r3}}{3}$ $V_r = 0.425$

$Vr := 42.5\%$

Markforged Specimens

1	*2*	*3*
$m_1 := 1.183 \cdot gm$	$m_2 := 1.180 \cdot gm$	$m_3 := 1.182 \cdot gm$
$M_1 := m_1 - n$	$M_2 := m_2 - n = 0.544\ gm$	$M_3 := m_3 - n$
$M_{01} := 0.444 \cdot gm$	$M_{02} := 0.441 \cdot gm$	$M_{03} := 0.440 \cdot gm$
$\rho_{s1} := \frac{M_{01}}{V}$	$\rho_{s2} := \frac{M_{02}}{V}$	$\rho_{s3} := \frac{M_{03}}{V}$
$V_{f1} := \left(\frac{M_1}{M_{01}}\right) \cdot \frac{\rho_{s1}}{\rho_f} \cdot 100$	$V_{f2} := \left(\frac{M_2}{M_{02}}\right) \cdot \frac{\rho_{s2}}{\rho_f} \cdot 100$	$V_{f3} := \left(\frac{M_3}{M_{03}}\right) \cdot \frac{\rho_{s3}}{\rho_f} \cdot 100$
$V_{f1} = 0.243$	$V_{f2} = 0.242$	$V_{f3} = 0.243$

$$V_f := \frac{V_{f1} + V_{f2} + V_{f3}}{3}$$

$V_f = 0.243$

$Vf := 24.3\%$